

ฟีนิลเอไทนิลีนคาลิกซ์[4]เอรีนเป็นตัวรับรู้ฟลูออเรสเซนซ์สำหรับสารประกอบไนโตรแอร์โรมแมติก



บทคัดย่อและแฟ้มข้อมูลฉบับเต็มของวิทยานิพนธ์ตั้งแต่ปีการศึกษา 2554 ที่ให้บริการในคลังปัญญาจุฬาฯ (CUIR)
เป็นแฟ้มข้อมูลของนิสิตเจ้าของวิทยานิพนธ์ ที่ส่งผ่านทางบัณฑิตวิทยาลัย

The abstract and full text of theses from the academic year 2011 in Chulalongkorn University Intellectual Repository (CUIR)
are the thesis authors' files submitted through the University Graduate School.

วิทยานิพนธ์นี้เป็นส่วนหนึ่งของการศึกษาตามหลักสูตรปริญญาวิทยาศาสตรดุษฎีบัณฑิต
สาขาวิชาปิโตรเคมี
คณะวิทยาศาสตร์ จุฬาลงกรณ์มหาวิทยาลัย
ปีการศึกษา 2558
ลิขสิทธิ์ของจุฬาลงกรณ์มหาวิทยาลัย

PHENYLETHYNYLENE CALIX[4]ARENES AS FLUORESCENCE SENSORS FOR
NITROAROMATIC COMPOUNDS

Miss Kanokthorn Boonkitpatarakul



A Dissertation Submitted in Partial Fulfillment of the Requirements
for the Degree of Doctor of Philosophy Program in Petrochemistry

Faculty of Science

Chulalongkorn University

Academic Year 2015

Copyright of Chulalongkorn University

Thesis Title	PHENYLETHYNYLENE CALIX[4]ARENES AS FLUORESCENCE SENSORS FOR NITROAROMATIC COMPOUNDS
By	Miss Kanokthorn Boonkitpatarakul
Field of Study	Petrochemistry
Thesis Advisor	Professor Mongkol Sukwattanasinitt, Ph.D.
Thesis Co-Advisor	Nakorn Niamnont, Ph.D.

Accepted by the Faculty of Science, Chulalongkorn University in Partial
Fulfillment of the Requirements for the Doctoral Degree

.....Dean of the Faculty of Science
(Associate Professor Polkit Sangvanich, Ph.D.)

THESIS COMMITTEE

.....Chairman
(Assistant Professor Warinthorn Chavasiri, Ph.D.)

.....Thesis Advisor
(Professor Mongkol Sukwattanasinitt, Ph.D.)

.....Thesis Co-Advisor
(Nakorn Niamnont, Ph.D.)

.....Examiner
(Associate Professor Nuanphun Chantarasiri, Ph.D.)

.....Examiner
(Associate Professor Voravee Hoven, Ph.D.)

.....Examiner
(Assistant Professor Apichat Imyim, Ph.D.)

.....External Examiner
(Gamolwan Tumcharern, Ph.D.)

กนกธร บุญกิจภัทรกุล : ฟีนิลเอไทนิลีนคาลิกซ์[4]เอรีนเป็นตัวรับรู้ฟลูออเรสเซนซ์สำหรับสารประกอบไนโตรอะโรแมติก (PHENYLETHYNYLENE CALIX[4]ARENES AS FLUORESCENCE SENSORS FOR NITROAROMATIC COMPOUNDS) อ.ที่ปรึกษาวิทยานิพนธ์หลัก: ศ. ดร.มงคล สุขวัฒน์สินธุ์, อ.ที่ปรึกษาวิทยานิพนธ์ร่วม: ดร. นคร เนียมมนนท์, 97 หน้า.

งานวิจัยนี้เกี่ยวกับการพัฒนาตัวรับรู้ฟลูออเรสเซนซ์สองชุด: ชุดแรกคืออนุพันธ์ของคาลิกซ์[4]เอรีนสำหรับการตรวจวัดไตรไนโตรโทลูอีน (ภาค ก) และชุดที่สองคืออนุพันธ์ซาลิไซลิคไดไฮดรอกไซด์สำหรับการตรวจวัดไอออนอลูมิเนียม(ภาค ข)

ภาค ก, ดัดแปลงด้านกว้างของวงคาลิกซ์[4]เอรีน (upper rim) ด้วยการทำปฏิกิริยาควบคู่โซโนกาซิระกับฟีนิลอะเซทิลีน เพื่อขยายขนาดของโพรงให้กว้างขึ้นสำหรับดักจับไตรไนโตรโทลูอีนซึ่งเป็นวัตถุระเบิดและเป็นสารเคมีที่มีพิษ เพื่อเป็นการเพิ่มความสามารถในการละลายน้ำของสาร เราจึงเลือกฟีนิลอะเซทิลีนที่มีหมู่ปลายที่มีขั้วได้แก่หมู่คาร์บอกซิลิก ไฮดรอกซิลและอะมิโน ผลที่ได้พบว่าไตรไนโตรโทลูอีนสามารถดับสัญญาณแสงฟลูออเรสเซนซ์ของคาลิกซ์[4]เอรีนที่มีหมู่อะมิโน (ANC) ในน้ำได้อย่างจำเพาะเจาะจงเมื่อเปรียบเทียบกับสารประกอบไนโตรอะโรมาติกชนิดอื่น ซึ่งเป็นผลมาจากความไม่ชอบน้ำของโพรงและขนาดของโพรงที่ขยายแล้ว นอกจากนี้หมู่ให้อิเล็กตรอนอย่างหมู่อะมิโนมีผลในการเพิ่มความไวในการตรวจวัดไตรไนโตรโทลูอีน เมื่อเปรียบเทียบกับพวกที่มีหมู่ดึงอิเล็กตรอนอย่าง BAC และ SAC โดยสารเรืองแสง ANC มีค่าคงที่ของการระงับสัญญาณต่อไตรไนโตรโทลูอีนเท่ากับ 1.09×10^5 ต่อโมลาร์ และให้ค่าต่ำสุดที่สามารถตรวจวัดได้ (LOD) คือ 0.3 ไมโครโมลาร์ และนอกจากนี้สารเรืองแสง ANC ยังสามารถนำมาเตรียมเป็นแผ่นกระดาษเรืองแสง เพื่อสะดวกในการตรวจวัดการตกค้างและไอระเหยของไตรไนโตรโทลูอีนนอกห้องปฏิบัติการ

ภาค ข, พัฒนาชุดของอนุพันธ์ N-ซาลิไซลิคไดไฮดรอกไซด์สามตัว ที่ใช้ในการตรวจวัดไอออนอลูมิเนียมในตัวกลางที่เป็นน้ำแบบขยายสัญญาณฟลูออเรสเซนซ์โดยให้การคายแสงฟลูออเรสเซนซ์ที่มีสีแตกต่างกัน และมีความแตกต่างของความยาวคลื่นของการคายและดูดกลืนแสงที่กว้าง (large stoke shift) โดยการขยายสัญญาณฟลูออเรสเซนซ์เป็นผลมาจาก chelation-enhanced fluorescence (CHEF) effects ซึ่งเกิดจากการยับยั้งกระบวนการ PET และ ESIP ในงานวิจัยนี้ได้เลือก Furan-2-carbohydrazide (F2) เป็นโครงสร้างหลักที่นำมาออกแบบดัดแปลงโครงสร้างให้มีช่วงการคายแสงที่ยาวขึ้นจากแสงสีฟ้า โดยสารประกอบ F3 ได้ออกแบบด้วยการเพิ่มหมู่ไฮดรอกซิลหมู่ที่สองลงไปตำแหน่งพารากับฟีนอล ส่วนสารประกอบ F4 ได้ทำการเพิ่มหมู่จับไฮดรอกไซด์กลุ่มที่สองลงบนวงฟีนอล ผลที่ได้พบว่าโครงสร้างที่ออกแบบมาใหม่นี้มีผลทำให้ลูมิเนียมคอมเพล็กซ์คายแสงในช่วงความยาวคลื่นที่ยาวขึ้นและยังเพิ่มความแข็งแรงในการจับกันของลิแกนด์กับลูมิเนียมไอออน นอกจากนี้ ลูมิเนียมคอมเพล็กซ์ F4-Al³⁺ มีคุณสมบัติที่น่าสนใจหลายอย่างได้แก่ คายแสงในช่วง 601 นาโนเมตรและมี stroke shifts ที่กว้างคือ 133 นาโนเมตร และให้ค่าต่ำสุดที่สามารถตรวจวัดได้ (LOD) คือ 3.1 นาโนโมลาร์

งานวิจัยของวิทยานิพนธ์นี้ประสบความสำเร็จในการออกแบบและสังเคราะห์สารเรืองแสงชนิดใหม่ขึ้นสองชุด ชุดแรกพัฒนาเพื่อการตรวจวัดไตรไนโตรโทลูอีน และชุดที่สองเพื่อการตรวจวัดไอออนอลูมิเนียมอย่างจำเพาะเจาะจง

สาขาวิชา ปีเตอร์เคมี

ปีการศึกษา 2558

ลายมือชื่อนิสิต

ลายมือชื่อ อ.ที่ปรึกษาหลัก

ลายมือชื่อ อ.ที่ปรึกษาร่วม

5373931023 : MAJOR PETROCHEMISTRY

KEYWORDS: FLUORESCENCE SENSORS / CALIX[4]ARENE-BASED FLUORESCENT SENSOR / HYDRAZIDE SENSORS

KANOKTHORN BOONKITPATARAKUL: PHENYLETHYNYLENE CALIX[4]ARENES AS FLUORESCENCE SENSORS FOR NITROAROMATIC COMPOUNDS. ADVISOR: PROF. MONGKOL SUKWATTANASINITT, Ph.D., CO-ADVISOR: NAKORN NIAMNONT, Ph.D.†, 97 pp.

This research deals with two novel fluorescent sensor series: the first series are calix[4]arene derivatives for TNT detection (part A) and the second series are salicylidenehydrazides for Al^{3+} detection (part B).

In part A, the upper-rim of calix[4]arene is modified with phenylacetylene derivatives via Sonogashira coupling reaction to produce a wider cavity for entrapping TNT, which is highly explosives and recognized as a toxic substance. To improve water solubility, hydrophilic groups such as carboxyl, hydroxyl and amino groups were placed on the modified wider rim (BAC, SAC and ANC). The modified calix[4]arene with amino groups on the wider rim (ANC) exhibits highly selective fluorescence quenching toward TNT compared to the other nitro aromatic compounds in an aqueous medium due to the shape and hydrophobicity of the modified cavity. In addition, the electron donating amino groups on the phenyl ring on ANC enhances the sensitivity toward TNT comparing with BAC and SAC. The Stern-Volmer fluorescence quenching constant of TNT is $1.09 \times 10^5 M^{-1}$ with limit of detection limit of $0.3 \mu M$. The paper-based sensor ANC was also fabricated for a visual on-site detection of trace residues of TNT and its vapor.

Part B, a series of *N*-salicylidenehydrazide derivatives has been developed for selective turn-on detection of Al^{3+} cation in aqueous media with large stroke shifts with three emissive colors, attributing to chelation-enhanced fluorescence (CHEF) effects which inhibit the non-radiative PET and ESIPT processes. Furan-2-carbohydrazide (F2) was chosen as a core structure for further design in shifting the blue emission to a longer wavelength. The addition of the second hydroxyl group at the para-position of a phenol (F3) and the additional of second hydrazide group on the phenol ring (F4) resulted in tuning the emission to longer wavelengths and also enhancing the ligand interaction with Al^{3+} cation. The developed F4- Al^{3+} complex integrates many attractive features into a single probe molecule, which includes emission at long wavelength (601 nm), remarkably large stroke shifts (133 nm) with the low detection limit of 3.1 nM.

This thesis research was successful in design and synthesis the two novel fluorescent sensor series for selective detection of TNT (series 1) and Al^{3+} ion (series 2).

Field of Study: Petrochemistry

Academic Year: 2015

Student's Signature

Advisor's Signature

Co-Advisor's Signature

ACKNOWLEDGEMENTS

First of all, I would like to express my sincere gratitude to my advisor, Professor Dr. Mongkol Sukwattanasinitt, for giving me opportunities, invaluable advice, guidance and encouragement throughout the course of this research. Sincere thanks are also extended to my Co-Advisor Dr. Nakorn Niamnont, Associate Professor Dr. Paitoon Rashatasakhon, Assistant Professor Dr. Anawat Ajavakom, Assistant Professor Dr. Sumrit Wacharasindhu and Dr. Sakulsuk Unarunotai for their generous advice, invaluable guidance and encouragement.

I am also greatly grateful to Professor Dr. Yi Pang at Department of Chemistry, The University of Akron, Ohio, USA for giving me a good opportunity to join their group for a year. I also would like to thank my colleagues for their friendship, especially Dr. Junfeng Wang for his help during the course of the year I was there.

I would like to gratefully acknowledge the committee, Assistant Professor Dr. Warinthorn Chavasiri, Associate Professor Dr. Nuanphun Chantarasiri, Associate Professor Dr. Voravee Hoven, Assistant Professor Dr. Apichat Imyim and Dr. Gamolwan Tumcharern for their kindness, valuable suggestion and recommendations.

I would like to thank Ms Yamonporn Yodta, Ms. Warathip Siripornnoppakhun, Mr. Akachai Khumsri Ms. Nattaporn Kimpitak, Ms. Daranee Homrarueng, and Mr. Watcharin Ngampueng for their helps, suggestions and guidance. I would like to thank Oran Pinrat, Natdanai Suta, Waroton Paisuwan, Atchareeporn Smata, Nattapong Srimuang, Chakrit Yimsukanan, Jadetapong Klahan, Jutawat Hojitsirsayanont and Apiwat Promchat for their help during the course of my graduate research. Moreover, I gratefully thank to everyone in MAPS group for a great friendships, spirit, smile, good wish and their helps in everything.

I would like to thank my financial support from the Thailand Research Fund through the Royal Golden Jubilee Ph. D. Program (Grant No. PHD/0234/2552), Nanotechnology Center (NANOTEC), through its program of Center of Excellence Network, National Research University of CHE and the Ratchadaphiseksomphot Endowment Fund (AM1006A), the University of Akron and the Coleman endowment for financial support and student scholarships.

Finally, I would like to express my thankfulness to my beloved parents who always stand by my side during both of my pleasant and hard time. I would like to

CONTENTS

	Page
THAI ABSTRACT	iv
ENGLISH ABSTRACT	v
ACKNOWLEDGEMENTS	vi
CONTENTS	vii
LIST OF FIGURES	xi
LIST OF TABLES	xvii
LIST OF ABBREVIATIONS	xviii
CHAPTER I INTRODUCTION.....	1
1.1 Fluorescent chemosensors.....	1
1.2 Fluorescence	2
1.3 Sensing mechanisms	3
1.4 Trinitrotoluene (Part A).....	5
1.4.1 Sensors for trinitrotoluene and other nitroaromatic compounds (NACs) ...	5
1.4.2 Calix[4]arene –based fluorescent sensors	11
1.4.3. Calix[4]arene–based fluorescence sensors for TNT and other nitroaromatic compounds (NACs).	12
1.4.4 Objectives of this research.....	14
1.5 Aluminium sensors (Part B)	16
1.5.1 Objectives of this research	23
CHAPTER II EXPERIMENT	24
2.1 Chemicals and materials	24
2.2 Analytical instruments	24
2.3 Synthesis of fluorophores.....	25

2.3.1 Synthesis of ANC, BAC and SAC	25
2.3.1.1 Preparation of p-tert-butyl calix[4]arene	25
2.3.1.2 Preparation of calix[4]arene	26
2.3.1.3 Preparation of 25,26,27,28-tetrapropoxy-calix[4]arene (1).....	27
2.3.1.4 Preparation of 25,26,27,28-tetrapropoxy-4-iodocalix[4]arene (2).....	27
2.3.1.5 Synthesis of 5,11,17,23-Tetrakis-[(4-methyl salicylate)ethynyl]- 25,26,27,28-tetra-(n-propoxy)-calix[4]arene (3b).....	29
2.3.1.6 Synthesis of 5,11,17,23-Tetrakis-[(4-N,N-dimethylaminophenyl) ethynyl]-25,26,27,28-tetra-(n-propoxy)-calix[4]arene (ANC).....	30
2.3.1.7 Preparation of 5,11,17,23-Tetrakis-[(4-benzoic)ethynyl]- 25,26,27,28-tetra-(n-propoxy)-calix[4]arene (BAC)	31
2.3.1.8 Preparation of 5,11,17,23-Tetrakis-[(4-salicylate)ethynyl]- 25,26,27,28-tetra-(n-propoxy)-calix[4]arene (SAC).....	31
2.3.2 Synthesis of F2-F4.....	32
2.3.2.1 Preparation of 2-furoic hydrazide.....	32
2.3.2.2 Synthesis of F2.....	32
2.3.2.3 Synthesis of F3.....	33
2.3.2.4 Synthesis of F4.....	33
2.4 Photophysical property study	34
2.4.1 UV-Visible spectroscopy	34
2.4.1.1. Molar Absorption Coefficients (ϵ)	34
2.4.2 Fluorescence spectroscopy	34
2.4.3 Fluorophore quantum yields	35

	Page
2.5 Electrochemical measurements.....	35
2.6 Fluorescent sensor study	36
2.6.1 Calix[4]arene-based fluorescence sensors (BAC, SAC and ANC) for nitroaromatic explosives	36
2.6.1.1 Selectivity study.....	36
2.6.1.2 Fluorescence titration.....	37
2.6.1.3 The Stern-Volmer plot	37
2.6.1.4 Preparation of ANC fluorescence paper strips	38
2.6.2 Hydrazone-based fluorescent sensors for Al ³⁺	38
2.6.2.1 Selectivity study.....	38
2.6.2.2 Fluorescence titration.....	39
2.6.2.3 Binding constant of the Al ³⁺ complexation	39
2.6.2.4 Competition with other metal ions.....	40
2.6.3 Limit of detection	40
2.6.3.1 Limit of detection for turn-off sensing.....	40
2.6.3.2 Limit of detection for turn-on sensing.....	40
CHAPTER III RESULTS AND DISCUSSION.....	42
3.1 Fluorescent phenylethyne calix[4]arenes (Part A).....	42
3.1.1 Synthesis and characterization of SAC, BAC and ANC	42
3.1.2 Photophysical properties of BAC, SAC and ANC.....	45
3.1.3 Electronic energy levels of the fluorophore	46
3.1.4 Fluorescence Quenching Studies with NACs in Aqueous solution.....	48
3.1.5 Fluorescence titration	49

	Page
3.1.6 Quenching mechanism	50
3.1.7 ANC fluorescent paper sensor.....	54
3.2 Fluorescent hydrazone sensor F2-F4 for sensing Al ³⁺ (Part B).....	55
3.2.1 Synthesis and characterization of F2-F4.....	55
3.2.2 Photophysical properties of F2-F4	56
3.2.3 Fluorescence studies of F2-F4 toward Al ³⁺ ion and other metal ions.	57
CHAPTER IV CONCLUSION	68
4.1 Conclusion of part A	68
4.2 Conclusion of part B	68
REFERENCES	70
APPENDIX A	81
APPENDIX B	96
PUBLICATIONS.....	96
VITA.....	97

LIST OF FIGURES

Figure 1.1 Changes of fluorescent signal.	2
Figure 1.2 Simple Jablonski diagram illustrating fluorescent processes.....	3
Figure 1.3 Principal photophysics of PET.....	4
Figure 1.4 Principal photophysics of ESIPT. Illustrated by 2-(20-hydroxyphenyl)-benzoxazole (HBO).....	4
Figure 1.5 Some fluorescent polymers for NACs sensing.....	6
Figure 1.6 (Top) Structures of 1,4-Diarylptentiptycenes 1a-1e . (Bottom) Photograph of the sensor slide before and after exposure to DNT and TNT in their equilibrium vapors at 22 °C for 30 min.....	7
Figure 1.7 (a) Structures of Hetero-oligophenylene carbazole derivatives S2 and S3 (b) selectivity graph of S2 and S3 toward electron deficient compounds. The inset shows the Stern–Volmer plot of %quenching vs TNT concentration.....	8
Figure 1.8 (a) Structure of Calix[2]pyreno[2]pyrrole (S4) (b) Fluorescence spectral changes of receptor S4 upon addition TNT in toluene ($\lambda_{\text{ex}} = 350 \text{ nm}$).....	8
Figure 1.9 Structure molecular of PQ and the fluorescence titration spectrum of PQ with PA in THF/H ₂ O 1:9 (v/v).	9
Figure 1.10 (a) Structure of sensors 5 and 6 (b) Histogram plot of the Ksv values of nine aromatic compounds tested on sensors 5 and 6 in CHCl ₃	9
Figure 1.11 Structure molecular of BisPy , AM1 optimized structures of BisPy •TNT and the fluorescence titration spectrum of BisPy with trinitrotoluene (0-55 equiv.) in CH ₃ CN/H ₂ O 2:8 (v/v), irradiated at 345 nm.	10
Figure 1.12 Some fluorescence sensors base on calix[4]arene.	11
Figure 1.13 (a) structure of 7 (b) Crystal structure of complex 7 -TNT (c) selectivity graph of 7 toward electron deficient compounds.	12
Figure 1.14 Molecular structures of TBP-p-PPE and Calix-p-PPE polymers.....	13

Figure 1.15 Molecular structures of Calix-PET and TBP-PET	13
Figure 1.16 (a) Structure of benzimidazole-functionalized calix[4]arene receptor (R) (b) selectivity graph of R toward nitroexplosive compounds and electron deficient compounds (c) Structures obtained from a 2 ns MD simulation for 1:3 complex of R with TNT.	14
Figure 1.17 (a) Structure of C4N4 (b) selectivity graph of C4N4 toward nitroexplosive compounds.	14
Figure 1.18 Target molecules BAC , SAC and ANC	15
Figure 1.19 (a) The plausible binding mode of complex of [8-HQP -Al ³⁺] (b) Changes in emission spectra of 8-HQP (25 μ M) in DMSO with increasing concentration of Al ³⁺	17
Figure 1.20 the mechanism of the sensing of Al ³⁺	18
Figure 1.21 Fluorescence enhancement mechanism of ISH -Al ³⁺ complex.....	18
Figure 1.22 the plausible binding mode of MPBH with Al ³⁺	19
Figure 1.23 Fluorescent enhancement mechanisms of the 8 -Al ³⁺ complex.	19
Figure 1.24 Fluorescent enhancement mechanisms of the MCNH -Al ³⁺ complex.....	20
Figure 1.25 Structure of F1 and fluorescent spectra of F1 with 5.0 equiv. of various metal ions in pure water.	20
Figure 1.26 Complexation of F1 and F2 with Al ³⁺	22
Figure 1.27 Target molecules F2-F4	23
Figure 2.1 the Stern-Volmer plot.....	38
Figure 2.2 the calibration curve for turn-on sensing.	41
Figure 3.1 Synthesis route of fluorophores BAC , SAC and ANC	42
Figure 3.2 ¹ H NMR spectra of compounds 1 and 2	43
Figure 3.3 ¹ H NMR spectra of compound 3a , 3b and ANC	44

Figure 3.4 ^1H NMR spectra of compounds of BAC and SAC	45
Figure 3.5 Electronic absorption and emission spectra of fluorophores in THF.	45
Figure 3.6 Cyclic voltammogram of (a) BAC (b) SAC (c) ANC in 0.1 M Bu_4NPF_6 dimethylformamide. Absorption spectra of (d) BAC (e) SAC (f) ANC	47
Figure 3.7 HOMO and LUMO energy levels calculated for BAC , SAC , ANC , and some explosive analytes such as DNT, TNT, and PA.	48
Figure 3.8 Fluorescence quenching effect of various electron deficient aromatic compounds (50 μM) on the fluorophores (0.5 μM) in 1%THF/ H_2O	49
Figure 3.9 Stern-Volmer plots of ANC for TNT, DNT and PA. Inset: The fluorescence quenching ratio of ANC upon the addition of TNT, DNT and PA.	50
Figure 3.10 ^1H NMR of ANC in CDCl_3 in the absence and presence of TNT (top). Chemical shift change ($\Delta\lambda$) plot (bottom).....	51
Figure 3.11 Proposed structure of ANC -TNT interaction.....	51
Figure 3.12 Job's plot of fluorescence responses of ANC upon addition of TNT showing 1:1 stoichiometry.	52
Figure 3.13 Stern-Volmer plots at 25 and 50 $^\circ\text{C}$	52
Figure 3.14 Fluorescence intensity of ANC 0.5 μM at $\lambda_{\text{max}} = 420$ nm in various pH.....	53
Figure 3.15 Fluorescence quenching of ANC for TNT 100 equiv in DMF and 1%THF/ H_2O	53
Figure 3.16 Fluorescence image (under 365 nm UV light) of ANC on a filter paper under different experimental conditions. (A) Vapor-mode detection of TNT (a) before (b) after exposing TNT vapors 5 min (c) 10 min.....	54
Figure 3.17 Impression of thumb (a) before rubbing with TNT (b) after rubbing with TNT.	54
Figure 3.18 Synthesis routes of fluorophores	55

Figure 3.19 1H NMR spectra of compound F2-F4	56
Figure 3.20 Quenching mechanism of F2	57
Figure 3.21 Fluorescence spectra of F2-F4 (10 μM in 0.1% DMSO/HEPES) before and after addition 10 equiv of metal ions: Na^+ , K^+ , Ag^+ , Mg^{2+} , Ca^{2+} , Hg^{2+} , Ba^{2+} , Pb^{2+} , Cd^{2+} , Mn^{2+} , Ni^{2+} , Co^{2+} , Cu^{2+} , Fe^{2+} , Zn^{2+} , Cr^{3+} , Fe^{3+} , Al^{3+} . The spectra were obtained after 10 minute mixing for F2 and F3 and 30 minute mixing for F4 with $\lambda_{\text{ex}} = 369$, 410 and 468 nm, respectively. Only Al^{3+} gives significant enhancement.....	58
Figure 3.22 Fluorescence enhancement mechanism of the F2-Al³⁺ complex.....	59
Figure 3.23 Fluorescence spectra of F2 (a), F3 (b) and F4 (c) (10 μM), respectively, upon addition of different concentrations of Al^{3+} in 0.1% DMSO/HEPES. Inset: Plots of intensity at each λ_{em} versus the amount of Al^{3+} added. The spectra were obtained after mixing for 10 minutes (sensor F2 and F3) and for 30 minutes (sensor F4) using $\lambda_{\text{ex}} = 369$, 410 and 468 nm, respectively.....	60
Figure 3.24 The Job's plot examined between Al^{3+} and (a) sensor F2 (b) F3 (c) F4 by fluorescence.	61
Figure 3.25 HRMS of sensor (a) F2-Al³⁺ , (b) F3-Al³⁺ and (c) F4-Al³⁺	61
Figure 3.26 Benesi-Hildebrand plots of (a) F2 , (b) F3 and (c) F4	62
Figure 3.27 Absorption spectra of (a) F2 (10 μM) (b) F3 (10 μM) (c) F4 (20 μM) after 10 minute mixing with Al^{3+} in 0.2% DMSO/HEPES for F2 and F3 but after 3 hour mixing with Al^{3+} in CH_3OH for F4	63
Figure 3.28 Calibration curves of ratio of fluorescence intensity of F4 to Al^{3+} concentration.	64
Figure 3.29 Relative fluorescence of F4 (10 μM) in 0.1% DMSO/HEPES pH 5.5 in the presence of Al^{3+} (100 μM) plus another interfering metal ion (100 μM) tested..	64
Figure 3.30 Fluorescence emission spectra of F2-F4 in the presence of Al^{3+} (1.0 equiv. for F2-F3 and 2.0 equiv. for F4) and signal restoration by EDTA (10.0 equiv.)..	65

Figure 3.31 Photographic image of metal ion (1 nmol) detection by F4 on filter paper tested by simple drop and dry from solutions of F4 and metal ions, consecutively. The sample was irradiated by UV-light (wavelength 365±50 nm).....	67
Figure 3.32 Fluorescence spectra of F4 (10 μM in 0.1% DMSO/HEPES) before and after addition 10 equiv of Al ³⁺ and Zn ²⁺ in CH ₃ CN (ACN).....	67
Figure 3.33 Photographic image for dual detection of Al ³⁺ and Zn ²⁺ by F4 using paper chromatography for separation: (a) before and (b) after elution with Et ₂ NH: DMF (5: 20 v/v). The sample was irradiated by UV-light (wavelength 365±50 nm).	67
Figure A.1 ¹ H NMR of 1 in CDCl ₃	81
Figure A.2 ¹ H NMR of 2 in CDCl ₃	81
Figure A.3 ¹ H NMR of 3a in CDCl ₃	82
Figure A.4 ¹³ C NMR of 3a in CDCl ₃	82
Figure A.5 HRMS of 3a	83
Figure A.6 ¹ H NMR of 3b in CDCl ₃	84
Figure A.7 ¹³ C NMR of 3b in CDCl ₃	84
Figure A.8 HRMS of 3b	85
Figure A.9 ¹ H NMR of ANC in CDCl ₃	86
Figure A.10 ¹³ C NMR of ANC in CDCl ₃	86
Figure A.11 HRMS of ANC	87
Figure A.12 ¹ H NMR of BAC in Acetone-d ₆	88
Figure A.13 ¹³ C NMR of BAC in Acetone-d ₆	88
Figure A.14 HRMS of BAC	89
Figure A.15 ¹ H NMR of SAC in Metanol-d ₄	89
Figure A.16 ¹³ C NMR of SAC in Metanol-d ₄	90
Figure A.17 HRMS of SAC	90

Figure A.18 ^1H NMR of F2 in DMSO-d_6	91
Figure A.19 ^{13}C NMR of F2 in DMSO-d_6	91
Figure A.20 HRMS of F1	92
Figure A.21 ^1H NMR of F3 in DMSO-d_6	92
Figure A.22 ^{13}C NMR of F3 in DMSO-d_6	93
Figure A.23 HRMS of F3	93
Figure A.24 ^1H NMR of F4 in DMSO-d_6	94
Figure A.25 ^{13}C NMR of F4 in DMSO-d_6	94
Figure A.26 HRMS of F4	95



LIST OF TABLES

Table 1.1 Summarize of some hydrazide fluorescent chemosensors for Al ³⁺ detection.....	21
Table 3.1 Photophysical properties of the fluorophores.....	46
Table 3.2 Photophysical properties of sensor F2-F4 in aqueous solution (~0.5% DMSO/H ₂ O).....	57



LIST OF ABBREVIATIONS

Ar	aromatic
calcd	calculated
^{13}C NMR	carbon-13 nuclear magnetic resonance
CDCl_3	deuterated chloroform
DMSO- d_6	deuterated dimethyl sulfoxide
DMSO	dimethylsulfoxide
d	doublet (NMR)
dd	doublet of doublet (NMR)
ESIMS	electrospray ionization mass spectrometry
equiv	equivalent (s)
FT-IR	fourier transform infrared spectroscopy
g	gram (s)
^1H NMR	proton nuclear magnetic resonance
Hz	Hertz
HRMS	high resolution mass spectrum
h	hour (s)
IR	infrared
J	coupling constant
K_a	Association constant
mg	milligram (s)
mL	milliliter (s)
mmol	millimole (s)

m/z	mass per charge
m	multiplet (NMR)
M.W.	molecular weight
M	molar
MHz	megaHerz
rt	room temperature
s	singlet (NMR)
THF	tetrahydrofuran
TLC	thin layer chromatography
UV	ultraviolet
δ	chemical shift
$^{\circ}\text{C}$	degree Celsius
μL	microliter (s)
μM	micromolar (s)
Φ	quantum yield
% yield	percentage yield

CHAPTER I

INTRODUCTION

1.1 Fluorescent chemosensors

Nowadays, fluorescent chemosensors play an important role in detection method in chemical, biological, and environmental fields, including detection of metal ion, anion, neutral molecules and biomolecules. Fluorescent technique has significant advantages over other methods such as high selectivity, high sensitivity, short response time, cost-effectiveness in instrumentation, operational simplicity, and also no destruction of samples. Most of the fluorescent chemosensors are composed of two main components: one is a receptor unit for selective binding of the analytes, the other is a fluorophore unit provides the means of signaling this bonding, whether by fluorescence quenching, enhancement or wavelength shift. The photophysical signaling mechanisms which controls the response of a fluorophore to analytes binding include photoinduced electron transfer (PET) [1-7], intramolecular charge transfer (ICT) [2-7], Förster resonance energy transfer (FRET) [8, 9], excited-state intramolecular proton transfer (ESIPT) [10, 11], Isomerization [12], aggregation-induced enhancement fluorescence (AIE) [13, 14], aggregation-caused quenching (ACQ), and excimer/exciplex formation [2-4, 7, 15]. In addition, a chemosensor may be designed by using more than one sensing mechanism in order to enhance response of signal transduction.

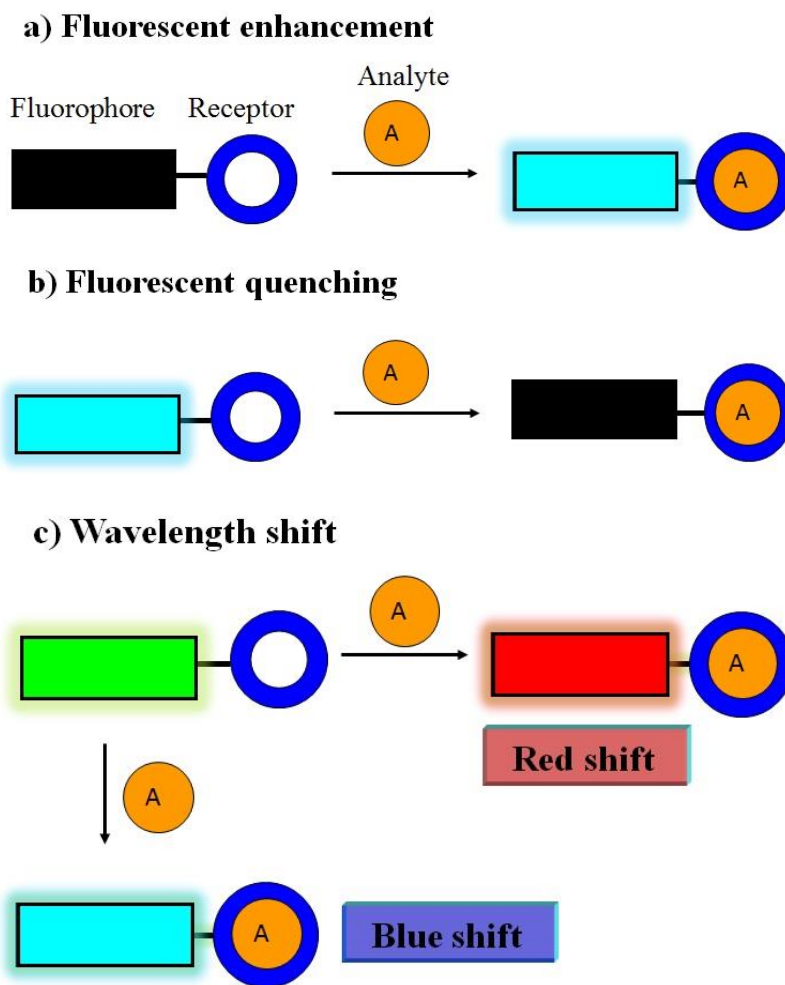


Figure 1.1 Changes of fluorescent signal.

1.2 Fluorescence

Fluorescence is the emission of light typically occurring with aromatic compounds or highly conjugated molecules. The fluorescence processes that occur between the absorption and emission of light can be usually described by the Jablonski diagram as shown in Figure 1.2 [16]. Upon the absorption of light energy, the molecule is excited to excited states (S_1 or S_2) and forms an excited molecule. The molecule rapidly relaxes to the lowest vibrational level of S_1 which this process is called internal conversion. The final process, the molecule returns to ground state (S_0) via emission of a longer wavelength photon. The time required to complete this process takes nano-second.

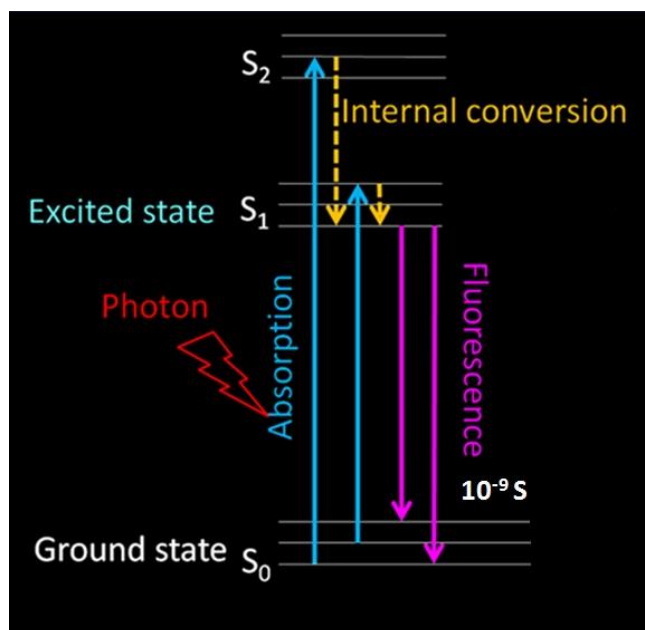


Figure 1.2 Simple Jablonski diagram illustrating fluorescent processes.

1.3 Sensing mechanisms

The sensing compounds in this thesis have been designed based on PET and ESIPT.

- Photoinduced electron transfer (PET)

PET process can occur when receptor or analyte has either its highest occupied molecular orbital (HOMO) (Donor) or the lowest unoccupied molecular orbital (LUMO) (acceptor) level between HOMO and LUMO gap of the fluorophore.

In the first case, when an electron of fluorophore is excited to its LUMO level. A HOMO electron of the donor presumably transfers to the HOMO level of the excited fluorophore which acts as the electron acceptor. After that, the excited electron in LUMO level can transfer to the HOMO level of the donor (Figure 1.3, left). In the latter case, the excited electron in LUMO level of the fluorophore transfer to the LUMO level of the acceptor before transferring back to the half-filled HOMO level of the fluorophore (Figure 1.3, right). In this case, the excited fluorophore acts as the electron donor. The electron transfer process is a non-radiative process which results in quenching of the fluorescence.

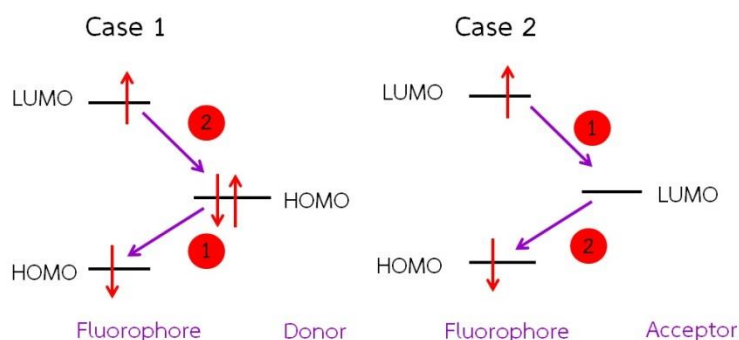


Figure 1.3 Principal photophysics of PET.

- Excited state intramolecular proton transfer (ESIPT)

The ESIPT process generally associates with the transfer of a proton of a hydroxyl (or amino) group to a carbonyl oxygen (or imine nitrogen) through a pre-existing six- or five-membered ring hydrogen bonding configuration [17]. The classic example of the ESIPT photophysical process was observed for 2-(20-hydroxyphenyl)-benzoxazole (HBO) as illustrated in Figure. 1.4. After irradiation, the HBO in enol form (E^*) is converted to the excited-state keto form (K^*) in the sub picosecond time scale resulting in significantly red shift emission compared with the absorption and unusually large Stoke shift. A large Stoke shift is beneficial in fluorescence sensing to avoid the self-absorption or the inner filter effect.

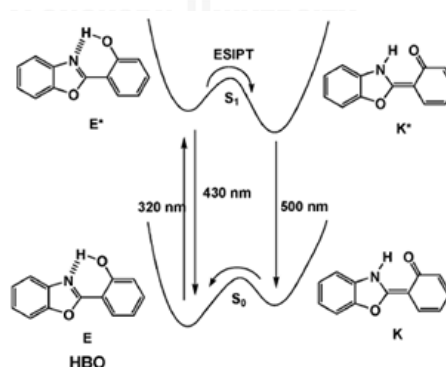


Figure 1.4 Principal photophysics of ESIPT. Illustrated by 2-(20-hydroxyphenyl)-benzoxazole (HBO).

1.4 Trinitrotoluene (Part A)

Trinitrotoluene (TNT) is an important nitroaromatic explosive and widely used as a part of many explosive mixtures partly due to its insensitivity to shock and friction [18, 19]. Besides TNT is highly explosive; it has also been considered as a hazardous material causing skin irritation, anemia, and liver cancer [18, 19]. TNT contamination in environment can occur through the TNT manufacture, the processing and destruction of bombshell. Amount of TNT in ground water and soil near munitions plants can be found at least 500 ppb [18]. The US Environmental Protection Agency (EPA) sets the limit of TNT in drinking water to be 2 ppb [20]. Until now, there are various techniques for TNT detections available such as chromatography coupled with mass spectrometry [21], surface-enhanced Raman spectroscopy [22], amperometry [23], X-ray dispersion [24], cyclic voltammetry [25] and ion mobility spectrometry [26]. However, these methods suffer from some obstacles for instance the cumbersome pretreatment of samples, interference from other compounds, or sophisticated instrumentation [26, 27]. On the other hand, using fluorescence chemsensors offer significant advantages over other method: high sensitivity and selectivity, short response time, cost-effectiveness in instrumentation and also operational simplicity suitable for on-site analysis [28-30].

1.4.1 Sensors for trinitrotoluene and other nitroaromatic compounds (NACs)

One property of nitroaromatics is their strong electron accepting capability due to substitution of the electron-withdrawing nitro groups on the aromatic ring. Therefore, the fluorescent sensory materials for NACs detection based mainly on photoinduced electron transfer (PET) fluorescent quenching process. In particular, fluorescent conjugated polymers films as good electron donors have been widely studied for detecting NACs both in solution and vapor phase. These polymers included poly(phenyleneethynylene) (PPEs) [28, 31-33], poly(p-phenylene vinylenes) (PPVs) [34, 35] and polymetalloles [26, 36-38]. Some fluorescent polymers for NACs sensing are shown in Figure 1.5. These conjugated fluorescent polymers can give high fluorescence quenching sensitivity due to excitonic migration amplifying mechanisms [39]. Nevertheless, their solid state dense films generally have low permeability for

analyte molecules [40]. Their random and unpredictable conformation of the polymer chains may also lead to molecular orientation at the film surface unsuitable for binding analysts.

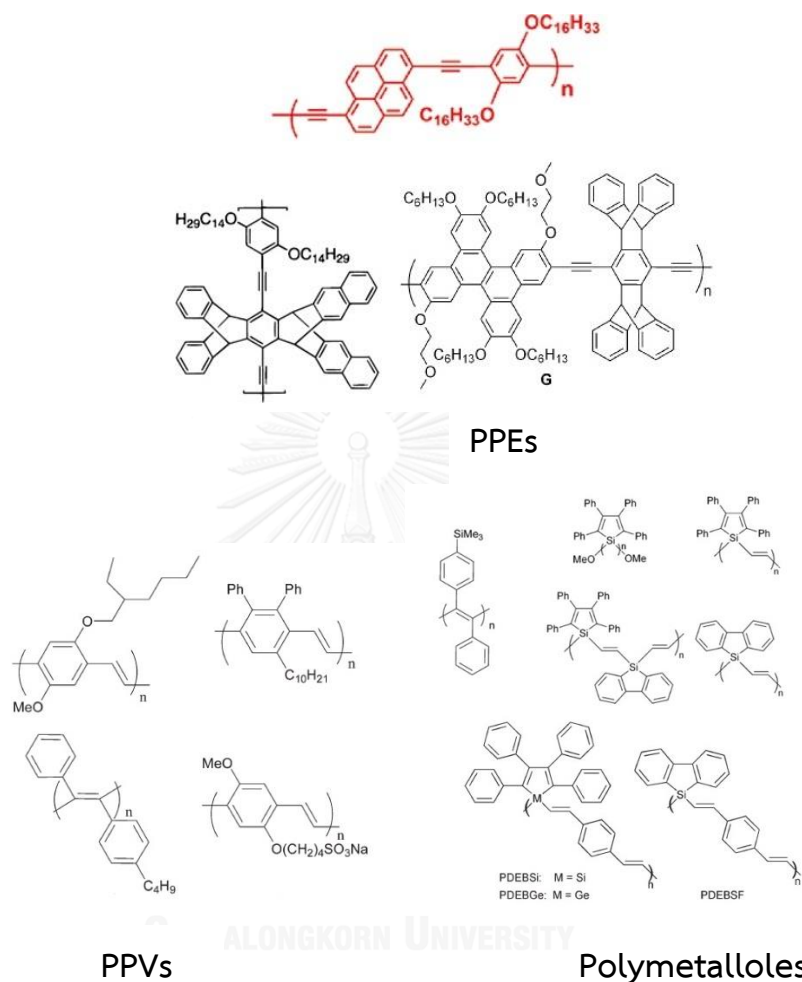


Figure 1.5 Some fluorescent polymers for NACs sensing.

Recently, development of single molecules as fluorescent sensors has gain more attention due to their well define structures, monodispersity, simpler synthesis and purification allowing better understanding of structure–property relationships [39, 40]. Some examples of literature related to single molecule-based fluorescent sensors for detecting NACs are as follows:

In 2008, Zyryanov et al. [41] synthesized a series of 1,4-Diaryl(pent)ptycene derivatives (1a-1e). Their fluorescence signals were selectively quenched by nitroaromatic compound such as TNT, DNT and NB in CH_2Cl_2 . The Stern-Volmer

constants were in the range of 1000-3000 M^{-1} in the case of TNT. To investigate the ability of the sensor for sensing nitroaromatic vapors, the sensor films were prepared by casting **1d** and **1e**, separately, in the glass wells. The fluorescence of **1d** and **1e** films was quenched upon exposure to TNT and DNT vapor in 30 minutes. Comparison with the standard HTPP film did not change the red fluorescence as shown in Figure 1.6.

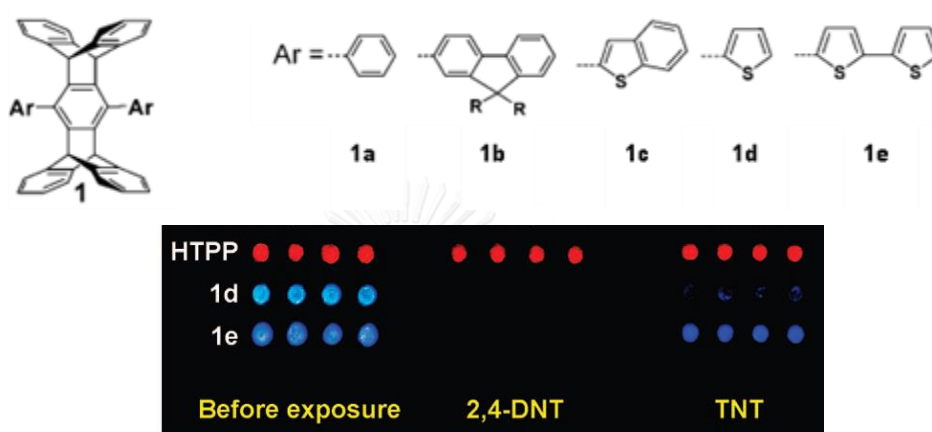


Figure 1.6 (Top) Structures of 1,4-Diarylpenttiptycenes **1a-1e**. (Bottom) Photograph of the sensor slide before and after exposure to DNT and TNT in their equilibrium vapors at 22 °C for 30 min.

In 2012, Kumar et al. [42] synthesized new AIEE-active hetero-oligophenylene carbazole derivatives (**S2** and **S3**) as fluorescent probes for the selective detection of TNT in aqueous media. Compound **S2** and **S3** themselves exhibited weak emission ($\Phi_f = 0.0018$ and 0.006) at 363 nm. In 80% H_2O/THF , the solutions gave bright fluorescence, with their quantum efficiency reaching as high as $\Phi_{AIEE} = 0.59$ and 0.43, respectively. Upon addition of 10 equiv. TNT, the fluorescence emissions of both sensors were selectively quenched about 90% (Figure 1.7b) with the limit of detection (LOD) as low as 30 nM for **S2** and 40 nM for **S3**. The Stern–Volmer fluorescence quenching constant of aggregates **S2** and **S3** to TNT are 13.3×10^5 and $10.0 \times 10^5 M^{-1}$, respectively.

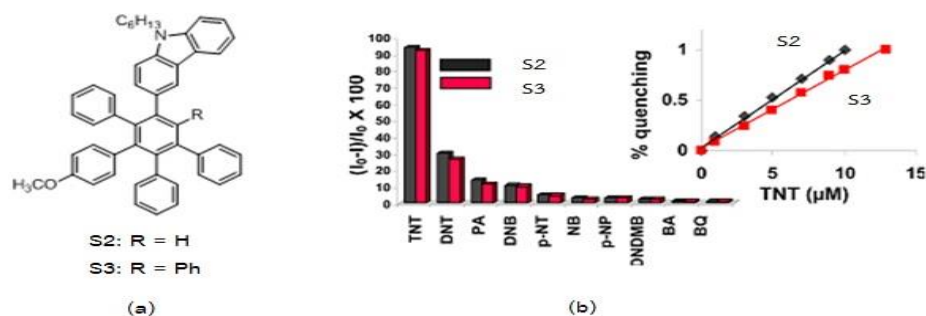


Figure 1.7 (a) Structures of Hetero-oligophenylene carbazole derivatives **S2** and **S3** (b) selectivity graph of **S2** and **S3** toward electron deficient compounds. The inset shows the Stern–Volmer plot of %quenching vs TNT concentration.

In 2012, Park et al. [43] synthesized calix[2]pyreno[2]pyrrole as fluorescence chemosensor for nitroaromatic compounds. The fluorescence emissions of the sensor **S4** was sensitively quenched in the presence of nitrobenzene (NB) and 2,4,6-trinitrotoluene (TNT) in toluene. The calculated binding constant from the fluorescence titration was found to be 1.2×10^6 and 1.1×10^6 for NB and TNT, respectively. These values were large enough to form strong host-anion charge transfer complex.

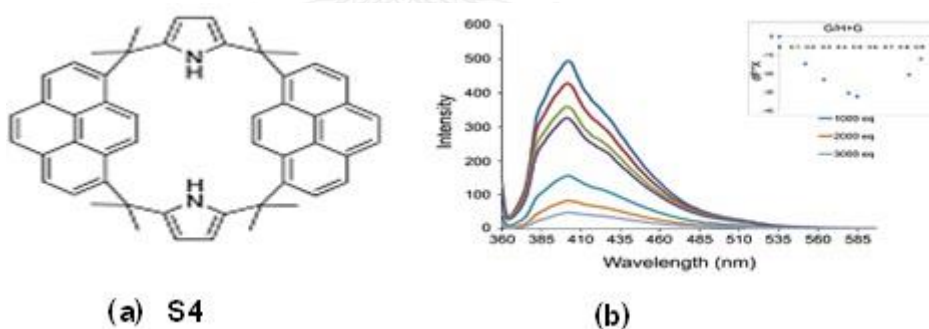


Figure 1.8 (a) Structure of Calix[2]pyreno[2]pyrrole (**S4**) (b) Fluorescence spectral changes of receptor **S4** upon addition of TNT in toluene ($\lambda_{\text{ex}} = 350$ nm).

In 2012, Bhalla et al. [44] designed and synthesized derivative of pentacenequinone **PQ** which exhibited aggregation-induced emission enhancement (AIEE) characteristics in aqueous media (10% THF/H₂O). The fluorescent nanoaggregate **PQ** showed selectively quenched toward picric acid (PA, $K_{\text{sv}} 6.9 \times 10^4 \text{ M}^{-1}$) more than TNT ($K_{\text{sv}} 4.3 \times 10^4 \text{ M}^{-1}$). The higher sensitivity of the aggregates toward PA than TNT could be explained by the energy transfer of the sensor to PA which

the absorption spectrum of PA overlapped the emission spectrum of the sensor in the wavelength region of 425-480 nm.

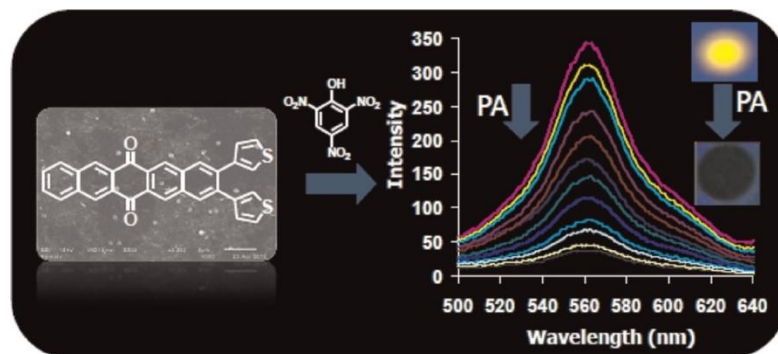


Figure 1.9 Structure molecular of PQ and the fluorescence titration spectrum of PQ with PA in THF/H₂O 1:9 (v/v).

In 2013, Niamnont et al. [45] synthesized triphenylamine-based fluorophores containing the electron rich aromatics (pyrene **5** and corannulene **6**). Compound **5** showed the high sensitivity and selectivity toward TNT with the Stern-Volmer constant to be $1.7 \times 10^4 \text{ M}^{-1}$ in CHCl₃. The lower sensitivity of the corannulene could be due to its bowl shape geometry which probably did not well accommodate the π - π interaction with TNT.

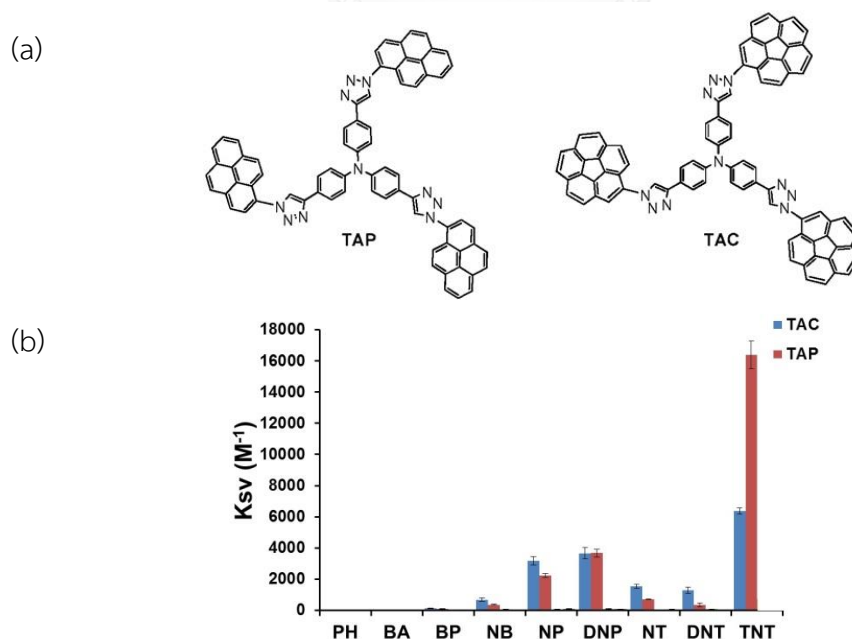


Figure 1.10 (a) Structure of sensors **5** and **6** (b) Histogram plot of the K_{sv} values of nine aromatic compounds tested on sensors **5** and **6** in CHCl₃.

In the same year, Kim et al. [46] designed and synthesized **BisPy** as a TNT receptor in semi-aqueous media (20% CH₃CN/H₂O). **BisPy** showed both monomer emission band (380, 384 nm) and excimer emission band (481 nm). The addition TNT decreased the excimer band but increased the monomeric band. These changes indicated the excimer formation was interfered. This result supported that the two pyrenyl groups in **BisPy** can arrange appropriately in the semi-aqueous medium. On the basis of Job plot, **BisPy** receptor formed a 1:1 complex between **BisPy** and TNT.

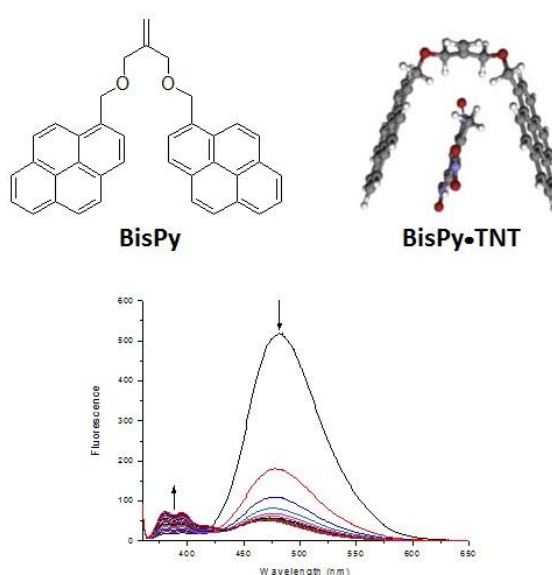


Figure 1.11 Structure molecular of **BisPy**, AM1 optimized structures of **BisPy•TNT** and the fluorescence titration spectrum of **BisPy** with trinitrotoluene (0-55 equiv.) in CH₃CN/H₂O 2:8 (v/v), irradiated at 345 nm.

From the literatures, it can be thus summarized that a highly sensitive fluorescent chemosensor for TNT sensing should have electron donating groups and aromatic moieties. However, most of fluorescent compounds have low selectivity between nitrotoluene and nitrophenol derivatives because both classes are strong electron acceptors [47]. Moreover, trinitrophenol (TNP) usually appeared to give higher quenching efficiencies than TNT in most cases because of its high absorptivity at the excitation wavelength [48]. To increase the selectivity toward TNT, it is interesting to include a binding site for nitrotoluene moiety. In this work, we selected

calix[4]arene scaffolds because of its pre-organized three-dimensional structures with suitable hydrophobic cavity.

1.4.2 Calix[4]arene –based fluorescent sensors

Calix[4]arene is a macrocycle composed four phenol rings linked together with four methylene units in the ring. Calix[4]arene forms three-dimensional cup shape with hydrophobic cavity. Calix[4]arene has two positions easy to be functionalized (phenolic hydroxyl groups and p-position), when they are modified appropriately capable of selectively interact and form specific host–guest complexes with neutral and ionic molecular guests. Some calix[4]arene-based fluorescent sensors are shown in Figure 1.12

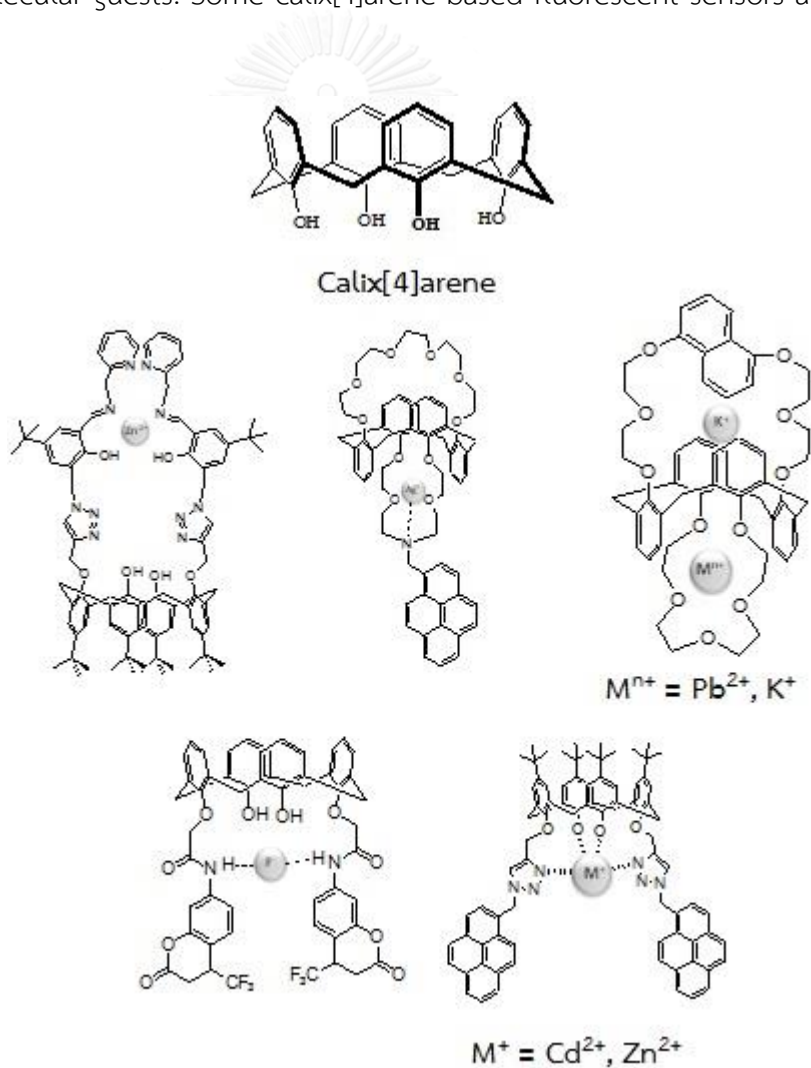


Figure 1.12 Some fluorescence sensors base on calix[4]arene.

1.4.3. Calix[4]arene-based fluorescence sensors for TNT and other nitroaromatic compounds (NACs).

In 2010, Lee et al. [49] synthesized dipyrenylcalix[4]arene (**7**) containing two facing pyreneamide groups. The molecule was used as a fluorescence chemosensor for nitroaromatic compounds in CH₃CN. The highly efficient quenching of TNB and TNT to the fluorescence emission of the sensor **7** was attributed to π - π interaction between the trinitroaromatics, TNB or TNT, and the pyrene moieties in the fluorophore as shown in Figure 1.12. The detection limit for TNT was determined to be down to the 1.1 ppb in CH₃CN.

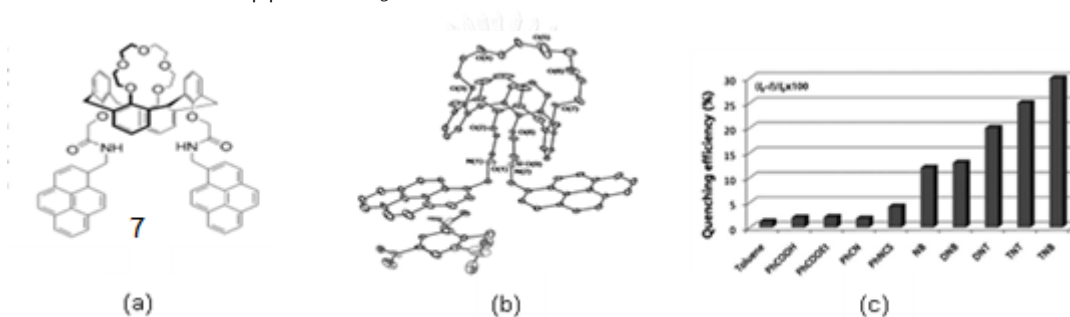


Figure 1.13 (a) structure of **7** (b) Crystal structure of complex **7**-TNT (c) selectivity graph of **7** toward electron deficient compounds.

In 2012, Costa et al. [50] prepared a PPE polymer film possessing calix[4]arene (**Calix-p-PPE**) moieties attach to the main chain. It was found that the **Calix-p-PPE** film showed high sensitivity and quick response time toward DNT and TNT vapors compared with a model **TBP-p-PPE** film. Upon exposure TNT vapor 10 second, the fluorescence quenching efficiency of **CALIX-p-PPE** is 54%. While, **TBP-p-PPE** used as a model showed no more than 20% upon 5 min of exposure.

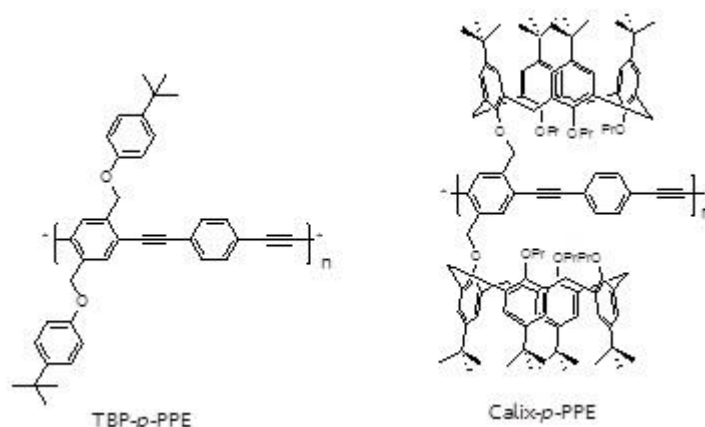


Figure 1.14 Molecular structures of **TBP-p-PPE** and **Calix-p-PPE** polymers.

In the same year and the same research group, [Costa et al., 2012] [51] *p*-phenylene ethynylene trimers integrating a non-macrocyclic analog *tert*-butylphenol (**TBP-PET**) and a macrocyclic calix[4]arene receptors (**Calix-PET**) moieties were synthesized. On the contrary what was expected, the results showed that the fluorescence quenching efficiency of the model structure, **TBP-PET** exhibited higher sensitivity toward NACs than that of **CALIX-PET** in both solution and solid state. In the solution, the K_{sv} constants of **Calix-PET** and **TBP-PET** for TNT in CHCl_3 were found to be 1248 and 1693 M^{-1} respectively.

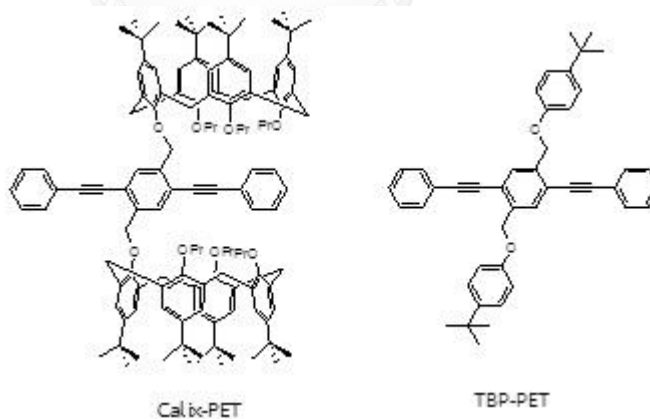


Figure 1.15 Molecular structures of **Calix-PET** and **TBP-PET**.

In 2013, Kandpal et al. [52] modified the upper rim of calix[4]arene with benzimidazole moiety (**R**) that served as a TNT receptor. The fluorescence emission of sensor **R** was high selectively and sensitively quenched toward TNT both in solution and solid state. In THF solution, the K_{sv} constant of **R** for TNT was found to be $30,000 \text{ M}^{-1}$ respectively.

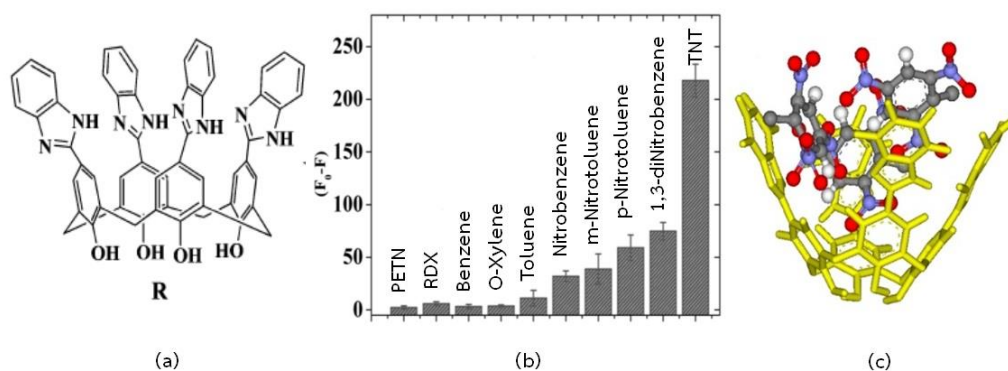


Figure 1.16 (a) Structure of benzimidazole-functionalized calix[4]arene receptor (**R**) (b) selectivity graph of **R** toward nitroexplosive compounds and electron deficient compounds (c) Structures obtained from a 2 ns MD simulation for 1:3 complex of **R** with TNT.

In 2014, Cao et al. [53] designed and synthesized a deep electron-rich cavity tetranaphthylcalix[4]arene which exhibited selectivity toward p-nitrophenol in acetonitrile. The association constant of **C4N4** for p-nitrophenol was determined using the Benesi–Hildebrand equation and was found to be $10.06 \times 10^3 \text{ M}^{-1}$. The NMR, AFM, IR, MALDI-TOF mass spectroscopy, and computational calculations revealed the formation of a host–guest complex driven by π – π stacking interactions.

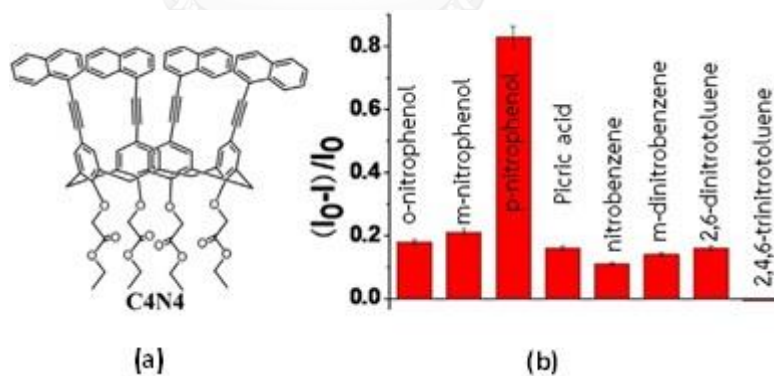


Figure 1.17 (a) Structure of **C4N4** (b) selectivity graph of **C4N4** toward nitroexplosive compounds.

1.4.4 Objectives of this research

The aim of this work has been focused on the synthesis of the fluorescent arylolethynyl calix[4]arenes (**BAC**, **SAC** and **ANC**) and study of photophysical properties of these compounds for sensing TNT in aqueous media. In our molecular design, the

upper-rim of calix[4]arene is extended with a π -conjugated system of phenylacetylene to produce a wider cavity for entrapping TNT. The sensing study in high water content media is particularly emphasized here as it is more relevant to real environmental samples. We hypothesized that the more hydrophilic TNP would be less likely to be included into the hydrophobic cavity of calix[4]arene in aqueous medium. To improve water solubility, hydrophilic groups such as carboxyl, hydroxyl and amino groups were placed on the modified wider rim as shown in Figure 1.18. The placement of these groups should also provide different electronically push-pull effects in connection with the electron donating alkoxy groups on the other rim, the narrow rim.

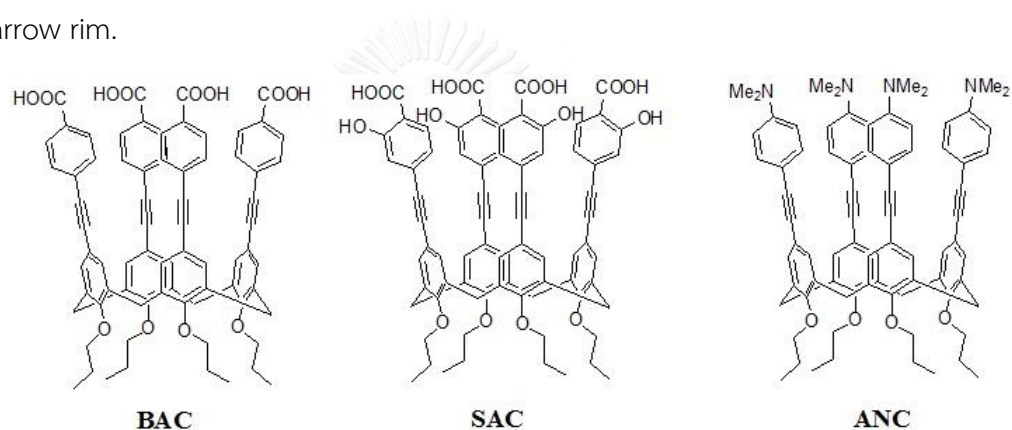


Figure 1.18 Target molecules BAC, SAC and ANC

1.5 Aluminium sensors (Part B)

Aluminum is one of the most abundant metallic elements in the earth's crust and it is extensively used in daily life [54, 55]. However, high levels of aluminum ion (Al^{3+}) in human body can cause many severe diseases including Alzheimer's disease, dialysis encephalopathy, and Parkinson's disease [56-61]. The World Health Organization (WHO) reports that human consume Al^{3+} about 3–10 mg/day while the weekly tolerable intake is 7 mg/kg of the body weight. The WHO also limits Al^{3+} concentration in drinking water to 200 $\mu\text{g/L}$ (7.41 μM) [62-64].

Nowadays, there are several analytical techniques available for detecting aluminum ion such as atomic absorption spectrometry [65], inductively coupled plasma mass spectrometry (ICP-MS) [66], voltammetry [67, 68], ion selective membrane [69] etc. However, these techniques are not easily applied for on-site and real time monitoring of environments and biological systems. In comparison, using fluorescence chemosensors offer significant advantages over other method as previously mentioned. Nevertheless, aluminium by itself has strong hydration with water, resulting in weak coordination with ligand [70-72] that makes the detection of the Al^{3+} by a chemosensor in highly aqueous system difficult. To achieve a high and selective binding, most fluorescent Al^{3+} sensors contain rather complicated ligand structures that are difficult to synthesize and poorly soluble in water [73, 74]. It is thus highly desirable to develop an aqueous soluble Al^{3+} sensor that can be easily synthesized and exhibit high selectivity to detect Al^{3+} ion in aqueous environments even at minimal concentration. In addition, ability in optical tuning of the probe is also highly desirable in bioimaging, especially for tuning toward the NIR region to minimize auto-fluorescence, cytotoxicity and photo damage of living cells [75-78]. A large stoke shift is also highly desirable in fluorescence sensing technology to avoid the self-absorption and interference from light source [79]. Thus, rational design of ligands with high sensitivity/selectivity and ability in spectroscopic tuning are of great value.

Hydrazides have been extensively used in several re-search fields due to their facile syntheses, tunable elec-tronic properties and good chelating capability [80].

Some hydrazide-based fluorescent sensors for selective detection of Al^{3+} have been reported herein.

In 2006, Zhao et al. [81] synthesized a two-branched amide-hydroxyquinoline ligand **8-HQP**. This ligand showed a selective fluorescence enhancement to Al^{3+} ion in DMSO. The enhancement of fluorescence resulted from the formation of the intramolecular excimer by the π - π^* stacking of the two quinoline rings as a consequence of coordination of two **8-HQP** didentate sites to the Al^{3+} . The association constant was determined as $\log K_a = 5.81$. The detection limit was found to be 1×10^{-6} M.

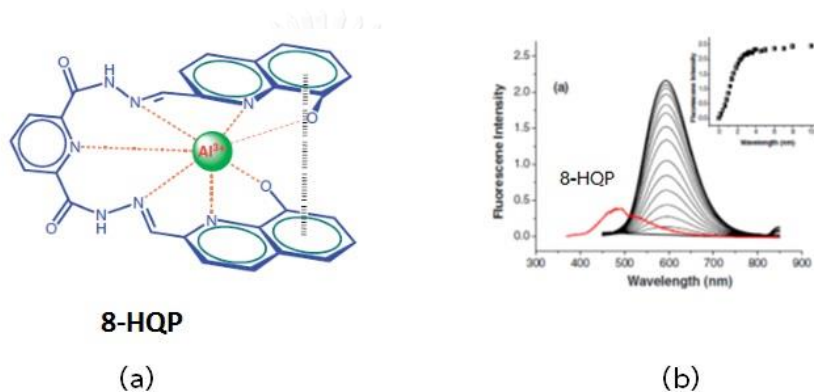


Figure 1.19 (a) The plausible binding mode of complex of $[\mathbf{8-HQP-Al}^{3+}]$ (b) Changes in emission spectra of **8-HQP** ($25 \mu\text{M}$) in DMSO with increasing concentration of Al^{3+} .

In 2013, Guo et al. [82] synthesized a selective fluorescent sensor for Al^{3+} ion, 2,2'-bipyridyl-3,3'-bis-(N,N)'disalicylidene)-formylhydrazone (**H2L**). The sensor showed high fluorescence turn-on after binding Al^{3+} in aqueous solution (HEPES-buffer, pH 7.4). Upon binding Al^{3+} , the molecular system formed nearly a planar structure that generated the chelation-enhanced fluorescence (CHEF) and also reduced the intramolecular charge transfer (ICT) process in the sensor. The association constant K_a value for the Al^{3+} complexation was determined to be $7.8 \times 10^4 \text{ M}^{-1}$ in aqueous solution (HEPES-buffer, pH 7.4) with the limit of detection (LOD) of $0.17 \mu\text{M}$.

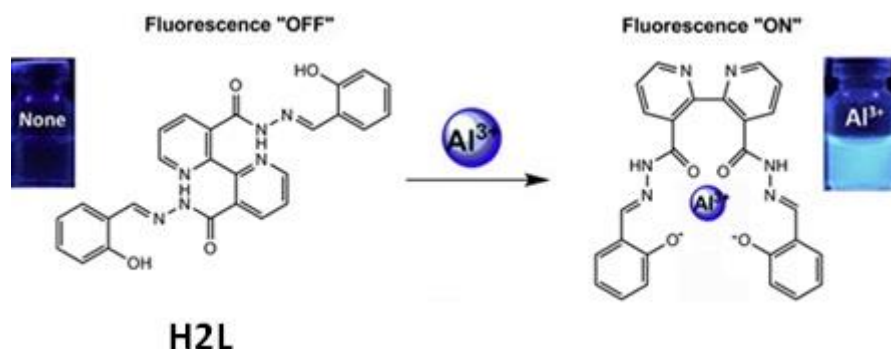


Figure 1.20 the mechanism of the sensing of Al^{3+} .

A Schiff base type isophthaloyl salicylaldehyde hydrazone (ISH) [83] was synthesized as a sensor for selectively detecting Al^{3+} in 50% MeOH/ H_2O with a fluorescence enhancement at wavelengths 455 nm. The fluorescence enhancement and blue shift from 527 nm to 455 nm could be explained by suppression of C=N isomerization and the more widespread formation of the π -conjugation system in ISH. The association constant (K_a) for the ISH-Al^{3+} complexation was $1.05 \times 10^5 \text{ M}^{-1}$ by using the Benesi-Hildebrand equation with the limit of detection (LOD) of $0.77 \mu\text{M}$.

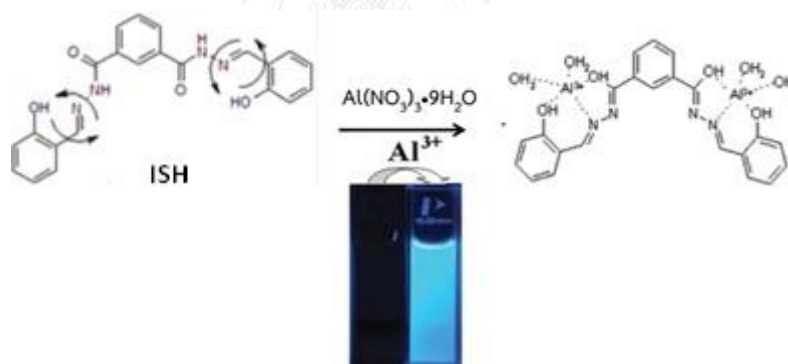


Figure 1.21 Fluorescence enhancement mechanism of ISH-Al^{3+} complex.

Liao et al. [84] synthesized a simple fluorescent turn-on chemosensor methyl pyrazinylketone benzoyl hydrazone (MPBH) by one-step Schiff base condensation. MPBH showed a high selectivity toward Al^{3+} with a turn-on fluorescence enhancement ratio over 800-fold in ethanol over other metal ions. After chelating Al^{3+} ion, the photoinduced electron-transfer (PET) process from the lone pair electrons of the Schiff base nitrogen atom was suppressed. The detection limit of MPBH for Al^{3+} was 10^{-7} M level.

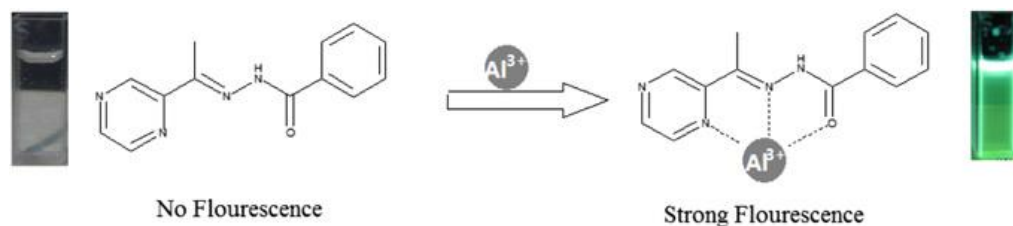


Figure 1.22 the plausible binding mode of MPBH with Al^{3+} .

In 2014, Lee et al. [85] developed a multifunctional hydrazide **HJBH** as a fluorescent sensor for Al^{3+} and colorimetric sensor for CN^- in aqueous solution (in bis-tris buffer–methanol (999/1, v/v)). Receptor **HJBH** exhibited an excellent selective fluorescence enhancement response toward Al^{3+} over other metals with the detection limit to be $0.193 \mu M$. Moreover, the sensor exhibited excellent detection ability in a broad range of pH 4–10 and also in living cells.

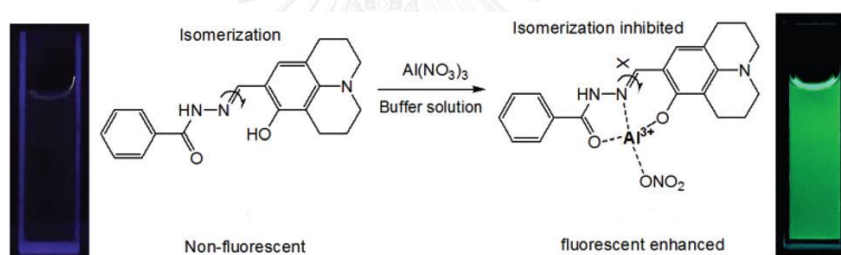


Figure 1.23 Fluorescent enhancement mechanisms of the **8**- Al^{3+} complex.

Fan et al. [86] synthesized a Schiff-base receptor 7-methoxychromone-3-carbaldehyde-(pyridylformyl) hydrazone (**MCNH**). This probe showed an “off-on-type” mode with high sensitivity toward Al^{3+} . The **MCNH**- Al^{3+} complex showed a significant green fluorescence enhancement with a turn-on ratio over 800-fold at 503 nm in EtOH. The detection limit of **MCNH** for Al^{3+} was as low as $0.19 \mu M$.

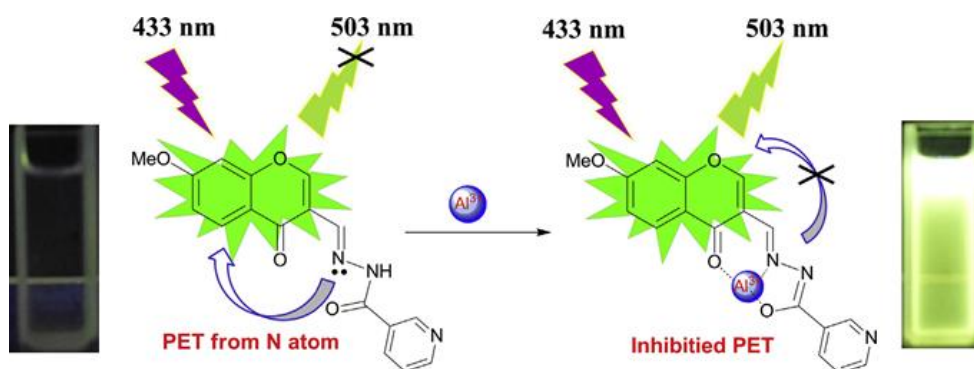


Figure 1.24 Fluorescent enhancement mechanisms of the MCNH–Al³⁺ complex.

Wang et al. [87] reported a very simple N-salicylidenehydrazide (**F1**) in which the hydrazide works synergistically with adjacent phenol group to selectively bind Al³⁺ cation in aqueous solution. The free ligand **F1** gave very weak green fluorescence (the emission $\lambda_{em} = 485$ nm, $\Phi = 0.01$), due to the PET effect from the amine and the ESIPt process. Upon addition Al³⁺ ion, the sensor exhibited bright blue fluorescence turn-on (441 nm) in aqueous solution, with its quantum efficiency reaching as high as $\Phi = 0.73$ based on suppression of non-radiative pathways. In addition, the turn-on of the sensor showed excellent selectivity to the Al³⁺ ion, with only a slight interference from Zn²⁺.

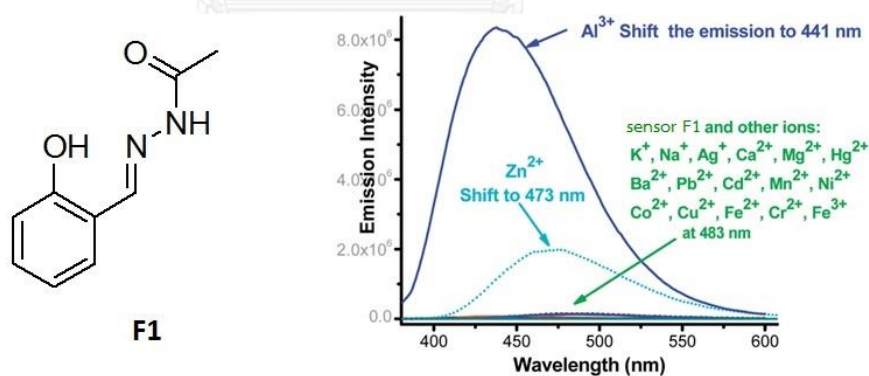
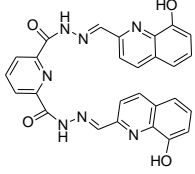
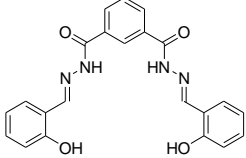
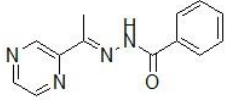
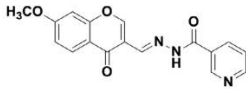
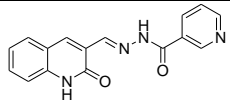
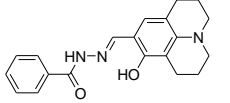
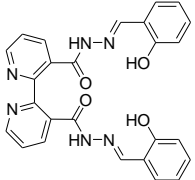
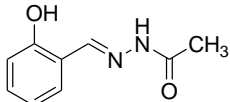


Figure 1.25 Structure of **F1** and fluorescent spectra of **F1** with 5.0 equiv. of various metal ions in pure water.

Table 1.1 Summarization of some hydrazone fluorescent chemosensors for Al³⁺ detection.

ligands	λ_{em} (nm)	Testing media	LOD	Φ of free ligand /Al ³⁺ complex	fold of I/I ₀	
	595	DMSO	1 μ M	-	50-fold	[81]
	455	50%MeOH/ H ₂ O	0.77 μ M	0.83/0.003	-	[83]
	506	Ethanol	~0.10 μ M	-	800- fold	[84]
	503	Ethanol	0.19 μ M	0.39/0.051	800- fold	[86]
	439	Ethanol	0.67 ppb	-	150- fold	[88]
	483	Bis-tris buffer	0.193 μ M	0.50/0.035	-	[85]
	466	HEPES- buffer	0.17 μ M	0.016/0.002	-	[82]
	441	H ₂ O	0.5 nM	0.73/0.01	-	[87]

From the literatures, it is thus summarized that these hydrazide ligands showed high sensitivity and sensitivity toward Al^{3+} giving remarkably fluorescence turn-on based on suppression of non-radiative pathways i.e. ESIPT and PET processes. In addition, some of them were synthesized by a facile one-step Schiff base reaction. However, most of them gave the emission color in the blue and green region with a few ligands in the orange.

In 2012, Bo et al. [89] registered a patent about the aluminium complex of furan-2-carbohydrazide (**F2**). Their studies revealed that the aluminium complex **F2**- Al^{3+} was in the enol form (form B) that could be stabilized by delocalization from the furyl ring which resulted in a limited spectral red-shifted of its photophysical properties in absorption λ_{max} (by ~ 17 nm) and λ_{em} emission (by ~ 24 nm) spectra in comparison with **F1**- Al^{3+} complex.

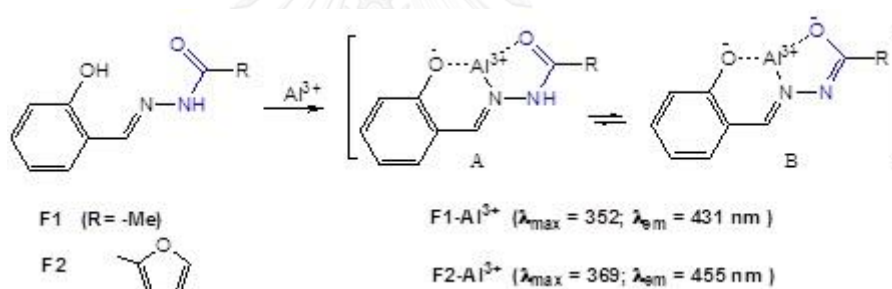


Figure 1.26 Complexation of **F1** and **F2** with Al^{3+} .

Since the *N*-salicylidenehydrazide ligands (such as **F1** and **F2**) showed both good selectivity toward Al^{3+} and large spectral response. In this work, we thus choose **F2** as a core structure for further design in shifting the blue emission to a longer wavelength.

1.5.1 Objectives of this research

The aim of this work is to develop a ligand series as Al^{3+} turn-on fluorescent sensors with large stroke shifts with three emissive colors. The inclusion of an additional hydroxyl substituent on the phenol ring to raise the HOMO level is exploited in the molecular design of compounds **F3**. Addition of the second hydrazide group on the phenol ring will further extend the π -conjugation to give **F4**. We expected the Al^{3+} complexes of **F3** and **F4** to give strong emission with notable red-shift useful for color tuning of the sensors.

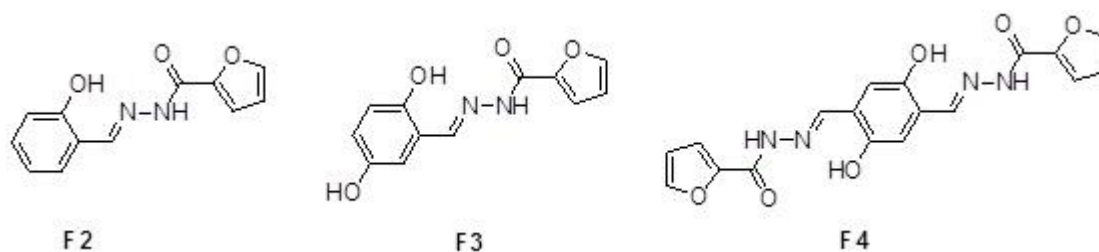


Figure 1.27 Target molecules F2-F4.



CHAPTER II

EXPERIMENT

2.1 Chemicals and materials

N,N-dimethylaniline, trimethylsilylacetylene, bis(triphenylphosphine)palladium(II)dichloride ($\text{PdCl}_2(\text{PPh}_3)_2$), sodium thiosulfate, benzyltrimethylammonium chloride, salicylaldehyde, 2,5-dihydroxybenzaldehyde, hydrazine monohydrate, Ethyl 2-furoate, potassium hydroxide, potassium carbonate, calcium carbonate, and bovine serum albumin (BSA) were purchased from Fluka (Switzerland). Triphenylamine, iodine monochloride, copper (I) iodide, 1, 8-diazabicyclo [5.4.0] undec-7-ene (DBU), 4-iodobenzoic acid and quinine sulfate were purchased from Aldrich. All other reagents were non-selectively purchased from Sigma-Aldrich, Fluka or Merck (Germany). For most reactions, solvents such as dichloromethane and acetonitrile were reagent grade stored over molecular sieves. In anhydrous reactions, solvents such as THF and toluene were dried and distilled before use according to the standard procedures. All column chromatography were operated using Merck silica gel 60 (70-230 mesh). Thin layer chromatography (TLC) was performed on silica gel plates (Merck F₂₄₅). Solvents used for extraction and chromatography such as dichloromethane, hexane, ethyl acetate and methanol were commercial grade and distilled before use while diethyl ether and chloroform were reagent grade. Milli-Q water was used in all experiments unless specified otherwise. The most reactions were carried out under positive pressure of N₂ filled in rubber balloons.

2.2 Analytical instruments

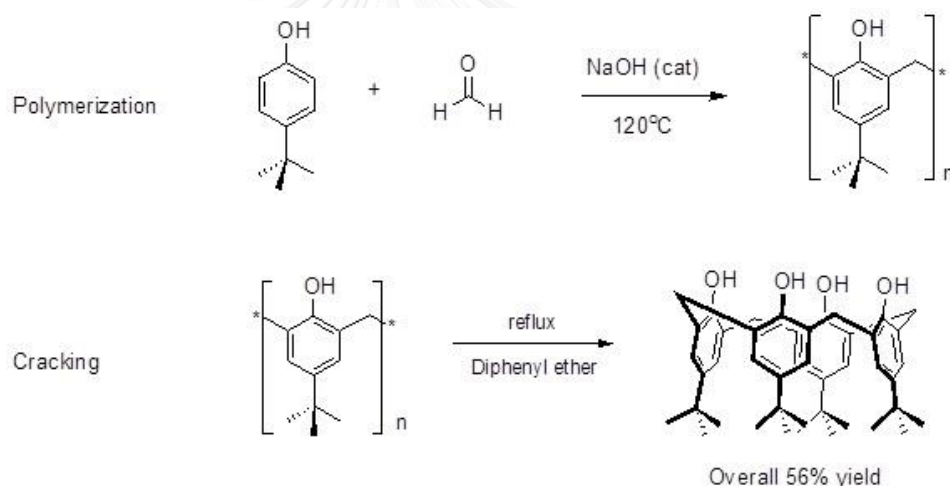
The melting points of all products were acquired from a melting point apparatus (Electrothermal 9100, Fisher Scientific, USA). Elemental (C, H, N) analyses were performed on a PE 2400 series II analyzer (Perkin-Elmer, USA). Mass spectra were recorded on a Microflex MALDI-TOF mass spectrometer (Bruker Daltonics) using doubly recrystallized α -cyano-4-hydroxy cinnamic acid (CCA) as a matrix. The HRMS spectra were measured on an electrospray ionization mass spectrometer (microTOF,

Bruker Daltonics). Fourier transform infrared spectra were acquired on Nicolet 6700 FT-IR spectrometer equipped with a mercury-cadmium telluride (MCT) detector (Nicolet, USA). $^1\text{H-NMR}$ and $^{13}\text{C-NMR}$ spectra were acquired from sample solution in CDCl_3 , acetone- d_6 , CD_3CN , CD_3OD and $\text{DMSO-}d_6$ on Varian Mercury NMR spectrometer (Varian, USA) at 400 MHz and 100 MHz, respectively. The UV-visible absorption spectra were obtained from a Varian Cary 50 UV-Vis spectrophotometer (Varian, USA) and the fluorescence emission spectra were recorded on a Varian Cary Eclipse spectrofluorometer (Varian, USA).

2.3 Synthesis of fluorophores

2.3.1 Synthesis of ANC, BAC and SAC

2.3.1.1 Preparation of *p*-tert-butyl calix[4]arene



First step: polymerisation

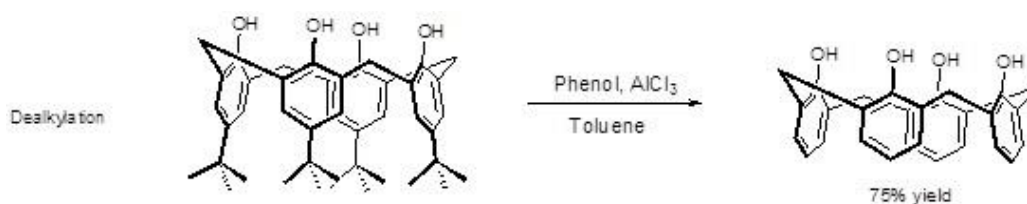
In a 1 L round-bottomed flask equipped with a magnetic stirring bar, a mixture of *p*-tert-butylphenol (25.00 g, 0.17 mol), 37% formaldehyde in ethanol (15.50 mL, 0.20 mol) and sodium hydroxide (0.30 g 7.50 mmol) was stirred and heated at 100-120°C on a heating mantle. The flask was left open to allow the water by-product to escape from the reaction mixture. The stirring and heating was continued until a colourless liquid turned into a spongy crispy yellow solid as the water evaporated. The reaction was then allowed to cool to room temperature. Overheating resulted in low yield of the desired product in the following step due to the formation of green

polymeric materials. The small amount of green polymer by-product, if formed, was disposed and only the yellow part of the precursor was brought to the next step, cracking. The precursor prepared should be used within one or two days to assure the high yield of *p-tert*-butylcalix[4]arene [90].

Second step: cracking

Two batches of the yellow polymer formed in the first step were crushed into powder. In a 2 L two-necked round-bottomed flask equipped with a magnetic stirring bar, condenser and a Dean-Stark trap, the precursor from polymerisation process (25.00 g) was stirred in diphenyl ether (250 mL). The reaction flask and the Dean-Stark side arm were wrapped with a heating jacket and cotton wool in aluminium foil in order to maintain the temperature. The mixture was refluxed on a heating mantle. The “pop” sound was produced indicating the removal of water from the reaction. When the “pop” sound was completely subsided, the reaction was allowed to cool to room temperature (around 2.5 hours). The pale brown product was precipitated out by addition of ethyl acetate (400 mL). The product was filtered and washed with 25% acetic acid in ethyl acetate (300 mL) and ethyl acetate (400 mL) yielding a white solid. The *p-tert*-butylcalix[4]arene was further purified by crystallisation in toluene giving a white crystal as a product in 56% yield.

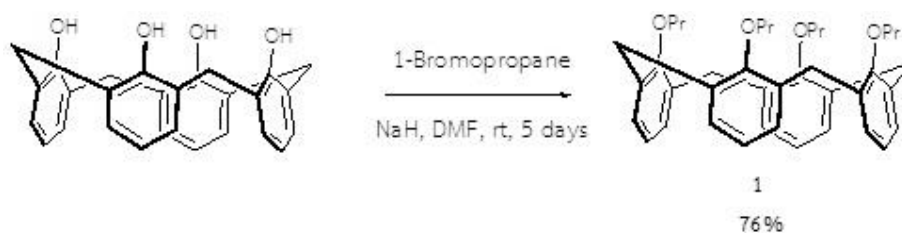
2.3.1.2 Preparation of calix[4]arene



In a 500 mL round-bottomed flask equipped with a magnetic stirring bar, a mixture of *p-tert*-butylcalix[4]arene (13.24 g, 0.02 mol), phenol (9.60 g, 0.10 mol) in anhydrous toluene (200 mL) was cooled to 0°C in an ice bath. AlCl₃ (14.00 g, 0.10 mol) was slowly added to the reaction mixture. The reaction mixture was allowed to warm to room temperature and stirred for 1 hour. HCl (3 M, 100 mL) was added to the reaction mixture at 0°C and extracted with water (2x30 mL). The organic phase was separated and dried over anhydrous Na₂SO₄. The solvent was evaporated under

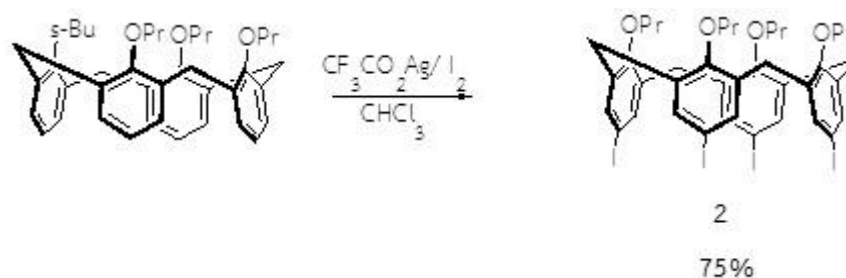
reduced pressure until the white solid was precipitated and methanol (100 mL) was poured into the residue. The product was precipitated out as a white solid. The precipitate was filtered and washed with cold toluene and methanol. The calix[4]arene was further purified by crystallization in toluene giving a white solid as a product in 75 % yield [91].

2.3.1.3 Preparation of 25,26,27,28-tetrapropoxy-calix[4]arene (**1**)



NaH (55% in oil, 1.0 g, 25 mmol) was added to a solution containing the Calix[4]arene 0.656 g (1.54 mmol) in DMF (25 ml) and then n-PrBr 80.8 mmol was added. The reaction mixture was stirred at room temperature for 5 days. Excess NaH was decomposed with methanol. The mixture was diluted with water (300 ml) and extracted with dichloromethane (100 ml x 2). The organic layer was separated and dried over anhydrous MgSO_4 . After solvent removal, the crude product was purified by column chromatography (SiO_2 , 5% EtOAc in hexanes) to give a white powder of 25,26,27,28-tetrapropoxy-calix[4]arene (**1**) [92, 93] (0.692 g, 76 % yield) ^1H NMR (400 MHz, CDCl_3): δ (ppm) 6.59 (m, 12H), 4.45 (d, $J = 13.3$ Hz, 4H), 3.84 (t, $J = 7.2$ Hz, 8H), 1.92 (q, $J = 8$ Hz, 8H), 1.56 (s, 4H), 0.99 (t, $J = 7.3$ Hz, 12H).

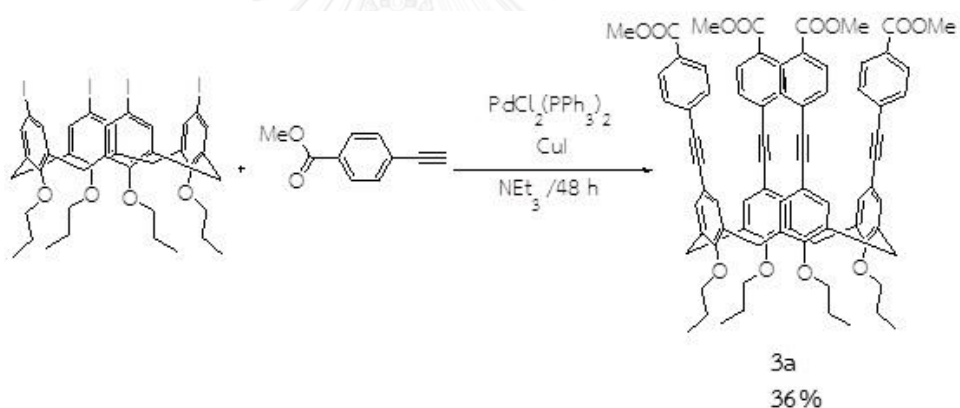
2.3.1.4 Preparation of 25,26,27,28-tetrapropoxy-4-iodocalix[4]arene (**2**)



A mixture of **1** (0.11 g, 0.14 mmol), CF_3COOAg (0.20 g, 0.91 mmol) and CHCl_3 (20 mL) was stirred and refluxed for 15 min and then the temperature was reduced

to 50-60°C and stirred for another 15 min period. Iodine (0.50 g, 1.97 mmol) was added and the stirring was continued at 50-60°C for 3 hours. The reaction mixture was allowed to cool to room temperature and filtered over Celite[®]. The filtrate was extracted with 20% aqueous NaHSO₃ (25 mL) and H₂O (25 mL). The organic phase was separated, dried over anhydrous MgSO₄, filtered and evaporated to dryness by rotary evaporator. The crude product was crystallized from CH₂Cl₂/CH₃OH yielding the desired product as a white solid of 25,26,27,28-tetrabenzoyloxy-4-iodocalix[4]arene (**2**) [94] (0.14 g, 75% yield) ¹H NMR (400 MHz, CDCl₃): δ (ppm) 6.99 (s, 8H), 4.29 (d, *J* = 13.1 Hz, 4H), 3.80 (t, *J* = 7.3 Hz, 8H), 3.05 (d, *J* = 13.5, 4H), 1.86 (q, *J* = 8.0 Hz, 8H), 1.55 (s, 8H), 0.96 (t, *J* = 7.3 Hz, 12H).

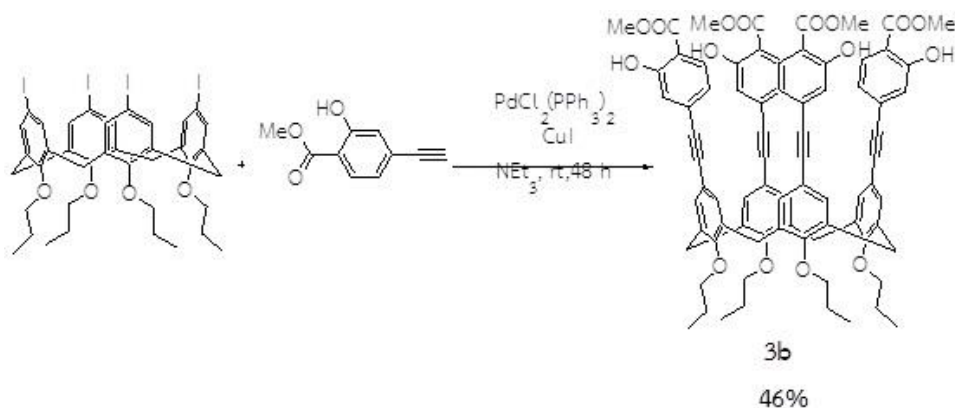
2.3.1.5 Synthesis of 5,11,17,23-Tetrakis-[(4-benzoic methyl ester)ethynyl]-25,26,27,28-tetra-(*n*-propoxy)-calix[4]arene (**3a**)



PdCl₂(PPh₃)₂ (10 mol %) and CuI (10 mol %) were added to a degassed solution of **2** (200 mg, 0.182 mmol) in dry triethylamine (40 ml) at rt and stirred for 30 min before methyl 4-ethynylbenzoate (175 mg, 1.1 mmol) was added. The mixture was stirred under nitrogen at rt for 48 h. After solvent removal, the residue was diluted with water (300 ml) and extracted with ethylacetate (100 ml x 3). The organic layer was separated and dried over anhydrous MgSO₄, filtered and evaporated. The crude product was purified by column chromatography (SiO₂, 10% CH₂Cl₂ in hexanes) to give a white powder of **3a** (80.6 mg, 36 % yield) ¹H NMR (400 MHz): δ (ppm) 7.79 (d, *J* = 8.2 Hz, 8H), 7.41 (d, *J* = 8.1 Hz, 8H), 6.95 (s, 8H), 4.44 (d, *J* = 13.4 Hz, 4H), 3.94-3.74 (m, 20H), 3.19 (d, *J* = 13.4 Hz, 4H), 1.98-1.88 (m, 8H), 1.00 (t, *J* = 7.4 Hz, 12H). ¹³C NMR

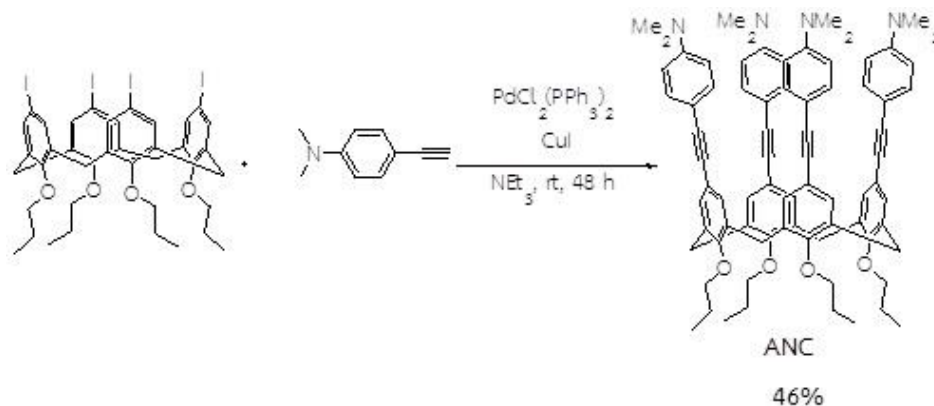
(100 MHz): δ (ppm) 166.68, 157.54, 135.06, 132.22, 131.34, 129.39, 128.96, 128.37, 116.67, 93.06, 87.80, 77.22, 52.22, 31.00, 23.36, 10.42. HRMS m/z Calcd for $C_{80}H_{72}NaO_{12}$ $[M + Na]^+$: 1247.4921 Found: 1247.4970.

2.3.1.5 Synthesis of 5,11,17,23-Tetrakis-[(4-methyl salicylate)ethynyl]-25,26,27,28-tetra-(*n*-propoxy)-calix[4]arene (**3b**)



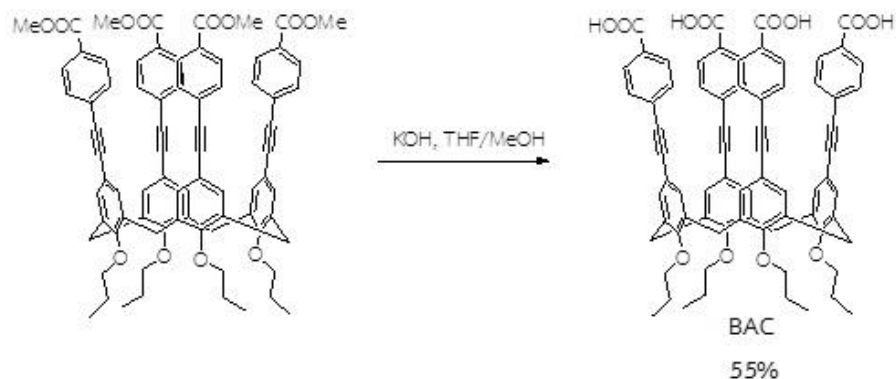
$PdCl_2(PPh_3)_2$ (10 mol %) and CuI (10 mol %) were added to a degassed solution of **2** (200 mg, 0.182 mmol) in dry triethylamine (40 ml) at rt and stirred for 30 min before 4-ethynyl-2-hydroxybenzoate (194 mg, 1.1 mmol) was added. The mixture was stirred under nitrogen at rt for 48 h. After solvent removal, the residue was diluted with water (300 ml) and extracted with ethylacetate (100 ml x 3). The organic layer was separated and dried over anhydrous $MgSO_4$, filtered and evaporated. The crude product was purified by column chromatography (SiO_2 , 10% CH_2Cl_2 in hexanes) to give a white powder of **3b** (107.6 mg, 46 % yield) 1H NMR (400 MHz): δ (ppm) 10.60 (s, 4H), 7.61 (d, $J = 8.1$ Hz, 4H), 7.05-6.84 (m, 16), 4.44 (d, $J = 13.4$ Hz, 8H), 3.92 (s, 12 H), 3.89 (t, $J = 7.5$ Hz, 8H), 3.18 (d, $J = 13.5$ Hz, 4H), 1.99-1.84 (m, 8H), 1.00 (t, $J = 7.2$ Hz, 12H). ^{13}C NMR (100 MHz): δ (ppm) 170.34, 161.16, 157.61, 135.07, 132.30, 131.07, 129.56, 122.51, 119.96, 116.58, 111.47, 93.25, 87.70, 77.16, 52.33, 30.97, 23.35, 10.41. HRMS m/z Calcd for $C_{80}H_{72}NaO_{16}$ $[M + Na]^+$: 1311.4718 Found: 1311.4684.

2.3.1.6 Synthesis of 5,11,17,23-Tetrakis-[(4-*N,N*-dimethylaminophenyl)ethynyl]-25,26,27,28-tetra-(*n*-propoxy)-calix[4]arene (**ANC**)



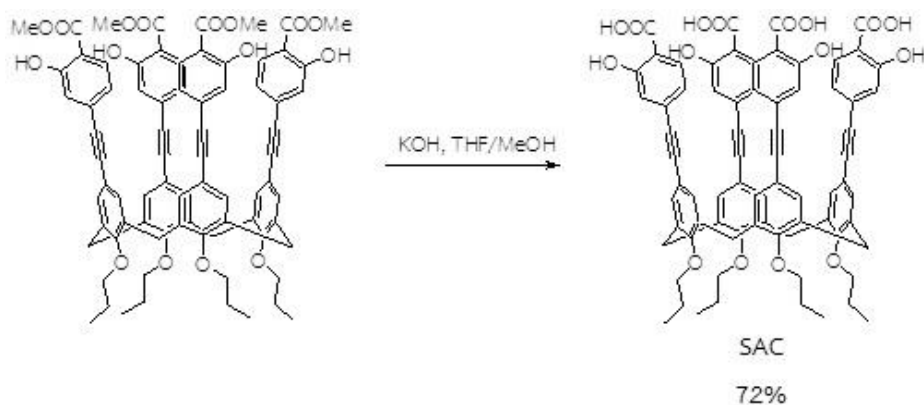
$\text{PdCl}_2(\text{PPh}_3)_2$ (10 mol %) and CuI (10 mol %) were added to a degassed solution of **2** (200 mg, 0.182 mmol) in dry triethylamine (40 ml) at rt and stirred for 30 min before 4-ethynyl-*N,N*-dimethylaniline (160 mg, 1.1 mmol) was added. The mixture was stirred under nitrogen at rt for 48 h. After solvent removal, the residue was diluted with water (300 ml) and extracted with ethylacetate (100 ml x 3). The organic layer was separated and dried over anhydrous MgSO_4 , filtered and evaporated. The crude product was purified by column chromatography (SiO_2 , 10% CH_2Cl_2 in hexanes) to give a white powder of **ANC** (107.6 mg, 46 % yield) ^1H NMR (400 MHz): δ (ppm) 7.31 (d, $J = 8.3$ Hz, 8H), 6.49 (d, $J = 8.6$ Hz, 8H), 4.40 (d, $J = 13.2$ Hz, 4H), 3.86 (t, $J = 7.5$ Hz, 8H), 3.14 (d, $J = 13.0$ Hz, 4H), 2.92 (s, 24H), 1.93 (m, 8 Hz, 8H), 0.99 (t, $J = 7.3$ Hz, 12H). ^{13}C NMR (100 MHz): δ (ppm) 156.42, 149.73, 134.66, 132.82, 131.73, 118.03, 111.94, 111.28, 89.09, 87.85, 77.06, 40.36, 31.00, 23.32, 10.45. HRMS m/z Calcd for $\text{C}_{80}\text{H}_{84}\text{N}_4\text{NaO}_4$ $[\text{M} + \text{Na}]^+$: 1187.6390 Found: 1187.6392.

2.3.1.7 Preparation of 5,11,17,23-Tetrakis-[(4-benzoic)ethynyl]-25,26,27,28-tetra-(*n*-propoxy)-calix[4]arene (**BAC**)



A mixture of **3a** (80 mg, 0.065 mmol) in THF (10 mL) and methanol (10 mL) was added with saturated KOH aqueous solution (0.5 mL) and the mixture was stirred at room temperature. After 24 h the solution was evaporated and the residue was dissolved in water (10 mL) and was added 1M HCl cool in ice-bath. The solution in suspension was centrifuge to afford **BAC** as a white solid (42 mg, 55% yield). ^1H NMR (400 MHz, CD_3OD): δ (ppm) 7.74 (d, $J = 8.2$ Hz, 2H), 7.36 (d, $J = 7.5$ Hz, 2H), 6.93 (s, 2H), 4.47 (d, $J = 13.2$ Hz, 4H), 3.93 (m, 2H), 3.24 (d, $J = 13.2$ Hz, 4H), 2.00-1.91 (m, 8H), 1.03 (t, $J = 7.4$ Hz, 12H). ^{13}C NMR (100 MHz, $(\text{CD}_3)_2\text{CO}$): δ (ppm) 167.13, 158.35, 136.12, 132.83, 131.86, 130.80, 130.33, 128.68, 117.43, 93.42, 88.16, 77.94, 31.23, 23.98, 10.57. HRMS m/z Calcd for $\text{C}_{76}\text{H}_{64}\text{O}_{12}$ [$\text{M} - \text{H}$] $^-$: 1167.4325 Found: 1167.4302.

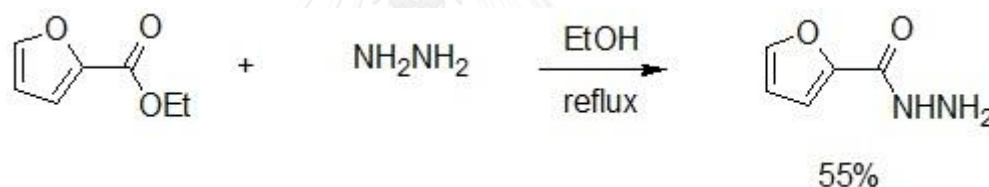
2.3.1.8 Preparation of 5,11,17,23-Tetrakis-[(4-salicylate)ethynyl]-25,26,27,28-tetra-(*n*-propoxy)-calix[4]arene (**SAC**)



A mixture of **3b** (98 mg, 0.08 mmol) in THF (10 mL) and methanol (10 mL) was added with saturated KOH aqueous solution (0.5 mL) and the mixture was stirred at room temperature. After 24 h the solution was evaporated and the residue was dissolved in water (10 mL) and was added 1M HCl cool in ice-bath. The solution in suspension was centrifuge to afford **SAC** as a white solid (67 mg, 72% yield). ^1H NMR (400 MHz, CD_3OD): δ (ppm) 7.58 (d, $J = 8.4$ Hz, 4H), 6.91 (bs, 2H), 6.80 (bs, 2H), 4.45 (d, $J = 13.6$ Hz, 4H), 3.91 (m, 8H), 3.22 (d, $J = 13.5$ Hz, 4H), 1.93 (dd, $J = 14.7, 7.5$ Hz, 8H), 1.01 (t, $J = 7.4$ Hz, 13H). ^{13}C NMR (100 MHz, CD_3OD): δ (ppm) 170.34, 161.16, 157.61, 135.07, 132.30, 131.07, 129.56, 122.51, 119.96, 116.58, 111.47, 93.25, 87.70, 52.33, 30.97, 23.35, 10.41. HRMS m/z Calcd for $\text{C}_{76}\text{H}_{64}\text{O}_{16}$ $[\text{M} - 2\text{H}]^{2-}$: 615.2019 Found: 615.2038

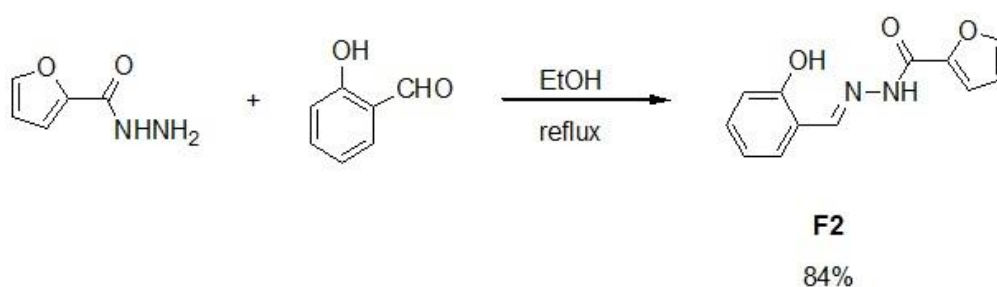
2.3.2 Synthesis of F2-F4

2.3.2.1 Preparation of 2-furoic hydrazide



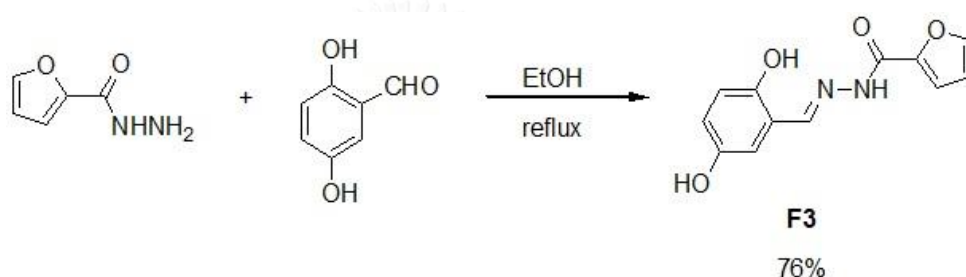
Ethyl 2-furoate 1.0 g was dissolved in EtOH (10.0 mL) and then the solution was added with hydrazine monohydrate 1 mL (excess). The mixture was refluxed for 6 hours. After that the resulting mixture was cooled to room temperature. After solvent removal, the crude product was purified by column chromatography (SiO_2 , 5%EtOAc in hexanes) to give a white solid of 2-furoic hydrazide (55% yield)

2.3.2.2 Synthesis of F2



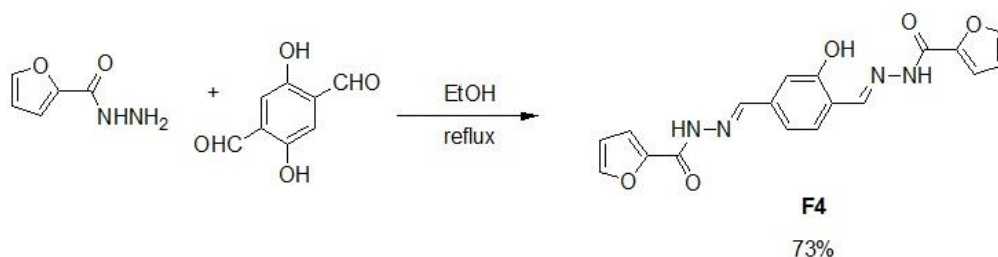
Salicylaldehyde (122 mg, 1.0 mmol) and 2-furoic hydrazide (130 mg, 1.05 mmol) were dissolved in EtOH (5 mL) and the mixture was heated to reflux for 3 hours. The resulting mixture was cooled down and the precipitate was collected by simple filtration to afford compound in 84 % as needle-like white crystal. ^1H NMR (400 MHz, DMSO): δ (ppm) 12.11 (1H, s), 11.15 (1H, s), 8.64 (1H, s), 7.97 (1H, s), 7.54 (1H, d, $J = 7.4$ Hz), 7.34-7.25 (2H, m), 6.95-6.89 (2H, m), 6.72 (1H, dd, $J = 3.5, 1.7$ Hz) ppm. ^{13}C NMR (400 MHz, DMSO): 157.3, 153.9, 148.2, 146.0, 131.4, 129.3, 119.3, 118.7, 116.4, 115.2 and 112.1 ppm.

2.3.2.3 Synthesis of **F3**



2,5-dihydroxybenzaldehyde [95] (138 mg, 1.0 mmol) and 2-furoic hydrazide (130 mg, 1.05 mmol) were dissolved in EtOH (5 mL) and the mixture was heated to reflux for 3 hours. The resulting mixture was cooled down and the precipitate was collected by simple filtration to afford compound in 76 % as a pale yellow solid. ^1H NMR (400 MHz, DMSO): δ (ppm) 11.99 (1H, s), 10.26 (1H, s), 8.98 (1H, s), 8.57 (1H, s), 7.96 (1H, s), 7.30 (1H, s), 6.97 (1H, s) and 6.75-6.70 (3H, m) ppm. ^{13}C NMR (400 MHz, DMSO): 153.9, 150.1, 149.9, 147.6, 146.4, 145.9, 118.9, 117.1, 115.0, 113.7 and 112.1 ppm. HRMS Cal. $\text{C}_{12}\text{H}_{11}\text{N}_2\text{O}_4$ 247.0719: found $\text{M}+\text{H}^+$ 247.0635; $\text{C}_{12}\text{H}_{10}\text{N}_2\text{NaO}_4$ 269.0538: found $\text{M}+\text{Na}^+$ 269.0179.

2.3.2.4 Synthesis of **F4**



2,5-dihydroxyterephthaldehyde (166 mg, 1.0 mmol) and 2-furoic hydrazide (255 mg, 2.05 mmol) were dissolved in EtOH (5 mL) and the mixture was heated to reflux for 3 hours. The resulting mixture was cooled down and the precipitate was collected by simple filtration to afford compound in 73 % as a yellow solid. ^1H NMR (500 MHz, DMSO): δ (ppm) 12.06 (1H, s), 10.25 (1H, s), 8.62 (1H, s), 7.94 (1H, s), 7.33 (1H, s), 7.22 (1H, s) and 6.72 (1H, s) ppm. ^{13}C NMR (500 MHz, DMSO): 154.5, 150.2, 146.8, 146.5, 146.3, 122.6, 115.6, 114.5 and 112.6 ppm. HRMS Cal. $\text{C}_{18}\text{H}_{15}\text{N}_4\text{O}_6$ 383.0986: found $\text{M}+\text{H}^+$ 383.1396; $\text{M}+\text{Na}^+$ $\text{C}_{18}\text{H}_{14}\text{N}_4\text{O}_6\text{Na}$ Cal. 405.0811, found 405.1244.

2.4 Photophysical property study

2.4.1 UV-Visible spectroscopy

The stock solutions of **BAC**, **SAC**, **ANC** (0.1 mM) in THF and **F1-F3** (10 mM) in DMSO were prepared. The absorption spectra of all fluorophores were recorded from 250 nm to 600 nm at ambient temperature.

2.4.1.1. Molar Absorption Coefficients (ϵ)

Molar Absorption Coefficients (ϵ) of all fluorophores were estimated from UV absorption spectra of analytical samples in THF for the sensors base on calix[4]arene derivatives and in DMSO for the hydrazide sensors at various concentrations. The intensities at absorption maximum wavelength (λ_{max}) of each compound were plotted against the concentrations. Each plot should be a straight line goes through origin. Molar Absorption Coefficients (ϵ) can be obtained from plotting of maximum absorption (A) vs concentration (C) represented into the following equation:

$$A = \epsilon b C$$

*b is the cell path length.

2.4.2 Fluorescence spectroscopy

The stock solutions of **BAC**, **SAC** and **ANC** were dilute to 1 μM in 1% THF/ H_2O . While, those of **F2-F4** were dilute to 10 μM in 0.1% DMSO/ H_2O . The emission spectra of fluorophores were recorded from 350 nm to 700 nm at ambient temperature using an excitation wavelength at 300 to 468 nm.

2.4.3 Fluorophore quantum yields

The fluorescence quantum yields of **BAC**, **SAC** and **ANC** were performed in THF, while, those of **F2-F4** and their Al complexes were performed in 0.1% DMSO/H₂O. Each sample used quinine sulphate ($\Phi_{ST} = 0.54$; λ_{ex} 336 nm) in 0.5 M H₂SO₄ or fluorescein ($\Phi_{ST} = 0.95$; λ_{ex} 496 nm) in 0.1 M NaOH as a reference [96]. The UV-Vis absorption spectra of five analytical samples and five reference samples at varied concentrations were recorded. The maximum absorbance of all samples should never exceed 0.1. The fluorescence emission spectra of the same solution using appropriate excitation wavelengths selected were recorded based on the absorption maximum wavelength (λ_{max}) of each compound. Graphs of integrated fluorescence intensities were plotted against the absorbance at the respective excitation wavelengths. Each plot should be a straight line with 0 interception and gradient m .

In addition, the fluorescence quantum yield (Φ_x) was obtained from plotting of integrated fluorescence intensity vs absorbance represented into the following equation:

$$\Phi_x = \Phi_{ST} \left(\frac{\text{Grad}_x}{\text{Grad}_{ST}} \right) \left(\frac{\eta_x^2}{\eta_{ST}^2} \right)$$

The subscripts Φ_{ST} denote the fluorescence quantum yield of a standard reference Φ_x is the fluorescence quantum yield of sample and η is the refractive index of the solvent.

2.5 Electrochemical measurements

Cyclic voltammetry (CV) experiments were carried out in a three-electrode system consisting of Ag/Ag⁺ (0.01 M AgNO₃) as the reference electrode, glassy carbon as the working electrode and the platinum-wire as the counter electrode using a scan rate of 50 mV/s under nitrogen atmosphere to find HOMO levels of the fluorophores. The ferrocene was used as external standard for calibration CV curves. Fluorophores **BAC**, **SAC**, **ANC** and the external standard were dissolved in the

supporting electrolyte (0.1 M of tetra-n-butylammonium hexafluorophosphate in anhydrous dimethylformamide) to give final concentrations of 1 mM.

The HOMO energy levels of the fluorophores were calculated from cyclic voltammetry using the equations:

$$E_{\text{HOMO}} = -[E_{\text{ox}} - E_{1/2} + 4.8] \text{ eV} \quad (1)$$

Where E_{ox} is the onset oxidation potential, $E_{1/2}$ is the average of the anodic and cathodic peak potentials. The LUMO energy levels were calculated according to the equation:

$$E_{\text{LUMO}} = E_{\text{HOMO}} + E_{\text{gap}} \quad (2)$$

The energy gaps (E_{gap}) were determined by using the onset of the longest wavelength absorption ($\lambda_{\text{cut off}}$) following equation:

$$E_{\text{gap}} = \frac{1240}{\lambda_{\text{cut off}}} \quad (3)$$

2.6 Fluorescent sensor study

2.6.1 Calix[4]arene-based fluorescence sensors (BAC, SAC and ANC) for nitroaromatic explosives

2.6.1.1 Selectivity study

All nitroaromatic compound and various electron deficient aromatic compounds such as 2,4,6-trinitrotoluene (TNT), 2,4-dinitrotoluene (DNT), picric acid (PA), 2,4-dinitrophenol (DNP), 2-nitrophenol (2-NP), 3-nitrophenol (3-NP), 4-nitrophenol (4-NP), 4-nitrobenzoic acid (4-NBA), benzoic acid (BA), and 2-chlorobenzoic acid (2-ClBA) were prepared in Milli-Q water and adjusted to 500 μM . The stock solution of the sensing compound in THF (50 μM , 10 μL) was diluted with Milli-Q water (900 μL) in a 1 mL quartz cuvette. 100 μL of various nitroaromatic and electron deficient aromatic compounds (500 μM) was separately added into the sensor solutions at the ratio 1:100 of fluorophore to analyte. The final volumes were adjusted to 1 mL by adding Milli-Q water. The final concentration of each

fluorophore is 0.5 μM in 1%THF/H₂O. The emission spectra of all sensors were recorded from 325 nm to 700 nm at ambient temperature using an excitation wavelength at 300-315 nm.

2.6.1.2 Fluorescence titration

The stock solution of the sensing compound in THF (50 μM , 10 μL) was diluted with Milli-Q water (900 μL) in a 1 mL quartz cuvette. Designated volumes (0-100 μL) of the nitroaromatic stock solution (10 mM) in Milli-Q water was added into the sensor solution. The final volumes were adjusted to 1 mL by adding Milli-Q water. The final concentration of each fluorophore is 0.5 μM in 1%THF/H₂O. The emission spectra of all sensors were recorded from 325 nm to 700 nm at ambient temperature using an excitation wavelength at 300-315 nm.

2.6.1.3 The Stern-Volmer plot

The efficiency of fluorescent quenching in solutions of quencher toward sensor is measured in terms of the Stern—Volmer constants. The quantity of quencher is estimated with the Stern-Volmer equation (4).

$$I_0/I = 1 + K_{sv}[Q] \quad (4)$$

In equation (4), the quencher concentration is [Q], the Stern-Volmer constant is K_{sv} , I_0 is the fluorescent intensity of the blank sample (sensor in the absence of quencher), I is the observed fluorescent intensity with [Q] present. After plotting (I_0/I) against [Q], the resulting graph will have an intercept of 1 and the slope can be determined to give the value of K_{sv} . Example of the Stern-Volmer plot is shown in Figure 2.1.

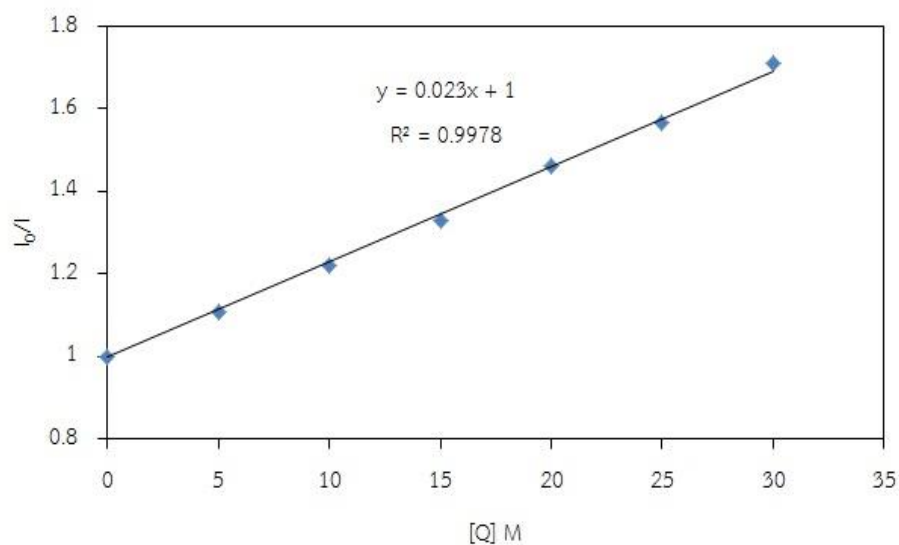


Figure 2.1 the Stern-Volmer plot.

2.6.1.4 Preparation of *ANC* fluorescence paper strips

A filter paper strip (Whatman No. 1, 4 cm x 1.1 cm²) was immersed in a CH₂Cl₂ solution of ANC 1 mM for 1 min. After removal from the solution, the coated filter paper was allowed to dry in the air at room temperature for 2 hours.

For the TNT vapor sensing, 0.50 g of TNT solid was placed in a 1 mL Eppendorf, covered with cotton gauze and cap-closed overnight to maintain a constant saturation vapor pressure before placed a fluorescent paper strip on top of the cotton in the Eppendorf and then cap-closed again for 5 and 10 minutes. The quenching results were recorded by a commercial digital camera.

For contact mode test, the glove-wearing thumb, rubbed with TNT was pressed on a fluorescent paper strip for 1 minute. The quenching results were recorded by a commercial digital camera.

2.6.2 Hydrazide-based fluorescent sensors for Al³⁺

2.6.2.1 Selectivity study

The stock solutions 10 mM of the fluorophores **F2-F4** were prepared in dimethyl sulfoxide (DMSO). All metal ion solutions were prepared in Milli-Q water and adjusted to 10 mM. The stock solutions of the fluorophore and analyte were mixed and diluted to the designated concentrations in 10 mM HEPES (pH 5.5). The

final volumes of the mixtures were adjusted to 1 mL to afford concentration of 10 μM for the fluorophores and 100 μM for metal ions at the ratio 1:10 in 0.1%DMSO/HEPES aqueous solution. The spectra were recorded after mixing for 10 minutes (sensor **F2** and **F3**) and for 30 minutes (sensor **F4**) using $\lambda_{\text{ex}} = 369, 410$ and 468 nm, respectively.

2.6.2.2 Fluorescence titration

The stock solution of the sensing compound in DMSO (10 mM, 1 μL) was diluted with HEPES buffer pH 5.5 (10 mM, 900 μL) in a 1 mL quartz cuvette. Designated volumes (0-100 μL) of the Al^{3+} stock solution (10 mM) in the HEPES buffer was added into the sensor solution. The final volumes were adjusted to 1 mL by adding the solution of HEPES buffer. The final concentration of each fluorophore is 10 μM in 0.1% DMSO/HEPES aqueous solution. The spectra were recorded after mixing for 10 minutes (sensor **F2** and **F3**) and for 30 minutes (sensor **F4**) using $\lambda_{\text{ex}} = 369, 410$ and 468 nm, respectively.

2.6.2.3 Binding constant of the Al^{3+} complexation

The binding constant of the Al^{3+} complexation with each ligand has been determined using the Benesi-Hildebrand plot [97-99] by using emission change. The Benesi-Hildebrand equation is $1/(I - I_0) = 1/(I_{\text{max}} - I_0) + (1/K[C]^n) \times (1/(I_{\text{max}} - I_0))$, where I_0 , I , and I_{max} are the emission intensities of each ligand in the absence of Al^{3+} , at an intermediate Al^{3+} concentration, and at a concentration of the complete interaction, respectively. K is the binding constant, C is the concentration of Al^{3+} and n is the number of Al^{3+} ions bound to each fluorophore (here $n = 1$). The association constant (K_a) could be determined from the slope of the straight line of the plot of $1/(I - I_0)$ against $1/[\text{Al}^{3+}]^n$ as shown in figure 3.24. K_a was calculated following the equation stated below.

$$K_a = \frac{\text{intercept}}{\text{slope}}$$

2.6.2.4 Competition with other metal ions

The mixture of each hydrazide sensors/ Al^{3+} /other metal ions in concentration of 10/100/100 μM with ratio 1/10/10 were used to investigate the interference of other metal ions to Al^{3+} binding with sensors.

2.6.3 Limit of detection

In fluorescent sensing, limit of detection (LOD) is the lowest concentration of analyte in a sample that is required to produce a signal greater than three times the standard deviation of the a blank sample. But the value is not necessarily quantitated as an exact value.

2.6.3.1 Limit of detection for turn-off sensing

For turn-off sensing, the limit of detection can be calculated according to the equation (5) and the Stern-Volmer equation (4). SD is the standard deviation of the response deriving from intensity of a fluorophore in the absence of an analyte ($n = 9$). I_0 is the fluorescent intensity of the blank sample (sensor in the absence of quencher), I is the observed fluorescent intensity with $[Q]$ present. The Stern-Volmer constant K_{sv} is determined from the slope of the Stern-Volmer plot as shown example in figure 2.1.

$$\text{LOD} = [I_0/(I_0 - 3SD) - 1]/K_{sv} \quad (5)$$

2.6.3.2 Limit of detection for turn-on sensing

For turn-on sensing, the limit of detection can be calculated according to the equation (6):

$$\text{LOD} = [(I_0 + 3SD)/I_0 - \text{Intercept}]/K \quad (6)$$

The variables were similar to those in turn-on sensing. Except K is the slope of the straight line of the plot of I/I_0 against the concentration of an analyte $[A]$. Example of the calibration curve is shown in Figure 2.2.

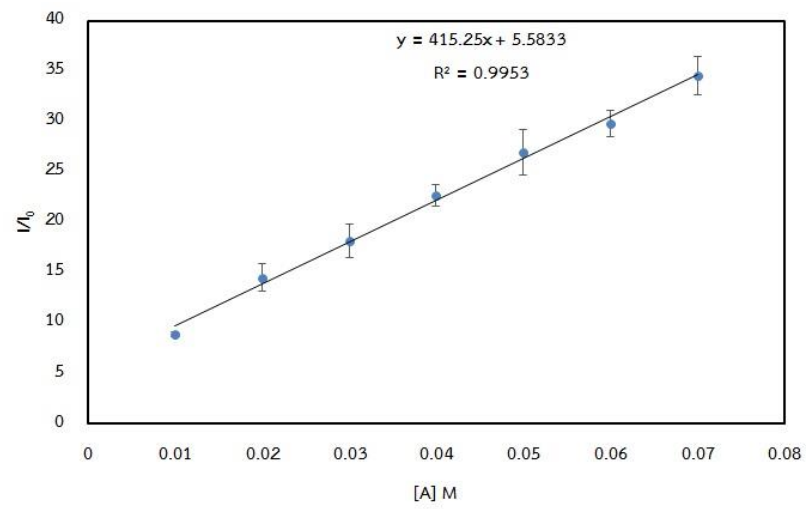


Figure 2.2 the calibration curve for turn-on sensing.



CHAPTER III

RESULTS AND DISCUSSION

3.1 Fluorescent phenylethynylene calix[4]arenes (Part A)

3.1.1 Synthesis and characterization of SAC, BAC and ANC

The phenylethynylene calix[4]arenes **SAC**, **BAC** and **ANC** were synthesized from calix[4]arene as shown in Figure 3.1. First, In order to fix calix[4]arene in cone conformation, four propyl groups were installed onto the narrow rim of the calix[4]arene. Tetrapropyloxy-calix[4]arene (**1**) was prepared in 76% yield from O-alkylation on the phenolic oxygen of calix[4]arene with propyl bromide. Then, the iodination of **1** at the para-position by using $\text{CF}_3\text{CO}_2\text{Ag}/\text{I}_2$ in CHCl_3 gave the corresponding tetraiodocalix[4]arene (**2**) in 75% yield. The key step was a Sonogashira copper-palladium catalyzed cross-coupling reaction between **2** and the ethynylbenzene derivative (i.e. methyl 4-ethynylbenzoate or methyl 4-ethynylsalicylate or N,N-dimethyl 4-ethynylaniline) to give **3a**, **3b**, and **ANC** in 36-46% yield. The base-catalyzed hydrolysis of ester **3a** and **3b** readily gave **BAC** and **SAC**, respectively in 55-72% yield.

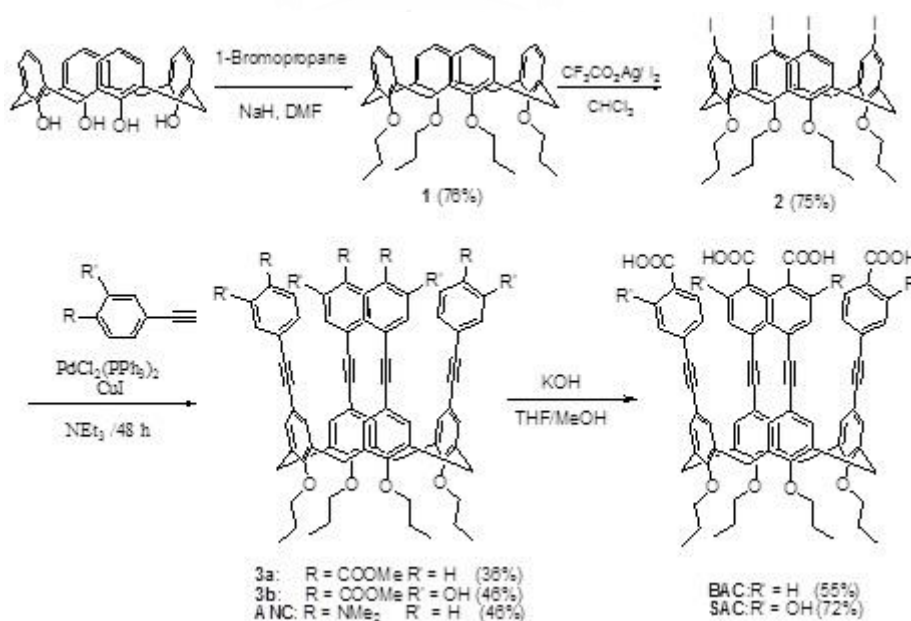


Figure 3.1 Synthesis route of fluorophores **BAC**, **SAC** and **ANC**.

The ^1H NMR spectra of compound **1** and **2** in CDCl_3 are shown in Figure 3.2. All the signals can be assigned to all the protons in each corresponding structure. The methylene bridge protons (ArCH_2Ar , $\text{H}_{\text{c-exo}}$ and $\text{H}_{\text{c-endo}}$) of calix[4]arene appeared as two doublets signals at 4.5 and 3.5 ppm that are characteristic for the cone conformation. After iodination of **1**, the multiplet signals of calix[4]arene phenyl ring around 6.59 was completely changed to a singlet peak at 6.99 ppm indicating a full iodination of the para position of all four phenyl rings of calix[4]arene.

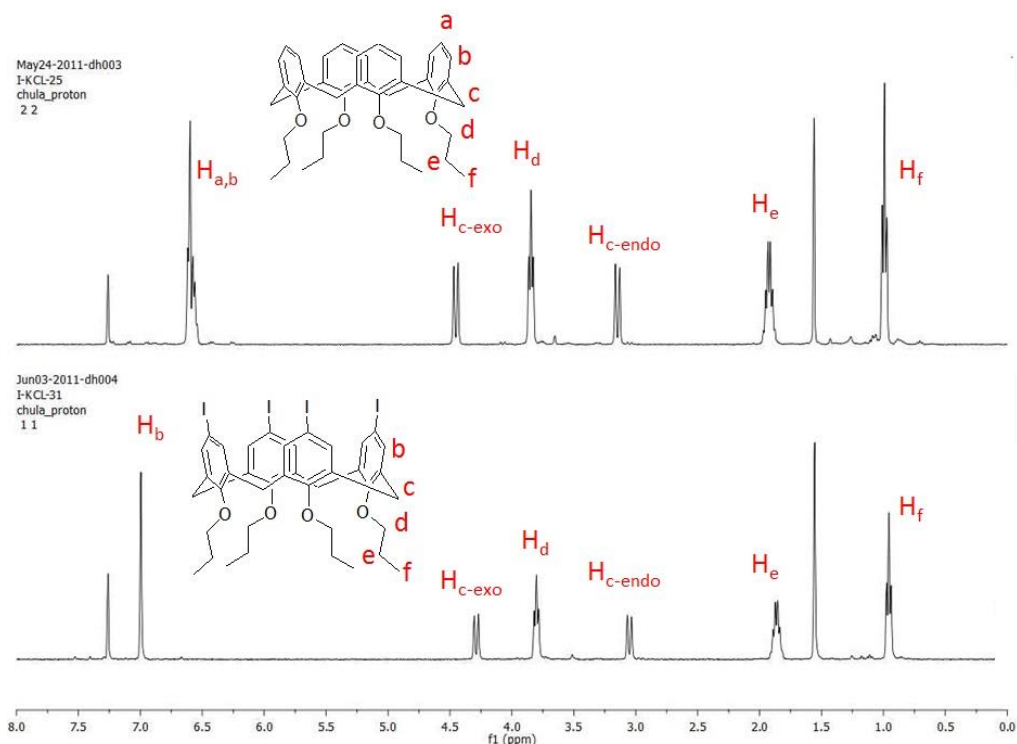


Figure 3.2 ^1H NMR spectra of compounds **1** and **2**.

The Sonogashira coupling of **2** with ethynylbenzene derivative (i.e. methyl 4-ethynylbenzoate or methyl 4-ethynylsalicylate or *N,N*-dimethyl 4-ethynylaniline) gave **3a**, **3b**, and **ANC**. In coupling products, the aromatic and methylene bridge protons of calix[4]arene ring did not have change to down-field and up-field shift, respectively (Figure. 3.3). Compound **3a** showed signal of methyl ester protons as a singlet at 3.90 ppm overlapping with OCH_2 of propyl and two new doublet signals at 7.42 and 7.89 ppm corresponding to the aromatic protons of *p*-substituted benzoate moieties. Compound **3b**, like compound **2** showed singlet signal of methyl ester protons around 3.90 ppm and also showed multiplet signal at 6.93 of aromatic protons of

salicylate moieties and singlet signal of OH at 10.61 ppm. In case of **ANC**, the aromatic protons of N,N dimethyl aniline appeared two doublet signals at 6.50 and 7.29 ppm and the methyl proton showed singlet signal at 2.92.

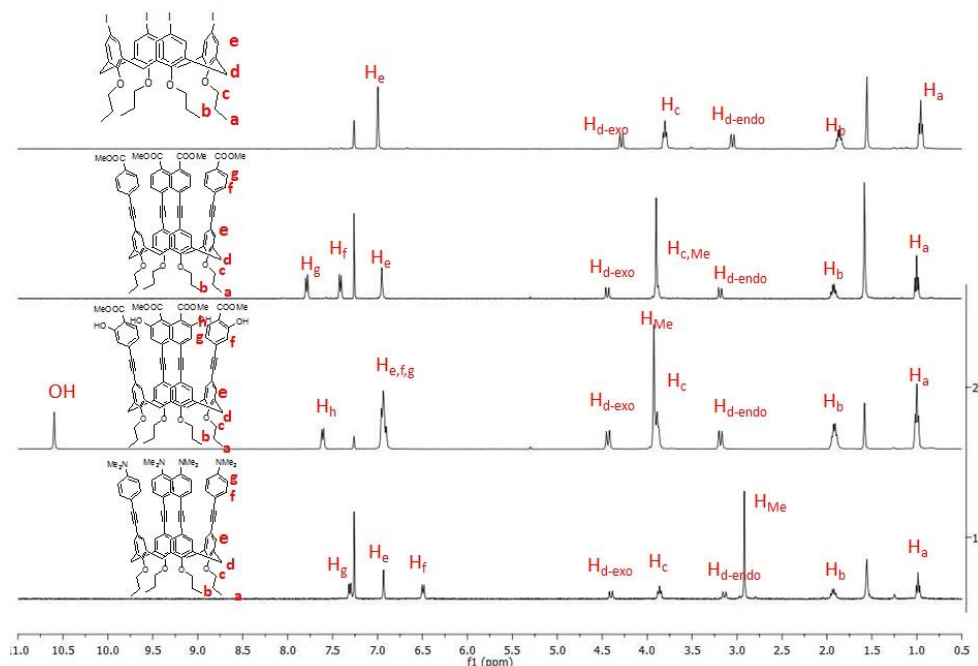


Figure 3.3 ^1H NMR spectra of compound **3a**, **3b** and **ANC**.

The ^1H NMR spectrum of **BAC** and **SAC** are shown in Figure 3.4. After base hydrolysis, the complete conversion from the methyl ester **3** to tetracarboxylic acid **BAC** and **SAC** was confirmed by the total disappearance of the methyl ester proton signal around 3.90 ppm. Moreover, the molecular weights of each fluorophore were confirmed by HRMS that are included in the experimental section at the end of each corresponding synthetic procedure.

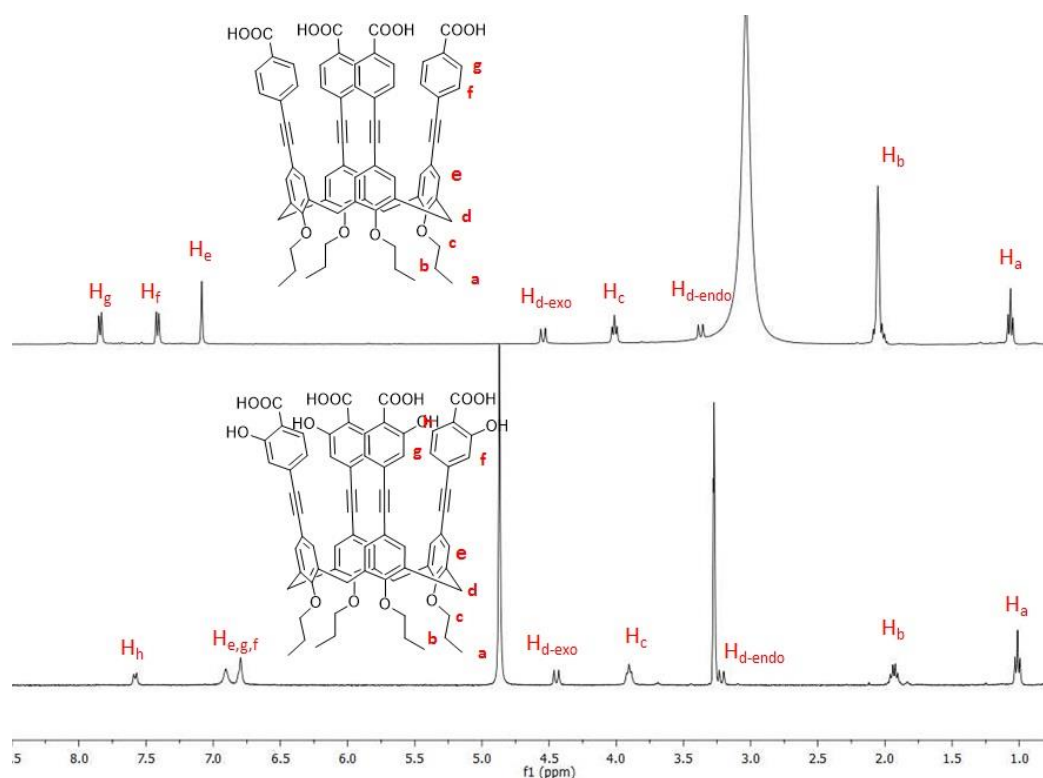


Figure 3.4 ^1H NMR spectra of compounds of BAC and SAC

3.1.2 Photophysical properties of BAC, SAC and ANC

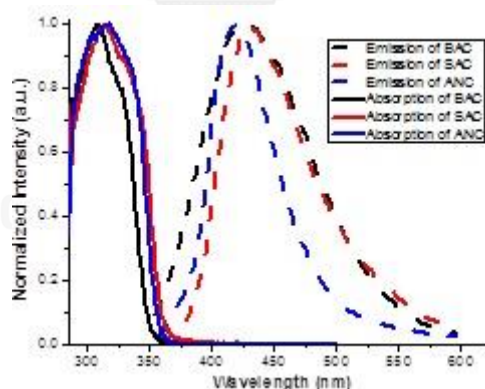


Figure 3.5 Electronic absorption and emission spectra of fluorophores in THF.

The absorption and emission of fluorophores were studied in THF. The photophysical properties are presented in Figure 3.5 and table 3.1. Each fluorophore showed a broad absorption band with λ_{max} around 310-315 nm corresponding to π - π^* electronic transitions of the substituted diphenylacetylene conjugated system with molar extinction coefficients of $9.7 \times 10^4 - 1.2 \times 10^5 \text{ M}^{-1} \text{ cm}^{-1}$. The maximum emission wavelengths of the fluorophores were in the range of 420 to 433 nm. **BAC**

and **SAC** have larger Stokes shifts comparing with that of **ANC**. These results may be because the fact that **SAC** and **BAC** possessed both electron donor and electron acceptor substituents allowing for an intramolecular charge transfer (ICT). Their fluorescent quantum yields (Φ_F) were in range of 5-10% in THF.

Table 3.1 Photophysical properties of the fluorophores.

Compound	Absorption		Fluorescence	
	λ_{\max} (nm)	ϵ ($M^{-1} cm^{-1}$)	λ_{\max} (nm)	Φ (%)
BAC	310	9.80×10^4	433	10.0
SAC	314	9.76×10^4	433	5.0
ANC	315	1.18×10^5	421	7.0

3.1.3 Electronic energy levels of the fluorophore

The onset oxidation appeared at -0.21 V, 0.24 V and 0.20 V which mean HOMO levels at -5.82 eV (for **BAC**; $E_{\text{half}} = 0.42$ V), -5.03 (for **SAC**; $E_{\text{half}} = 0.01$ V) and -4.99 (for **ANC**; $E_{\text{half}} = 0.01$ V) calculated from equation (1). The energy gaps were estimated to be 3.55 (for **BAC**), 3.44 (for **SAC**) and 3.48 (for **ANC**) eV from the onset of UV absorption spectra (Figure 3.6). Therefore, LUMO energy levels were calculated to be -2.27 (for **BAC**), -1.59 (for **SAC**) and -1.51 (for **ANC**). The HOMO and LUMO electronic energy levels of the fluorophores were summarized in Figure 3.7. Their LUMO energy levels in the range of -1.51 to -2.27 eV are higher than those of TNT, DNT and PA, which allow for an electron transfer from the excited fluorophores to TNT, DNT and PA in the PET process.

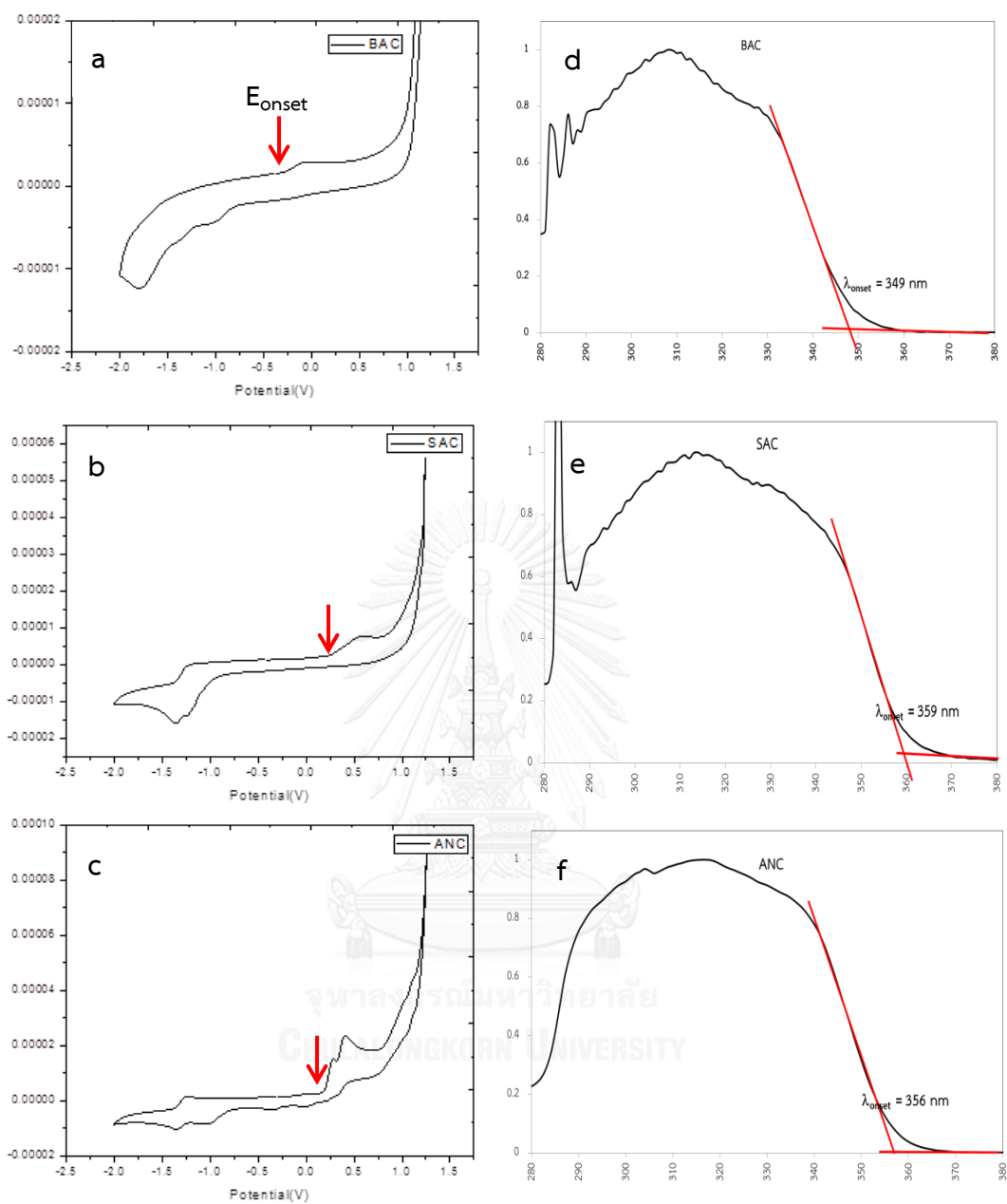


Figure 3.6 Cyclic voltammogram of (a) BAC (b) SAC (c) ANC in 0.1 M Bu_4NPF_6 dimethylformamide. Absorption spectra of (d) BAC (e) SAC (f) ANC.

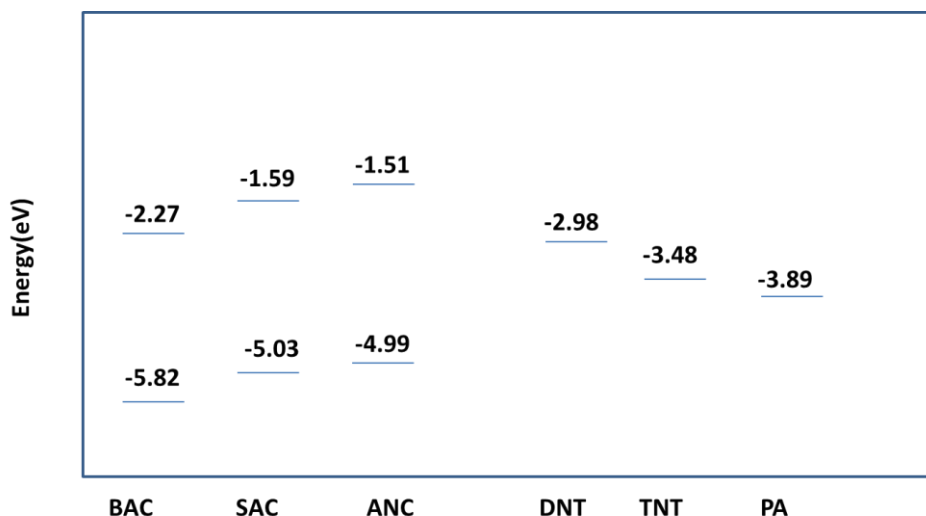


Figure 3.7 HOMO and LUMO energy levels calculated for **BAC**, **SAC**, **ANC**, and some explosive analytes such as **DNT**, **TNT**, and **PA**.

3.1.4 Fluorescence Quenching Studies with NACs in Aqueous solution.

The fluorescence responses of all fluorophores towards various electron deficient aromatic compounds such as (2,4,6-trinitrotoluene (TNT), 2,4-dinitrotoluene (DNT), picric acid (PA), 2,4-dinitrophenol (DNP), 2-nitrophenol (2-NP), 3-nitrophenol (3-NP), 4-nitrophenol (4-NP), 4-nitrobenzoic acid (4-NBA), benzoic acid (BA), 2-chlorobenzoic acid (2-ClBA)) were primarily evaluated in aqueous solutions (1% THF). As shown in figure 3.8, **ANC** showed high sensitivity toward the detection of TNT and DNT. On the other hand, the fluorescence emissions of **BAC** and **SAC** were quenched by about 2 times or less by the electron deficient aromatic compounds. For **ANC**, the quenching effect of nitrophenol compounds was also much lesser than nitrotoluene compounds in aqueous solution as designed due to the more hydrophilicity of nitrophenols. The quenching is consistent with the nonradiative PET from the LUMO energy level of the electron rich of a fluorophore in its excited state to the LUMO of the electron poor nitroaromatic compounds. **ANC** showed good selectivity for TNT over DNT as the results of the more suitable matching of the LUMO energy of TNT with that of ANC and the higher reduction potential of TNT (-0.7 V) than those of DNT (-0.9 V). In other words, the electron donating amino groups on the phenyl ring on **ANC** enhances the sensitivity toward TNT comparing

with **BAC** and **SAC**. The results imply that TNT molecule interacts with the phenyl rings on the wider rim of the fluorophore.

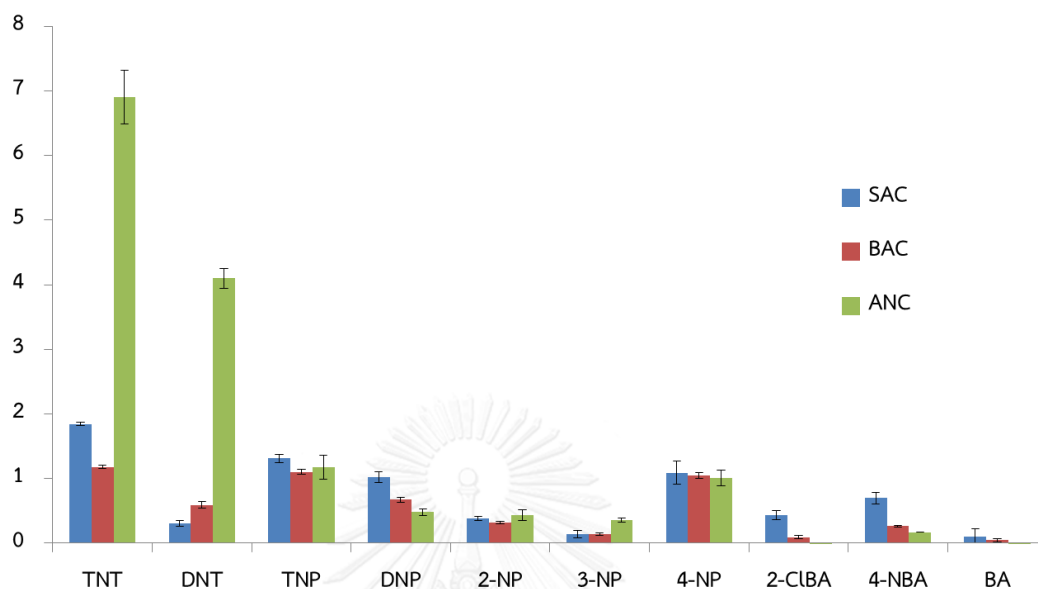


Figure 3.8 Fluorescence quenching effect of various electron deficient aromatic compounds (50 μM) on the fluorophores (0.5 μM) in 1%THF/H₂O

3.1.5 Fluorescence titration

In order to access a quantitative measurement of fluorescence quenching, Stern Volmer plots of TNT, DNT and PA were performed by fluorescence titrations as shown in Figure 3.9. The Stern-Volmer equation was used to evaluate the differences in quenching efficiencies for various analytes. The Stern–volmer equation is $I_0/I - 1 = K_{sv}[Q]$, where I_0 and I are the fluorescence intensities in the absence and presence of quencher, respectively, $[Q]$ is the quencher concentration, K_{sv} is the Stern–volmer constant. The Stern–volmer constant of **ANC** to TNT was found to be $1.09 \times 10^5 \text{ M}^{-1}$ with the detection limit of 0.3 μM (68 ppb) which is lower than TNT level typically found in ground water and soil sites near munitions plants (LOD = $3\text{std}/K$; std is the standard deviation of the blank measurements and K is the slope of the calibration curve). While, a linear relationship was also observed for DNT and PA with K_{sv} constants of $5.97 \times 10^4 \text{ M}^{-1}$ and $2.09 \times 10^4 \text{ M}^{-1}$ respectively.

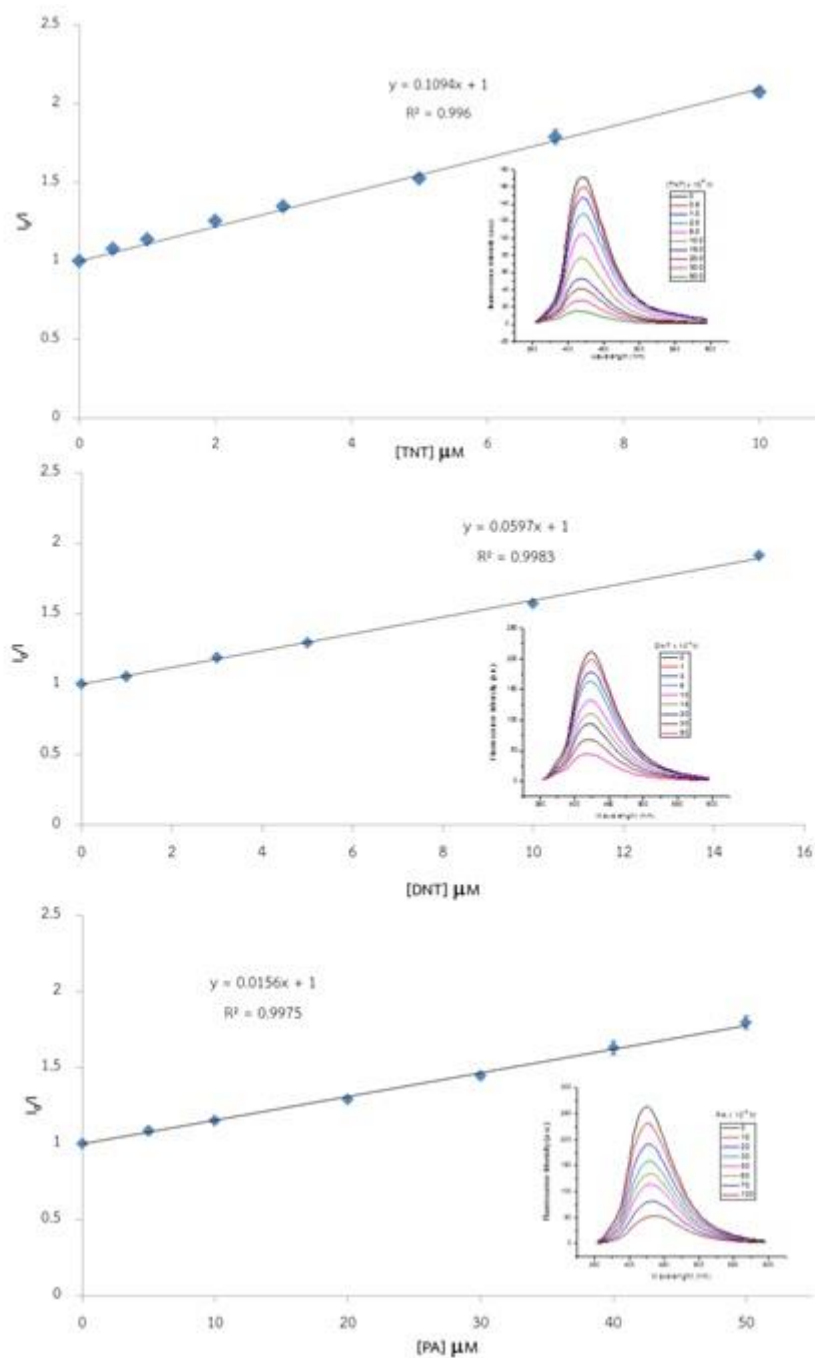


Figure 3.9 Stern-Volmer plots of **ANC** for TNT, DNT and PA. Inset: The fluorescence quenching ratio of **ANC** upon the addition of TNT, DNT and PA.

3.1.6 Quenching mechanism

The interaction between **ANC** and TNT was confirmed by ^1H NMR titration as shown in Figure 3.10. Upon increasing amount of TNT added to **ANC** solution, the aromatic proton signals (b and c) of the phenyl ring at the wider rim gradually upfield

shifted, whereas aromatic proton signals at the narrower rim did not show significant shifts confirming the interaction of TNT with the aniline rings at the extended wider rim of calix[4]arene, probably via an insertion into the **ANC** cavity. The interaction between TNT and **ANC** was proposed in Figure 3.11. On the basis of Job plot, the complex ratio between **ANC** and TNT obtained from emission data showed 1:1 stoichiometric complexation as shown in Figure 3.12.

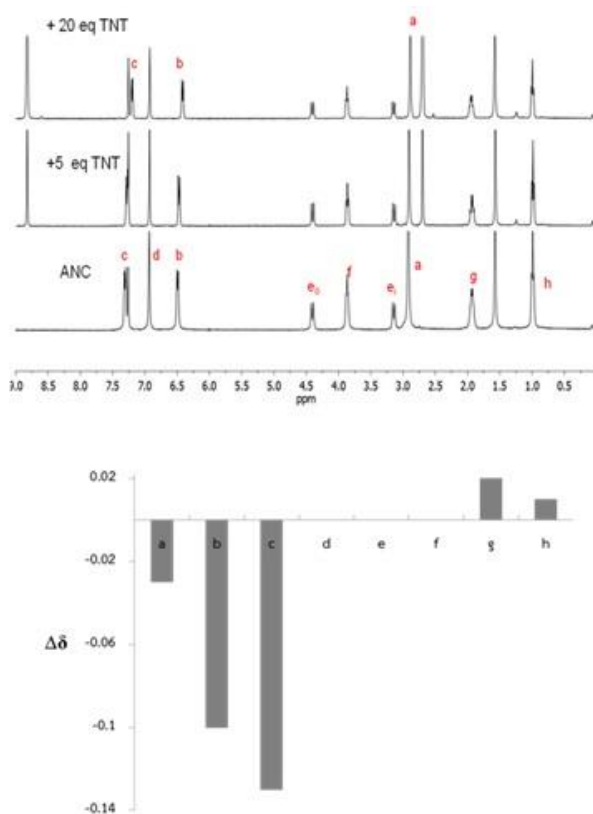


Figure 3.10 ¹H NMR of **ANC** in CDCl₃ in the absence and presence of TNT (top). Chemical shift change ($\Delta\delta$) plot (bottom).



Figure 3.11 Proposed structure of **ANC**-TNT interaction.

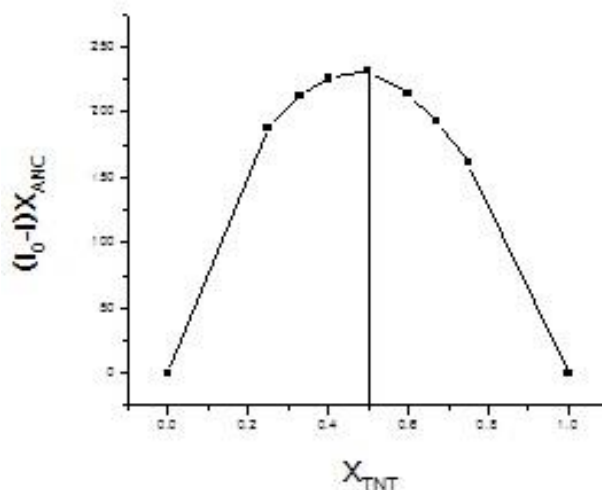


Figure 3.12 Job's plot of fluorescence responses of ANC upon addition of TNT showing 1:1 stoichiometry.

In typical, there are two basic mechanisms of quenching: dynamic (collisional) and static quenching. Both types require molecular contact between the fluorophore and quencher. For dynamic quenching, this contact can be due to diffusive encounters. For static quenching, a ground-state nonfluorescent complex is formed between the fluorophore and the quencher. To investigate quenching mechanism, linear K_{sv} plots of TNT were carried out at two different temperatures. Figure 3.13 shows Stern-Volmer plots at 25 and 50 °C with the K_{sv} values of $1.09 \times 10^5 \text{ M}^{-1}$ and $5.08 \times 10^4 \text{ M}^{-1}$, respectively. The decrease in K_{sv} values with the increase in temperature supports a static quenching mechanism.

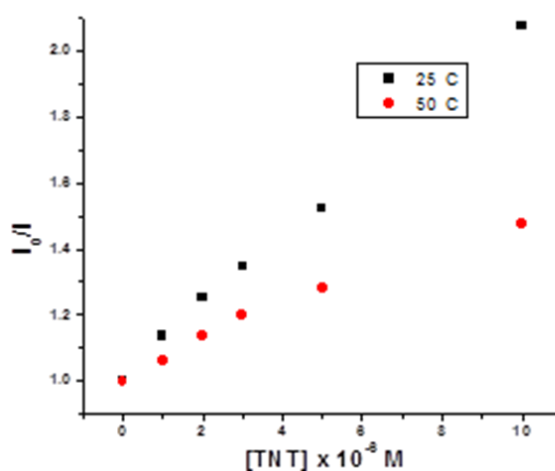


Figure 3.13 Stern-Volmer plots at 25 and 50 °C

The effects of pH on fluorescent intensity of fluorophore **ANC** were investigated using phosphate buffers in the range of 3-10. As shown in Figure 3.14, there was no significant change of the intensity indicating that the protonation at dimethyl amine system on **ANC** did not affect the fluorescence of **ANC**. Moreover, we also compared the quenching of fluorescence of **ANC** to TNT in DMF with aqueous solution (1% THF). Furthermore, we also compared the quenching of fluorescence of **ANC** to TNT in DMF with aqueous solution (1%THF) (Figure 3.12). The quenching in aqueous solution (~90%) was much higher than in DMF (~20%). The result showed that water can forced TNT to insert into **ANC** cavity.

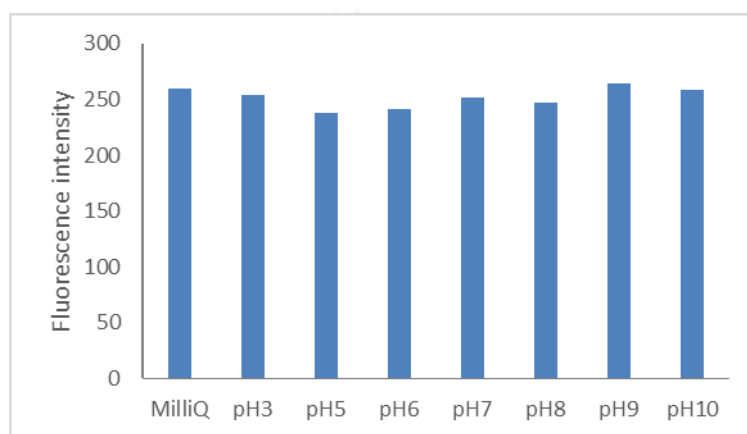


Figure 3.14 Fluorescence intensity of **ANC** 0.5 μM at $\lambda_{\max} = 420$ nm in various pH.

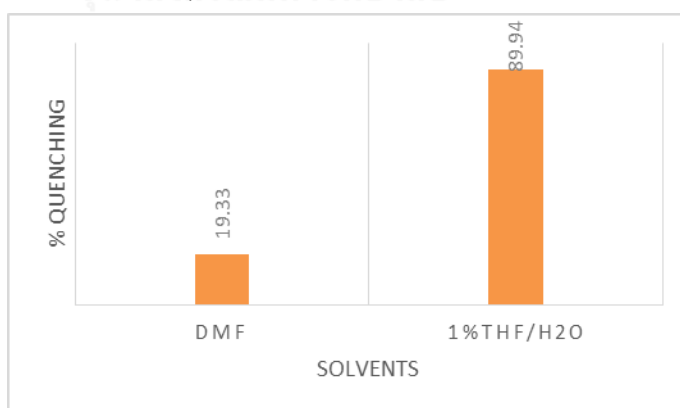


Figure 3.15 Fluorescence quenching of **ANC** for TNT 100 equiv in DMF and 1%THF/H₂O

3.1.7 ANC fluorescent paper sensor

To investigate the practical application of **ANC** sensor, we further carried out TNT detection both in vapor mode and contact mode by using paper strips for rapid on-site detection of TNT. The fluorescence paper test strips were placed on the Eppendorf that contained TNT solid and was covered with cotton gauze to expose to TNT vapor in (8.02×10^{-6} mm Hg at 25° C) 5 and 10 min. The fluorescence was quenched upon exposure to TNT vapor as shown in Figure 3.16.

In contact mode test, the glove-wearing thumb, rubbed with TNT was pressed down a paper strip. Under UV light, the dark finger print of the thumb appeared (Figure 3.17). These results displayed that the **ANC** paper strips can easily use for the on-site prompt visualization of trace residues of TNT and its vapor.



Figure 3.16 Fluorescence image (under 365 nm UV light) of **ANC** on a filter paper under different experimental conditions. (A) Vapor-mode detection of TNT (a) before (b) after exposing TNT vapors 5 min (c) 10 min.

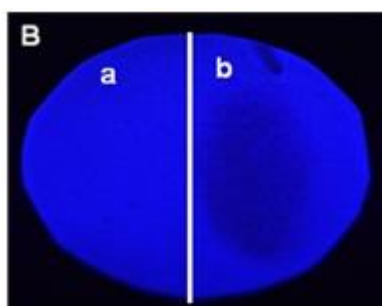


Figure 3.17 Impression of thumb (a) before rubbing with TNT (b) after rubbing with TNT.

3.2 Fluorescent hydrazone sensor F2-F4 for sensing Al³⁺ (Part B)

3.2.1 Synthesis and characterization of F2-F4

As shown in Figure 3.18, the key step in the synthesis of the hydrazone fluorophores was the schiff base reaction between 2-furoic hydrazide and benzaldehyde derivatives (salicylaldehyde, 2,5-dihydroxybenzaldehyde and 2,5-dihydroxyterephthalaldehyde) to afford compounds **F2-F4** in 73-84% yield.

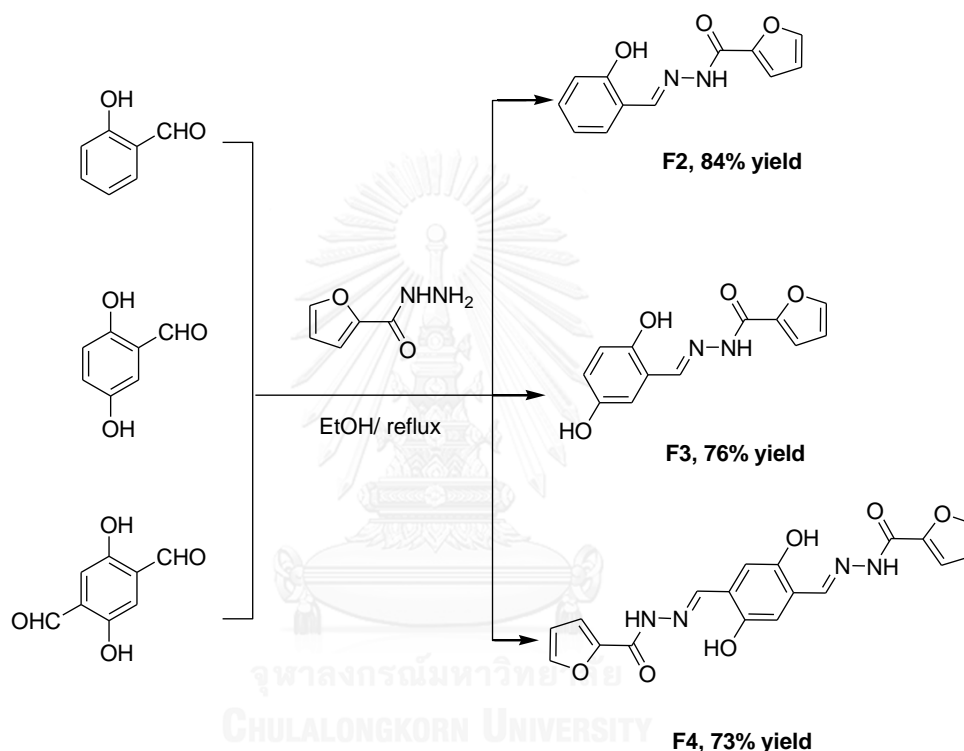


Figure 3.18 Synthesis routes of fluorophores

For the NMR characterization, ¹H NMR spectrum of fluorophores **F2-F4** is shown in Figure 3.19. All fluorophores **F2-F4** showed the imine proton signal (HC=N) around 8.6 ppm, amide proton (NH) around 12.0 ppm and the characteristic furan peaks (H₁, H₂ and H₃) around 8.0, 6.7 and 7.3 ppm, respectively.

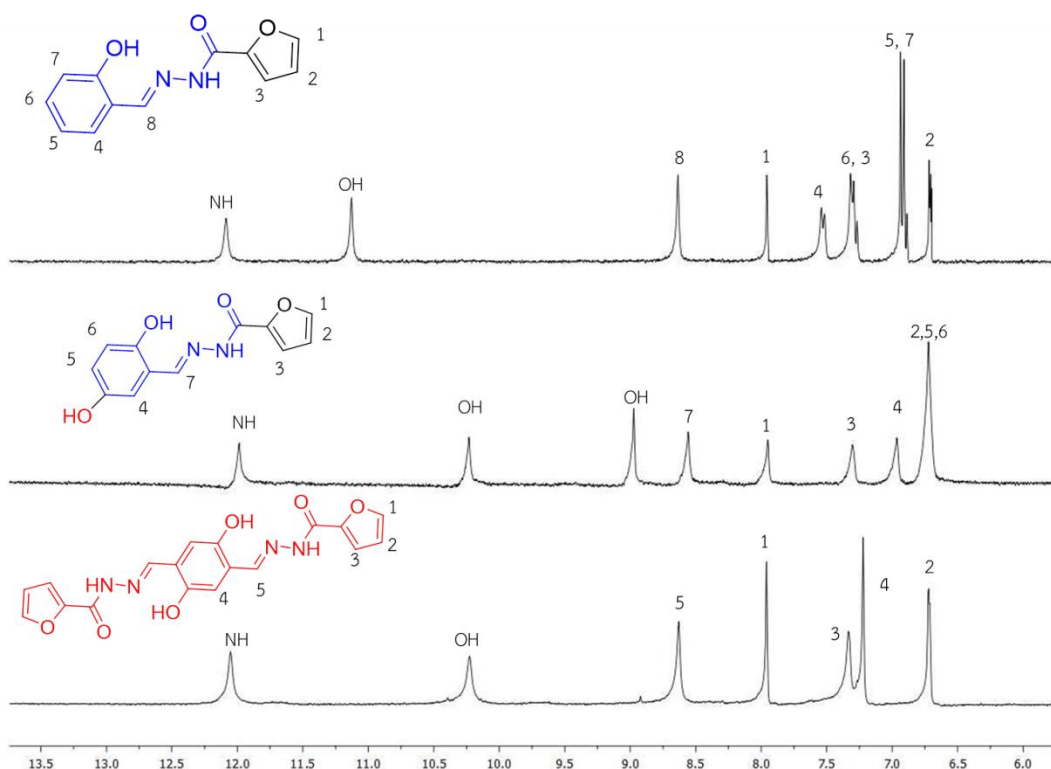


Figure 3.19 ^1H NMR spectra of compound F2-F4

3.2.2 Photophysical properties of F2-F4

The absorption and emission of fluorophores **F2-F4** were studied in aqueous solution (0.5% DMSO/ H_2O). The photophysical properties are summarized in Table 3.2. The UV-Vis absorption spectrum of each compound exhibited two major absorption regions corresponding to $\pi\text{-}\pi^*$ and $n\text{-}\pi^*$ transitions. The molar absorptivity of **F4** was low when comparing with those of **F2** and **F3** because it has low solubility in water. As expected, the absorption and emission spectra of **F3** and **F4** showed significantly red-shifted compared with **F2** as the results of the additional hydroxyl group (**F2**) and increasing π conjugation (**F4**). In aqueous solution, all of the compounds gave very weak fluorescence owing to the PET and ESIPT processes as depicted in Figure 3.20. The PET process occurs from the electron transfer of amine. For ESIPT process, phenolic proton can transfer to Schiff base nitrogen atom ($\text{C}=\text{N}$) act as proton acceptor. The ESIPT process was also evidenced by the extraordinary large Stokes' shift.

Table 3.2 Photophysical properties of sensor **F2-F4** in aqueous solution (~0.5% DMSO/H₂O)

Sensor	λ_{ab} (nm)	$\log \epsilon$	λ_{em} (nm)	Φ
F2	302, 328	4.40, 4.28	457	0.02
F3	297, 350	4.46, 4.10	531	0.001
F4	309, 396	4.01, 3.87	615	0.003

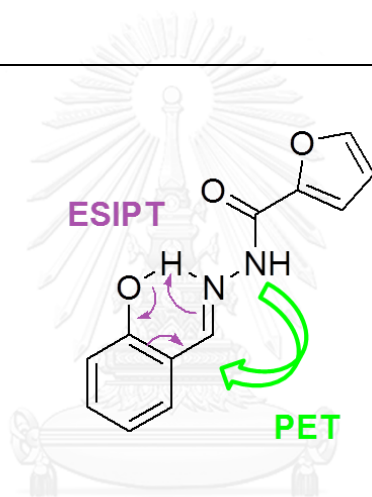


Figure 3.20 Quenching mechanism of **F2**

3.2.3 Fluorescence studies of **F2-F4** toward Al^{3+} ion and other metal ions.

Upon addition of 10 equiv. Al^{3+} (100 μM), the fluorescent intensity of each sensor showed significant enhancement, but in different emission wavelengths and apparent colors: blue for **F2**, green for **F3** and orange red for **F4** as shown in Figure 3.21. The strong fluorescence turn-on was associated with the formation of the complex formation between Al^{3+} and each sensing compound which suppressed both the PET and ESIPT in the sensors and induced rigidity in the complexes resulting in CHEF (chelation enhanced fluorescence) [19] as shown in Figure 3.22. The solution of **F2**- Al^{3+} complex has strong blue emission with the maximum emission wavelength $\lambda_{em} \approx 455$ nm (Stokes shift ($\Delta\lambda_{em-ex}$) = 89 nm) with high quantum efficiencies of 0.49. As designed, the **F3**- Al^{3+} complex exhibited green fluorescence at $\lambda_{em} \approx 524$

nm ($\Phi = 0.16$) which was red-shifted by 70 nm from **F2**-Al³⁺ and the Stokes shift was 114 nm as a result of an extra hydroxyl substituent. Impressively, the emission peak of 4-Al³⁺ complex moved even further to 601 nm ($\Phi = 0.18$) which also gave the largest Stokes shift of 133 nm. The significant emission bathochromic shifts and larger Stokes shifts of **F3**-Al³⁺ and **F4**-Al³⁺ from **F2**-Al³⁺ revealed the presence of the additional hydroxyl and hydrazine substituents thus has intriguing impact on the radiative decay process besides lowering the HOMO-LUMO band gap.

The fluorescence sensing selectivity of **F2-F4** was also studied with other common metal ions (Na⁺, K⁺, Ag⁺, Mg²⁺, Ca²⁺, Hg²⁺, Ba²⁺, Pb²⁺, Cd²⁺, Mn²⁺, Ni²⁺, Co²⁺, Cu²⁺, Fe²⁺, Zn²⁺, Cr³⁺, Fe³⁺) at 10 equiv (100 μ M) in aqueous solution (0.1%DMSO/HEPES). Except Al³⁺ ion, the fluorescence signals of all fluorophores showed no significant change with other metal ions as shown in Figure. 3.21. Therefore, these hydrazide compounds are highly selective for Al³⁺ detection.

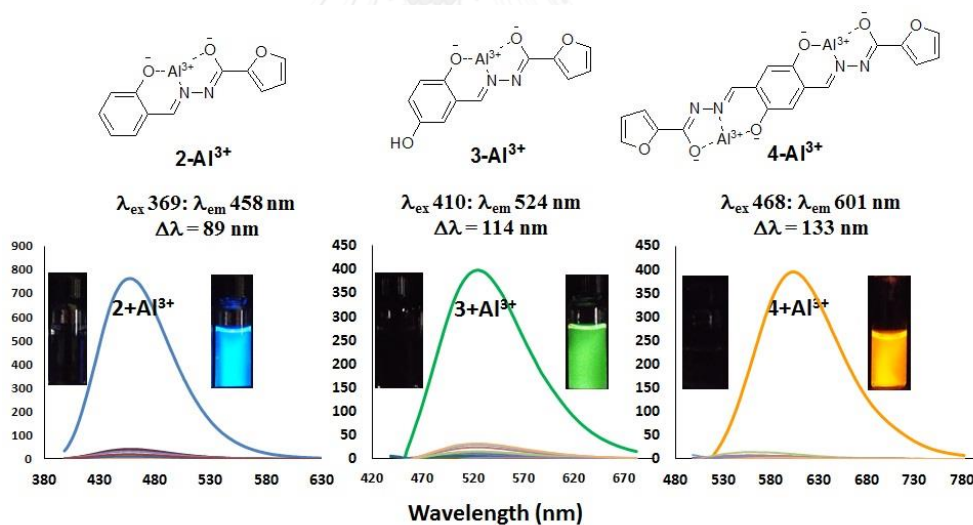


Figure 3.21 Fluorescence spectra of **F2-F4** (10 μ M in 0.1% DMSO/HEPES) before and after addition 10 equiv of metal ions: Na⁺, K⁺, Ag⁺, Mg²⁺, Ca²⁺, Hg²⁺, Ba²⁺, Pb²⁺, Cd²⁺, Mn²⁺, Ni²⁺, Co²⁺, Cu²⁺, Fe²⁺, Zn²⁺, Cr³⁺, Fe³⁺, Al³⁺. The spectra were obtained after 10 minute mixing for **F2** and **F3** and 30 minute mixing for **F4** with $\lambda_{ex} = 369, 410$ and 468 nm, respectively. Only Al³⁺ gives significant enhancement.

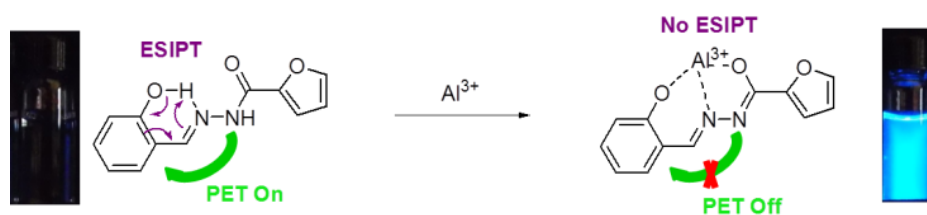


Figure 3.22 Fluorescence enhancement mechanism of the **F2**- Al^{3+} complex.

Quantitative studies of the binding affinity of three fluorophores with Al^{3+} ion were carried out by fluorescence titrations as shown in Figure. 3.23. The intensity of fluorescence signal increased almost linearly with the increasing Al^{3+} concentration up to 1 equiv. (for **F2** and **F3**) and 2 equiv. (for **F4**). On the basis of Job plot, the complexation ratios of Al^{3+} and the ligand **F2** and **F3** were 1:1 (Figure 3.24). Meanwhile, the job plot of the Al^{3+} complexed with **F4** gave 2:1 stoichiometric metal:ligand ratio. The assumption was supported by ESI-mass spectrometry analysis. For **F2** and **F3**, the mass spectrum showed peaks at m/z 381.3 and 366.7 corresponding to the mass of $[\text{AlNO}_3 \cdot (\text{F2-H}) \cdot 2(\text{MeOH})]^+$ and $[\text{AlNO}_3 \cdot (\text{F3-H}) \cdot \text{MeOH}]^+$ (Figure 3.25a and 3.25b). In the case of **F4**, the ESI-MS spectrum showed both 1:1 and 2:1 ion peaks at 502.9 for $[\text{AlNO}_3 \cdot (\text{F4-H}) \cdot \text{MeOH}]^+$ and 562.9 for $[2\text{Al} \cdot (\text{F4-4H})\text{NO}_3 \cdot \text{MeOH} \cdot 2\text{H}_2\text{O}]^+$ (Figure 3.25c).

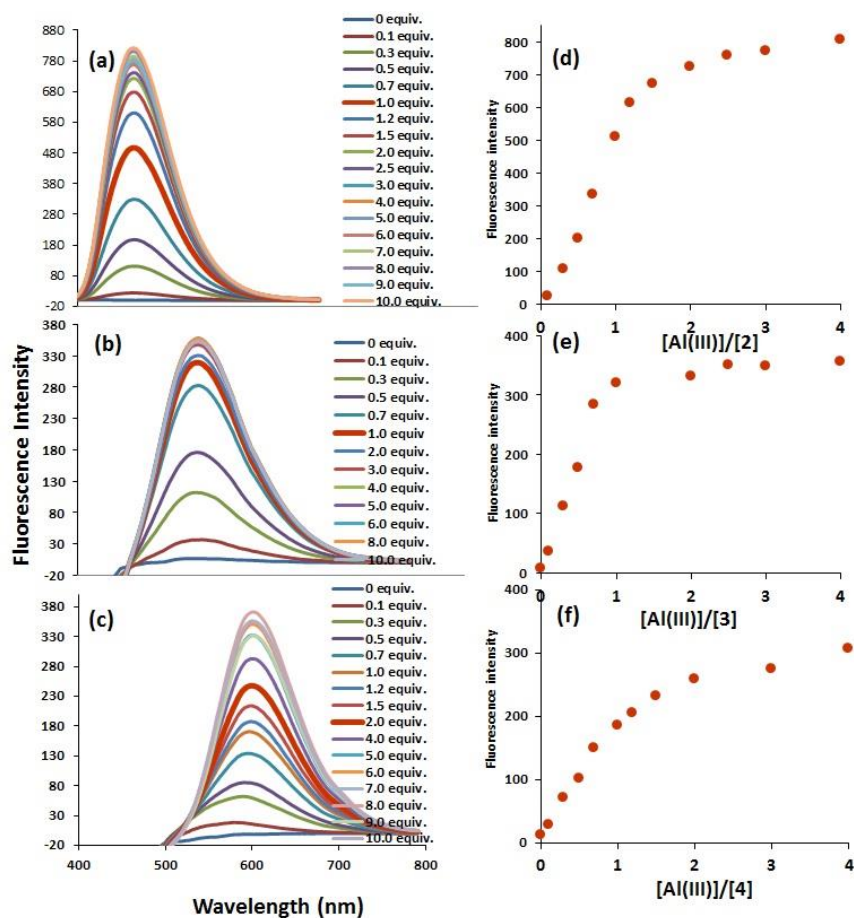


Figure 3.23 Fluorescence spectra of F2 (a), F3 (b) and F4 (c) (10 μM), respectively, upon addition of different concentrations of Al^{3+} in 0.1% DMSO/HEPES. Inset: Plots of intensity at each λ_{em} versus the amount of Al^{3+} added. The spectra were obtained after mixing for 10 minutes (sensor F2 and F3) and for 30 minutes (sensor F4) using $\lambda_{\text{ex}} = 369, 410$ and 468 nm, respectively.

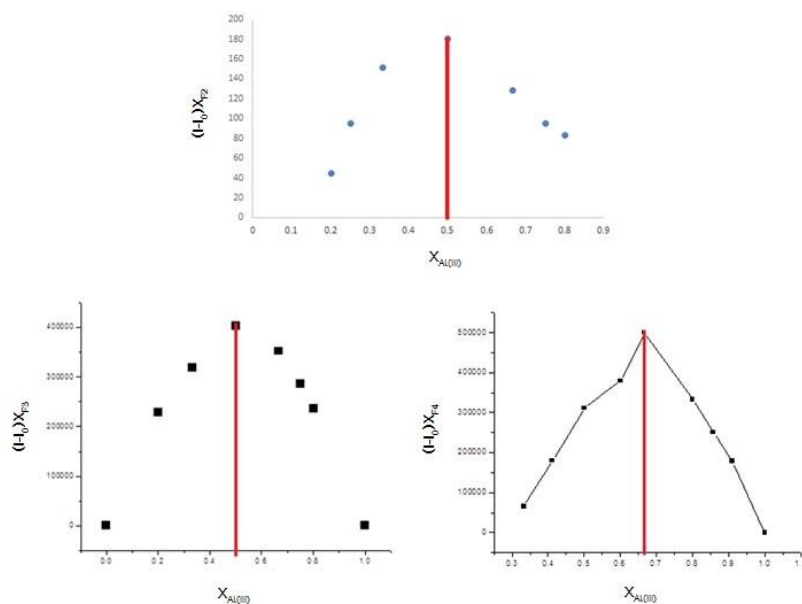


Figure 3.24 The Job's plot examined between Al^{3+} and (a) sensor F2 (b) F3 (c) F4 by fluorescence.

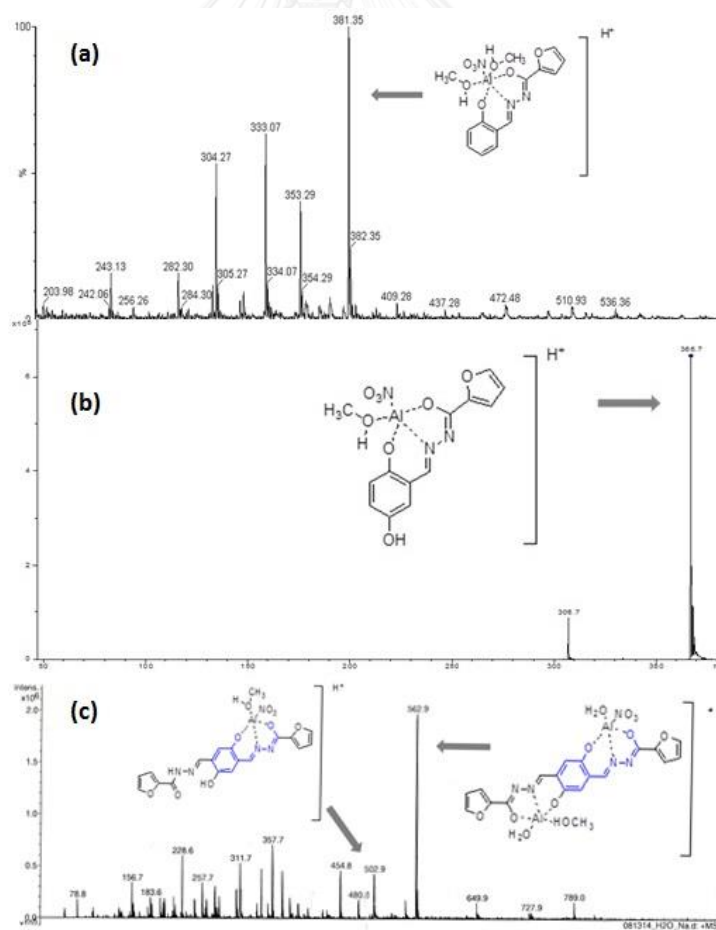


Figure 3.25 HRMS of sensor (a) F2- Al^{3+} , (b) F3- Al^{3+} and (c) F4- Al^{3+}

The K_a values for the complexation with **F2-F4** are 1.6×10^5 , 5.4×10^5 and $2.0 \times 10^{10} \text{ M}^{-1}$, respectively. The particularly large K_a value for the complex of **F4** is the result of two association constants supporting the formation of 2:1 complex.

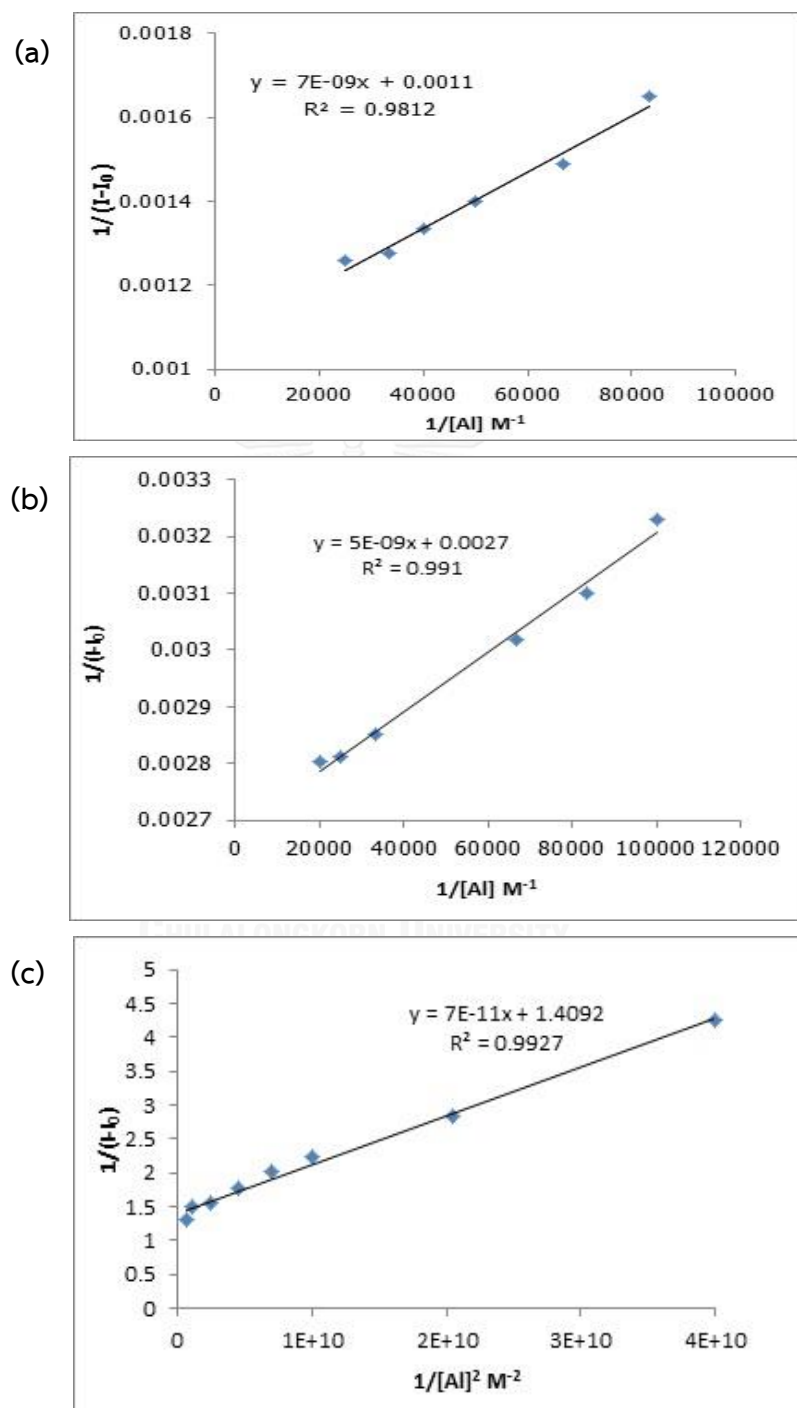


Figure 3.26 Benesi-Hildebrand plots of (a) **F2**, (b) **F3** and (c) **F4**

Upon the addition of Al^{3+} , the absorption band of each compound showed the large spectral bathochromic shift inferring deprotonation of the phenolic proton to enable its binding with Al^{3+} . The λ_{max} of **F2** and **F3** exhibited a single shift from 325 to 369 nm and 352 to 397 nm, respectively (Figure 3.27a and b). On the other hand, **F4** exhibited a two-stepped spectral shift in methanol. The first step was from 408 nm to 457 with the addition of Al^{3+} up to 1 equiv, and the second step was from 457 nm to 504 nm with the addition of 1 to 2 equiv that corresponded to the stepwise deprotonation of the two phenolic protons upon the complexation (Figure 3.27c).

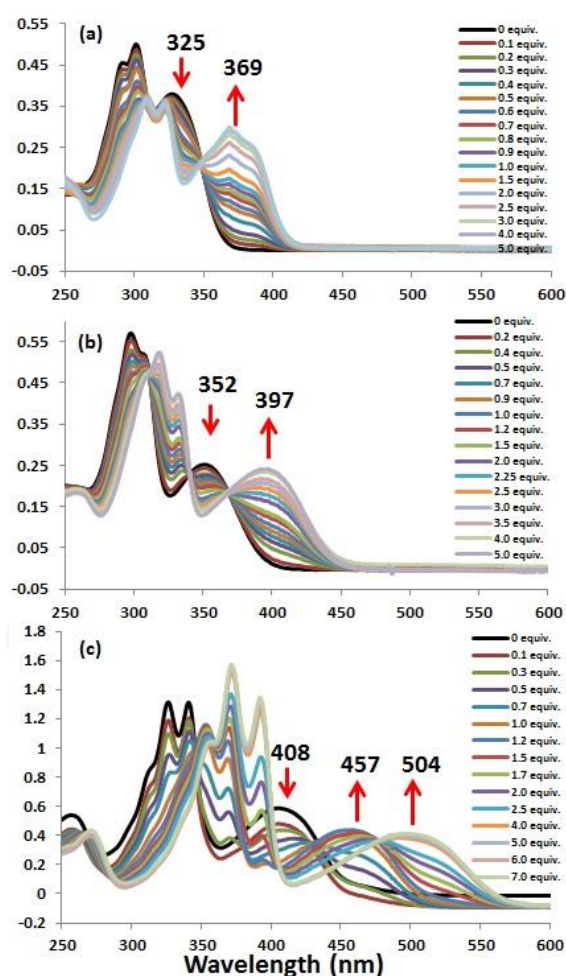


Figure 3.27 Absorption spectra of (a) **F2** (10 μM) (b) **F3** (10 μM) (c) **F4** (20 μM) after 10 minute mixing with Al^{3+} in 0.2% DMSO/HEPES for **F2** and **F3** but after 3 hour mixing with Al^{3+} in CH_3OH for **F4**.

To determine the detection limit of **F4**, the fluorescence response to Al^{3+} concentration in nanomolar range was investigated in HEPES buffered aqueous solution pH 5.5. A good linear response was obtained in the range of 20-120 nM Al^{3+} ($R^2 = 0.9969$) giving the detection limit of 3.1 nM (Figure 3.28). The detection limit is much lower than the permissible limit of 7.41 μM for Al^{3+} in drinking water established by WHO.

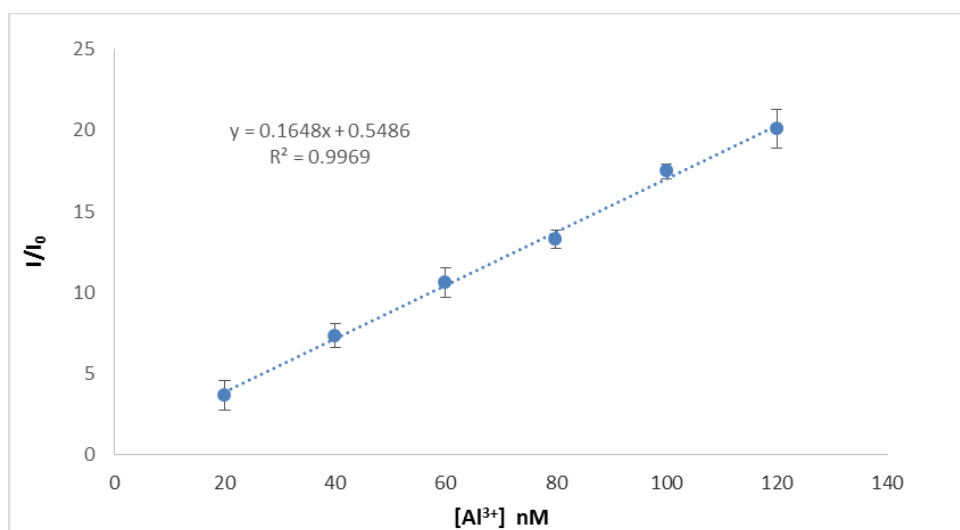


Figure 3.28 Calibration curves of ratio of fluorescence intensity of **F4** to Al^{3+} concentration.

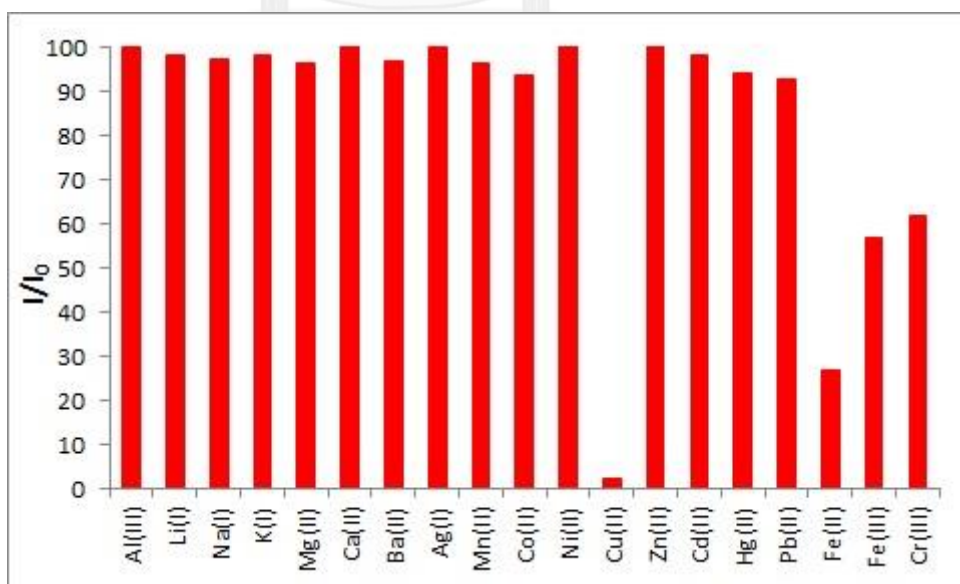


Figure 3.29 Relative fluorescence of **F4** (10 μM) in 0.1% DMSO/HEPES pH 5.5 in the presence of Al^{3+} (100 μM) plus another interfering metal ion (100 μM) tested.

To evaluate the possible interference from other metal ions in Al^{3+} detection, we measured the fluorescence responses of **F4** to Al^{3+} in the presence of another metal ion in HEPES. At the same concentration, most metal ions did not interfere with the detection of Al^{3+} by **F4** (Figure 3.29). However, Fe^{3+} , Fe^{2+} and Cr^{3+} partially reduced the fluorescence intensity of the **F4**- Al^{3+} complex. Only Cu^{2+} completely quenched the fluorescence signal. Therefore, positive turn-on fluorescence signal of this sensor is a good indication for the predominant presence of Al^{3+} . In quantitative determination of Al^{3+} , samples however should be free from these interfering metal ions. In addition, The Al^{3+} complexation with each ligand was reversible as the fluorescence turn on signal could be nullified with the addition of 10 equiv EDTA (Figure 3.30).

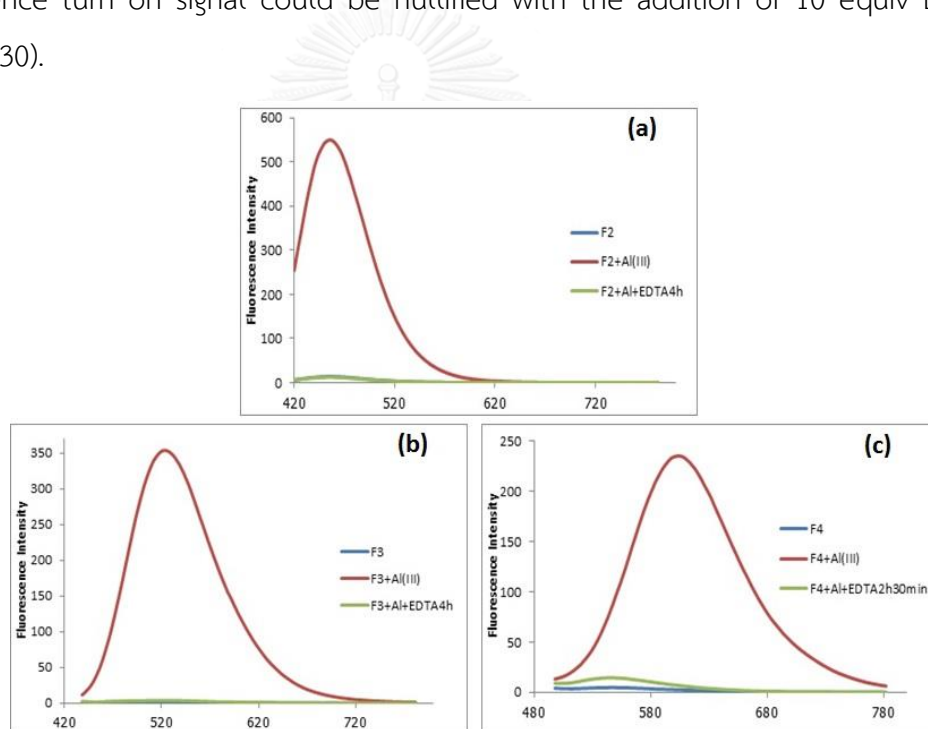


Figure 3.30 Fluorescence emission spectra of **F2-F4** in the presence of Al^{3+} (1.0 equiv. for **F2-F3** and 2.0 equiv. for **F4**) and signal restoration by EDTA (10.0 equiv.)

For convenient use in an on-site analysis, we developed paper-based fluorescent sensors for Al^{3+} detection. A series of 3.0 μL of 0.5 mM **F4** solution in EtOH were dropped on to filter paper strips and then dried to get light blue fluorescence spots (Figure 3.31). Each spot was dropped with 1 μL containing 1.0 nmol of various metal ions. Al^{3+} gave a yellow while Zn^{2+} gave an orange emission area within the blue spot. Co^{2+} , Ni^{2+} , Cu^{2+} and Fe^{2+} generated a dark quenching area

within the blue spots while other metal ion tested did not change the appearance of the spots.

Interestingly, this detection test in solid state not only Al^{3+} but also Zn^{2+} showed the turn-on fluorescence responses, despite the fact that Zn^{2+} did not give significant change in aqueous media. In aqueous solution, both phenolic and hydrazidic protons are readily deprotonated to form the hard-base donor sites, phenoxide ($\text{Ar}-\text{O}^-$) and enolate ($\text{N}=\text{C}-\text{O}^-$), that prefers Al^{3+} coordination (form B in Figure 1.26). In an aprotic medium, the acidic protons are presumably less labile that both ArOH and $\text{NHC}=\text{O}$ remain in neutral form (starting form A in Figure 1.26) providing soft-base binding sites. To support this hypothesis, the fluorescence sensing study of **F4** was carried out in CH_3CN and found that Zn^{2+} gave significantly higher fluorescence turn-on signal in CH_3CN than that of Al^{3+} (Figure 3.32). On cellulosic material such as paper, **F4** was probably in intermediate environment between water and CH_3CN that allows the formation of fluorescent complexes with both Al^{3+} and Zn^{2+} .

The result prompted us to explore for the application of **F4** in dual detection of Al^{3+} and Zn^{2+} with the aid of paper chromatography separation. The 0.5 μL of solution of Al^{3+} , Zn^{2+} and their mixture containing the total ions of 5 nmol were spotted on a filter paper strip (Whatman No. 1, 8 x 2.5 cm^2). The solution of **F4** (0.5 μL of 2 mM) was then spotted on the metal spots as shown in Figure 3.33a. After drying, the strips were placed in a closed chamber containing 5:20 (v/v) of Et_2NH :DMF as mobile phase²¹ and developed to achieve the solvent front distance of 5.5 cm. After developing, the strip clearly showed well separated orange fluorescent spot of Al^{3+} and Zn^{2+} complexes as shown in Figure 3.33b. To the best of our knowledge, this is the first simultaneous fluorescence detection of Al^{3+} and Zn^{2+} . These results demonstrate a convenient application of **F4** for dual detection of Al^{3+} and Zn^{2+} .

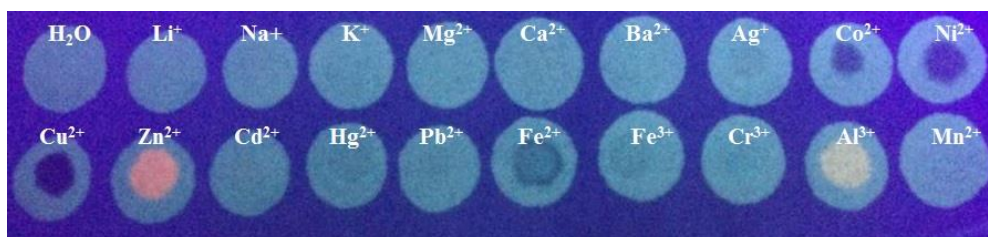


Figure 3.31 Photographic image of metal ion (1 nmol) detection by **F4** on filter paper tested by simple drop and dry from solutions of **F4** and metal ions, consecutively.

The sample was irradiated by UV-light (wavelength 365 ± 50 nm)

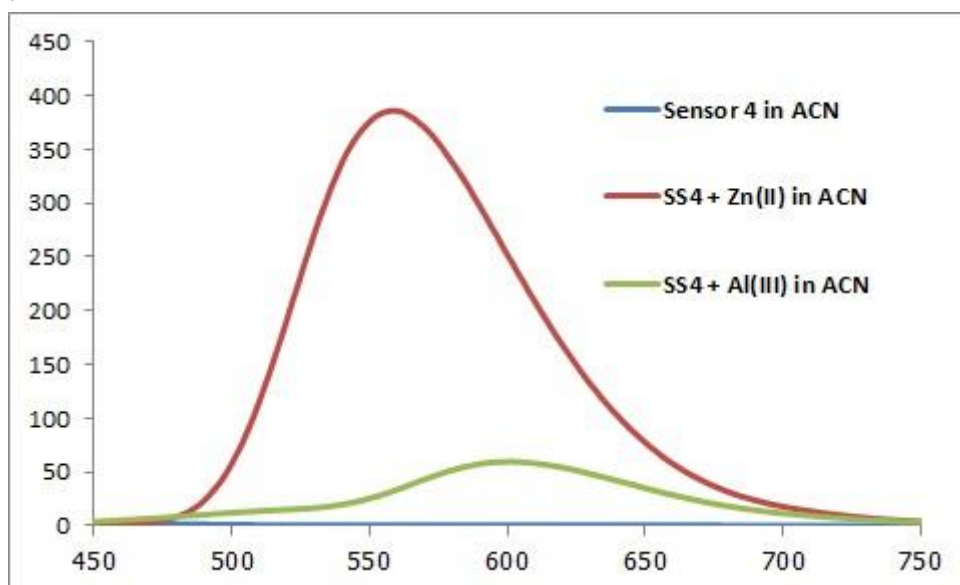


Figure 3.32 Fluorescence spectra of **F4** ($10\ \mu\text{M}$ in 0.1% DMSO/HEPES) before and after addition 10 equiv of Al^{3+} and Zn^{2+} in CH_3CN (ACN).

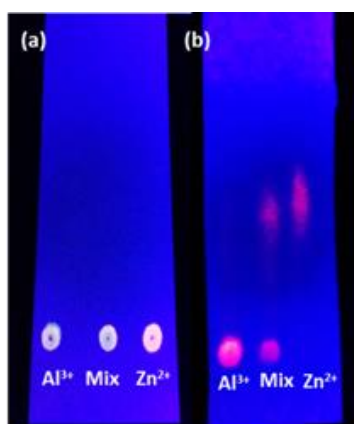


Figure 3.33 Photographic image for dual detection of Al^{3+} and Zn^{2+} by **F4** using paper chromatography for separation: (a) before and (b) after elution with Et_2NH :DMF (5: 20 v/v). The sample was irradiated by UV-light (wavelength 365 ± 50 nm).

CHAPTER IV

CONCLUSION

4.1 Conclusion of part A

In conclusion, a series of arylolethynyl calix[4]arenes was successfully synthesized and developed as new fluorescent sensors for TNT detection. With aniline rings on the wider rim, **ANC** exhibited high sensitivity and selectivity of fluorescence quenching by TNT in aqueous medium. The electron rich aniline rings provide high sensitivity while the size and hydrophobicity of the cavity of the modified calix[4]arene provide high selectivity as evidenced by the shift of ^1H NMR signals. The selective quenching effect was associated with the photo electron transfer (PET) process between the sensor and the electron deficient TNT. The Stern-Volmer fluorescence quenching constant of TNT is $1.09 \times 10^5 \text{ M}^{-1}$ with limit of detection limit of $0.3 \mu\text{M}$ (68ppb). In addition, the filter paper strips coated with ANC are potentially useful for visual detection of trace residues of TNT and its vapor.

4.2 Conclusion of part B

Part B, a series of *N*-salicylidenehydrazide derivatives was successfully synthesized and developed for selectively turn-on detection of Al^{3+} cation in aqueous media with large stroke shifts with three emissive colors: blue for **F2**, green for **F3** and orange for **F4**. The study illustrates that addition of the second hydroxyl group at the *para*-position of a phenol could have a large impact on the response of the probe, which not only tunes the emission to a longer wavelength but also enhances the ligand interaction with Al^{3+} cation. This *para*-substitution effect is further enhanced in the new double hydrazide compound **F4**, which also exhibits strong fluorescence response selectively to Al^{3+} in a highly aqueous environment. The high Al^{3+} chelation-enhanced fluorescence (CHEF) is probably due to multiple mechanisms including inhibition of PET and ESIPT. The developed **F4**- Al^{3+} complex thus integrates many attractive features into a single probe molecule, which includes

emission at long wavelength, remarkably large stroke shifts (133 nm), and large fluorescence turn-on. Therefore, the current aluminum sensors could find wide use for aluminum detection, since they are easier to synthesize and exhibit excellent response to Al^{3+} cation. In paper-based chromatography, compound **F4** can also be used for fluorescent detection of both Al^{3+} and Zn^{2+} simultaneously.



REFERENCES

- [1] Gunnlaugsson, T., Ali, H., Glynn, M., Kruger, P., Hussey, G., Pfeffer, F., dos Santos, C.G. and Tierney, J. Fluorescent Photoinduced Electron Transfer (PET) Sensors for Anions; From Design to Potential Application. Journal of Fluorescence 15(3) (2005): 287-299.
- [2] Callan, J.F., de Silva, A.P. and Magri, D.C. Luminescent Sensors and Switches in the Early 21st century. Tetrahedron 61(36) (2005): 8551-8588.
- [3] de Silva, A.P., Gunaratne, H.Q.N., Gunnlaugsson, T., Huxley, A.J.M., McCoy, C.P., Rademacher, J.T. and Rice, T.E. Signaling Recognition Events with Fluorescent Sensors and Switches. Chemical Reviews 97(5) (1997): 1515-1566.
- [4] Martínez-Máñez, R. and Sancenón, F. Fluorogenic and Chromogenic Chemosensors and Reagents for Anions. Chemical Reviews 103(11) (2003): 4419-4476.
- [5] Valeur, B. and Leray, I. Design Principles of Fluorescent Molecular Sensors for Cation Recognition. Coordination Chemistry Reviews 205(1) (2000): 3-40.
- [6] Xu, Z., Yoon, J. and Spring, D.R. Fluorescent Chemosensors for Zn²⁺. Chemical Society Reviews 39(6) (2010): 1996-2006.
- [7] Kim, J.S. and Quang, D.T. Calixarene-Derived Fluorescent Probes. Chemical Reviews 107(9) (2007): 3780-3799.
- [8] Sapsford, K.E., Berti, L. and Medintz, I.L. Materials for Fluorescence Resonance Energy Transfer Analysis: Beyond Traditional Donor–Acceptor Combinations. Angewandte Chemie International Edition 45(28) (2006): 4562-4589.
- [9] Carlson, H.J. and Campbell, R.E. Genetically Encoded FRET-Based Biosensors for Multiparameter Fluorescence Imaging. Current Opinion in Biotechnology 20(1) (2009): 19-27.
- [10] Wu, J., Liu, W., Ge, J., Zhang, H. and Wang, P. New Sensing Mechanisms for Design of Fluorescent Chemosensors Emerging in Recent Years. Chemical Society Reviews 40(7) (2011): 3483-3495.

- [11] Peng, X., Wu, Y., Fan, J., Tian, M. and Han, K. Colorimetric and Ratiometric Fluorescence Sensing of Fluoride: Tuning Selectivity in Proton Transfer. The Journal of Organic Chemistry 70(25) (2005): 10524-10531.
- [12] Wu, J.-S., Liu, W.-M., Zhuang, X.-Q., Wang, F., Wang, P.-F., Tao, S.-L., Zhang, X.-H., Wu, S.-K. and Lee, S.-T. Fluorescence Turn On of Coumarin Derivatives by Metal Cations: A New Signaling Mechanism Based on C=N Isomerization. Organic Letters 9(1) (2007): 33-36.
- [13] Hong, Y., Lam, J.W.Y. and Tang, B.Z. Aggregation-Induced Emission: Phenomenon, Mechanism and Applications. Chemical Communications (29) (2009): 4332-4353.
- [14] Wang, M., Zhang, G., Zhang, D., Zhu, D. and Tang, B.Z. Fluorescent Bio/Chemosensors Based on Silole and Tetraphenylethene Luminogens with Aggregation-Induced Emission Feature. Journal of Materials Chemistry 20(10) (2010): 1858-1867.
- [15] Lodeiro, C. and Pina, F. Luminescent and Chromogenic Molecular Probes Based on Polyamines and Related Compounds. Coordination Chemistry Reviews 253(9-10) (2009): 1353-1383.
- [16] Introduction to Fluorescence. in Lakowicz, J. Principles of Fluorescence Spectroscopy, pp. 1-26: Springer US, 2006.
- [17] Henary, M.M. and Fahrni, C.J. Excited State Intramolecular Proton Transfer and Metal Ion Complexation of 2-(2'-Hydroxyphenyl)benzazoles in Aqueous Solution. The Journal of Physical Chemistry A 106(21) (2002): 5210-5220.
- [18] Toxicological Profile for 2,4,6-Trinitrotoluene (TNT). U.S. Department of Health and Human Services, Public Health Service (1995).
- [19] Ownby, D.R., Belden, J.B., Lotufo, G.R. and Lydy, M.J. Accumulation of Trinitrotoluene (TNT) in Aquatic Organisms: Part 1—Bioconcentration and Distribution in Channel Catfish (*Ictalurus punctatus*). Chemosphere 58(9) (2005): 1153-1159.

- [20] Fant, F., De Sloovere, A., Matthijsen, K., Marlé, C., El Fantroussi, S. and Verstraete, W. The Use of Amino Compounds for Binding 2,4,6-Trinitrotoluene in Water. Environmental Pollution 111(3) (2001): 503-507.
- [21] Håkansson, K., Coorey, R.V., Zubarev, R.A., Talrose, V.L. and Håkansson, P. Low-Mass Ions Observed in Plasma Desorption Mass Spectrometry of High Explosives. Journal of Mass Spectrometry 35(3) (2000): 337-346.
- [22] Sylvia, J.M., Janni, J.A., Klein, J.D. and Spencer, K.M. Surface-Enhanced Raman Detection of 2,4-Dinitrotoluene Impurity Vapor as a Marker To Locate Landmines. Analytical Chemistry 72(23) (2000): 5834-5840.
- [23] Hilmi, A. and Luong, J.H.T. Electrochemical Detectors Prepared by Electroless Deposition for Microfabricated Electrophoresis Chips. Analytical Chemistry 72(19) (2000): 4677-4682.
- [24] Luggar, R.D., Farquharson, M.J., Horrocks, J.A. and Lacey, R.J. Multivariate Analysis of Statistically Poor EDXRD Spectra for the Detection of Concealed Explosives. X-Ray Spectrometry 27(2) (1998): 87-94.
- [25] Krausa, M. and Schorb, K. Trace Detection of 2,4,6-Trinitrotoluene in the Gaseous Phase by Cyclic Voltammetry¹. Journal of Electroanalytical Chemistry 461(1-2) (1999): 10-13.
- [26] Toal, S.J. and Trogler, W.C. Polymer Sensors for Nitroaromatic Explosives Detection. Journal of Materials Chemistry 16(28) (2006): 2871-2883.
- [27] He, G., Yan, N., Yang, J., Wang, H., Ding, L., Yin, S. and Fang, Y. Pyrene-Containing Conjugated Polymer-Based Fluorescent Films for Highly Sensitive and Selective Sensing of TNT in Aqueous Medium. Macromolecules 44(12) (2011): 4759-4766.
- [28] McQuade, D.T., Pullen, A.E. and Swager, T.M. Conjugated Polymer-Based Chemical Sensors. Chemical Reviews 100(7) (2000): 2537-2574.
- [29] Albert, K.J., Lewis, N.S., Schauer, C.L., Sotzing, G.A., Stitzel, S.E., Vaid, T.P. and Walt, D.R. Cross-Reactive Chemical Sensor Arrays. Chemical Reviews 100(7) (2000): 2595-2626.

- [30] Naddo, T., Che, Y., Zhang, W., Balakrishnan, K., Yang, X., Yen, M., Zhao, J., Moore, J.S. and Zang, L. Detection of Explosives with a Fluorescent Nanofibril Film. Journal of the American Chemical Society 129(22) (2007): 6978-6979.
- [31] Thomas, S.W., Joly, G.D. and Swager, T.M. Chemical Sensors Based on Amplifying Fluorescent Conjugated Polymers. Chemical Reviews 107(4) (2007): 1339-1386.
- [32] Yang, J.-S. and Swager, T.M. Porous Shape Persistent Fluorescent Polymer Films: An Approach to TNT Sensory Materials. Journal of the American Chemical Society 120(21) (1998): 5321-5322.
- [33] Yang, J.-S. and Swager, T.M. Fluorescent Porous Polymer Films as TNT Chemosensors: Electronic and Structural Effects. Journal of the American Chemical Society 120(46) (1998): 11864-11873.
- [34] Chen, L., McBranch, D., Wang, R. and Whitten, D. Surfactant-Induced Modification of Quenching of Conjugated Polymer Fluorescence by Electron Acceptors: Applications for Chemical Sensing. Chemical Physics Letters 330(1-2) (2000): 27-33.
- [35] Chang, C.-P., Chao, C.-Y., Huang, J.H., Li, A.-K., Hsu, C.-S., Lin, M.-S., Hsieh, B.R. and Su, A.-C. Fluorescent Conjugated Polymer Films as TNT Chemosensors. Synthetic Metals 144(3) (2004): 297-301.
- [36] Sohn, H., Calhoun, R.M., Sailor, M.J. and Trogler, W.C. Detection of TNT and Picric Acid on Surfaces and in Seawater by Using Photoluminescent Polysiloles. Angewandte Chemie International Edition in English 113(11) (2001): 2162-2163.
- [37] Sohn, H., Sailor, M.J., Magde, D. and Trogler, W.C. Detection of Nitroaromatic Explosives Based on Photoluminescent Polymers Containing Metalloles. Journal of the American Chemical Society 125(13) (2003): 3821-3830.
- [38] Sanchez, J.C., DiPasquale, A.G., Rheingold, A.L. and Trogler, W.C. Synthesis, Luminescence Properties, and Explosives Sensing with 1,1-Tetraphenylsilole- and 1,1-Silafluorene-vinylene Polymers. Chemistry of Materials 19(26) (2007): 6459-6470.

- [39] Zhou, Q. and Swager, T.M. Fluorescent Chemosensors Based on Energy Migration in Conjugated Polymers: The Molecular Wire Approach to Increased Sensitivity. Journal of the American Chemical Society 117(50) (1995): 12593-12602.
- [40] Kumar, S., Venkatramaiah, N. and Patil, S. Fluoranthene Based Derivatives for Detection of Trace Explosive Nitroaromatics. The Journal of Physical Chemistry C 117(14) (2013): 7236-7245.
- [41] Zyryanov, G.V., Palacios, M.A. and Anzenbacher, P. Simple Molecule-Based Fluorescent Sensors for Vapor Detection of TNT. Organic Letters 10(17) (2008): 3681-3684.
- [42] Kumar, M., Vij, V. and Bhalla, V. Vapor-Phase Detection of Trinitrotoluene by AIEE-Active Hetero-oligophenylene-Based Carbazole Derivatives. Langmuir 28(33) (2012): 12417-12421.
- [43] Park, K.H.Y., Jae D., Lee, C.H. and Ka, J.W. Calix[2]pyreno[2]pyrrole as a Fluorescence Chemical Probe for Polynitroaromatics. Bulletin of the Korean Chemical Society 33(2) (2012): 675-577.
- [44] Bhalla, V., Gupta, A. and Kumar, M. Fluorescent Nanoaggregates of Pentacenequinone Derivative for Selective Sensing of Picric acid in Aqueous Media. Organic Letters 14(12) (2012): 3112-3115.
- [45] Niamnont, N., Kimpitak, N., Wongravee, K., Rashatasakhon, P., Baldrige, K.K., Siegel, J.S. and Sukwattanasinitt, M. Tunable Star-Shaped Triphenylamine Fluorophores for Fluorescence Quenching Detection and Identification of Nitroaromatic explosives. Chemical Communications 49(8) (2013): 780-782.
- [46] Kim, S.-B., Lee, E.-B., Choi, J.-H. and Cho, D.-G. Simple Fluorescent Chemosensors for TNT: One-Step Synthesis. Tetrahedron 69(23) (2013): 4652-4656.
- [47] Xu, B., Wu, X., Li, H., Tong, H. and Wang, L. Selective Detection of TNT and Picric Acid by Conjugated Polymer Film Sensors with Donor-Acceptor Architecture. Macromolecules 44(13) (2011): 5089-5092.

- [48] Ma, Y., Li, H., Peng, S. and Wang, L. Highly Selective and Sensitive Fluorescent Paper Sensor for Nitroaromatic Explosive Detection. Analytical Chemistry 84(19) (2012): 8415-8421.
- [49] Lee, Y.H., Liu, H., Lee, J.Y., Kim, S.H., Kim, S.K., Sessler, J.L., Kim, Y. and Kim, J.S. Dipyrenylcalix[4]arene—A Fluorescence-Based Chemosensor for Trinitroaromatic Explosives. Chemistry – A European Journal 16(20) (2010): 5895-5901.
- [50] Costa, A.I., Pinto, H.D., Ferreira, L.F.V. and Prata, J.V. Solid-State Sensory Properties of CALIX-poly(phenylene ethynylene)s toward Nitroaromatic Explosives. Sensors and Actuators B: Chemical 161(1) (2012): 702-713.
- [51] Costa, A.I. and Prata, J.V. Substituted p-Phenylene Ethynylene Trimers as Fluorescent Sensors for Nitroaromatic Explosives. Sensors and Actuators B: Chemical 161(1) (2012): 251-260.
- [52] Kandpal, M., Bandela, A.K., Hinge, V.K., Rao, V.R. and Rao, C.P. Fluorescence and Piezoresistive Cantilever Sensing of Trinitrotoluene by an Upper-Rim Tetrabenzimidazole Conjugate of Calix[4]arene and Delineation of the Features of the Complex by Molecular Dynamics. ACS Applied Materials & Interfaces 5(24) (2013): 13448-13456.
- [53] Cao, X., Luo, L., Zhang, F., Miao, F., Tian, D. and Li, H. Synthesis of a Deep Cavity Calix[4]arene by Fourfold Sonogashira Cross-Coupling Reaction and Selective Fluorescent Recognition toward p-Nitrophenol. Tetrahedron Letters 55(12) (2014): 2029-2032.
- [54] Robinson, G.H. Aluminum. Chemical & Engineering News Archive 81(36) (2003): 54.
- [55] Exley, C. Guest Editorial. Journal of Inorganic Biochemistry 99(9) (2005): 1747-1748.
- [56] Berthon, G. Aluminium Speciation in Relation to Aluminium Bioavailability, Metabolism and Toxicity. Coordination Chemistry Reviews 228(2) (2002): 319-341.
- [57] Nayak, P. Aluminum: Impacts and Disease. Environmental Research 89(2) (2002): 101-115.

- [58] Cronan, C.S., Walker, W.J. and Bloom, P.R. Predicting Aqueous Aluminium Concentrations in Natural Waters. Nature 324(6093) (1986): 140-143.
- [59] Perl, D., Gajdusek, D., Garruto, R., Yanagihara, R. and Gibbs, C. Intraneuronal Aluminum Accumulation in Amyotrophic Lateral Sclerosis and Parkinsonism-Dementia of Guam. Science 217(4564) (1982): 1053-1055.
- [60] Perl, D. and Brody, A. Alzheimer's Disease: X-ray Spectrometric Evidence of Aluminum Accumulation in Neurofibrillary Tangle-Bearing Neurons. Science 208(4441) (1980): 297-299.
- [61] Crapper, D.R., Krishnan, S.S. and Dalton, A.J. Brain Aluminum Distribution in Alzheimer's Disease and Experimental Neurofibrillary Degeneration. Science 180(4085) (1973): 511-513.
- [62] Valeur, B. and Leray, I. Design Principles of Fluorescent Molecular Sensors for Cation Recognition. Coordination Chemistry Reviews 205(1) (2000): 3-40.
- [63] Barceló, J. and Poschenrieder, C. Fast Root Growth Responses, Root Exudates, and Internal Detoxification as Clues to the Mechanisms of Aluminium Toxicity and Resistance: a Review. Environmental and Experimental Botany 48(1) (2002): 75-92.
- [64] Han, T., Feng, X., Tong, B., Shi, J., Chen, L., Zhi, J. and Dong, Y. A Novel "Turn-on" Fluorescent Chemosensor for the Selective Detection of Al³⁺ Based on Aggregation-Induced Emission. Chemical Communications 48(3) (2012): 416-418.
- [65] Frankowski, M., Ziola-Frankowska, A. and Siepak, J. New Method for Speciation Analysis of Aluminium Fluoride Complexes by HPLC-FAAS Hyphenated Technique. Talanta 80(5) (2010): 2120-2126.
- [66] Sanz-Medel, A., Soldado Cabezuelo, A.B., Milačič, R. and Bantan Polak, T. The Chemical Speciation of Aluminium in Human Serum. Coordination Chemistry Reviews 228(2) (2002): 373-383.
- [67] Goyal, R.N., Gupta, V.K. and Chatterjee, S. A Sensitive Voltammetric Sensor for Determination of Synthetic Corticosteroid Triamcinolone, Abused for Doping. Biosensors and Bioelectronics 24(12) (2009): 3562-3568.

- [68] Di, J., Bi, S., Yang, T. and Zhang, M. Voltammetric Determination of Aluminum(III) Using a Reagentless Sensor Fabricated by Sol–Gel Process. Sensors and Actuators B: Chemical 99(2–3) (2004): 468-473.
- [69] Ma, Y.-H., Yuan, R., Chai, Y.-Q. and Liu, X.-L. A New Aluminum(III)-Selective Potentiometric Sensor Based on N,N'-Propanediamide bis(2-salicylideneimine) as a Neutral Carrier. Materials Science and Engineering: C 30(1) (2010): 209-213.
- [70] Soroka, K., Vithanage, R.S., Phillips, D.A., Walker, B. and Dasgupta, P.K. Fluorescence Properties of Metal Complexes of 8-Hydroxyquinoline-5-Sulfonic Acid and Chromatographic Applications. Analytical Chemistry 59(4) (1987): 629-636.
- [71] Ma, T.-H., Dong, M., Dong, Y.-M., Wang, Y.-W. and Peng, Y. A Unique Water-Tuning Dual-Channel Fluorescence-Enhanced Sensor for Aluminum Ions Based on a Hybrid Ligand from a 1,1'-Binaphthyl Scaffold and an Amino Acid. Chemistry – A European Journal 16(34) (2010): 10313-10318.
- [72] Sahana, A., Banerjee, A., Das, S., Lohar, S., Karak, D., Sarkar, B., Kanti Mukhopadhyay, S., Mukherjee, A.K. and Das, D. A Naphthalene-Based Al³⁺ Selective Fluorescent Sensor for Living Cell Imaging. Organic & Biomolecular Chemistry 9(15) (2011): 5523-5529.
- [73] Lu, Y., Huang, S., Liu, Y., He, S., Zhao, L. and Zeng, X. Highly Selective and Sensitive Fluorescent Turn-on Chemosensor for Al³⁺ Based on a Novel Photoinduced Electron Transfer Approach. Organic Letters 13(19) (2011): 5274-5277.
- [74] Gupta, V.K., Singh, A.K. and Mergu, N. Antipyrine Based Schiff Bases as Turn-on Fluorescent Sensors for Al (III) Ion. Electrochimica Acta 117 (2014): 405-412.
- [75] Frangioni, J.V. In Vivo Near-Infrared Fluorescence Imaging. Current Opinion in Chemical Biology 7(5) (2003): 626-634.
- [76] Smith, B.A., Akers, W.J., Leevy, W.M., Lampkins, A.J., Xiao, S., Wolter, W., Suckow, M.A., Achilefu, S. and Smith, B.D. Optical Imaging of Mammary and Prostate Tumors in Living Animals using a Synthetic Near Infrared Zinc(II)-

- Dipicolylamine Probe for Anionic Cell Surfaces. Journal of the American Chemical Society 132(1) (2010): 67-69.
- [77] Koide, Y., Urano, Y., Hanaoka, K., Terai, T., and Nagano, T. Evolution of Group 14 Rhodamines as Platforms for Near-Infrared Fluorescence Probes Utilizing Photoinduced Electron Transfer. ACS Chemical Biology 6(6) (2011): 600-608.
- [78] Sivaraman, G., Anand, T. and Chellappa, D. Quick Accessible Dual Mode Turn-on Red Fluorescent Chemosensor for Cu(ii) and its Applicability in Live Cell Imaging. RSC Advances 3(38) (2013): 17029-17033.
- [79] Zhao, J., Ji, S., Chen, Y., Guo, H. and Yang, P. Excited State Intramolecular Proton Transfer (ESIPT): from Principal Photophysics to the Development of New Chromophores and Applications in Fluorescent Molecular Probes and Luminescent Materials. Physical Chemistry Chemical Physics 14(25) (2012): 8803-8817.
- [80] Bessy Raj, B.N. and Kurup, M.R.P. N-2-Hydroxy-4-Methoxyacetophenone-N'-4-Nitrobenzoyl Hydrazine: Synthesis and Structural Characterization. Spectrochimica Acta Part A: Molecular and Biomolecular Spectroscopy 66(4-5) (2007): 898-903.
- [81] Zhao, Y., Lin, Z., Liao, H., Duan, C. and Meng, Q. A Highly Selective Fluorescent Chemosensor for Al³⁺ Derived from 8-Hydroxyquinoline. Inorganic Chemistry Communications 9(9) (2006): 966-968.
- [82] Guo, Y.-Y., Yang, L.-Z., Ru, J.-X., Yao, X., Wu, J., Dou, W., Qin, W.-W., Zhang, G.-L., Tang, X.-L. and Liu, W.-S. An "OFF-ON" Fluorescent Chemosensor for Highly Selective and Sensitive Detection of Al (III) in Aqueous Solution. Dyes and Pigments 99(3) (2013): 693-698.
- [83] Goswami, S., Manna, A., Paul, S., Aich, K., Das, A.K. and Chakraborty, S. Dual Channel Selective Fluorescence Detection of Al(III) and PPI in Aqueous Media with an 'Off-On-Off' Switch which Mimics Molecular Logic Gates (INHIBIT and EXOR gates). Dalton Transactions 42(22) (2013): 8078-8085.
- [84] Liao, Z.-C., Yang, Z.-Y., Li, Y., Wang, B.-D. and Zhou, Q.-X. A Simple Structure Fluorescent Chemosensor for High Selectivity and Sensitivity of Aluminum Ions. Dyes and Pigments 97(1) (2013): 124-128.

- [85] Lee, S.A., You, G.R., Choi, Y.W., Jo, H.Y., Kim, A.R., Noh, I., Kim, S.-J., Kim, Y. and Kim, C. A New Multifunctional Schiff Base as a Fluorescence Sensor for Al³⁺ and a Colorimetric Sensor for CN⁻ in Aqueous Media: an Application to Bioimaging. Dalton Transactions 43(18) (2014): 6650-6659.
- [86] Fan, L., Li, T.-r., Wang, B.-d., Yang, Z.-y. and Liu, C.-j. A Colorimetric and Turn-on Fluorescent Chemosensor for Al(III) Based on a Chromone Schiff-base. Spectrochimica Acta Part A: Molecular and Biomolecular Spectroscopy 118 (2014): 760-764.
- [87] Wang, J. and Pang, Y. A Simple Sensitive ESIPT on-off Fluorescent Sensor for Selective Detection of Al³⁺ in Water. RSC Advances 4(12) (2014): 5845-5848.
- [88] Zhang, K., Yang, Z.-y., Wang, B.-d., Sun, S.-B., Li, Y.-D., Li, T.-r., Liu, Z.-c. and An, J.-m. A Highly Selective Chemosensor for Al³⁺ Based on 2-Oxo-Quinoline-3-Carbaldehyde Schiff-Base. Spectrochimica Acta Part A: Molecular and Biomolecular Spectroscopy 124 (2014): 59-63.
- [89] Shi, X., Cui, G., Tang, B., Wang M., Zhang, G., Dong, Y. and Dong Y. Process for Synthesizing Al-Salicylic Aldehyde Acylhydrazone Complexes. 2012, Patents CN101434613 B.
- [90] Iqbal, C.D.G.a.M. p-tert-Butylcalix[4]arene. Org. Synth. 68 (1990): 234-236.
- [91] Gutsche, C.D., Levine, J.A., and Sujeeth, P.K. Calixarenes. 17. Functionalized Calixarenes: the Claisen Rearrangement Route. The Journal of Organic Chemistry 50(26) (1985): 5802-5806.
- [92] Kelderman, E., Verboom, W., Engbersen, J.F.J., Reinhoudt, D.N., Heesink, G.J.T., van Hulst, N.F., Derhaeg, L. and Persoons, A. Nitrocalix[4]arenes as Molecules for Second-Order Nonlinear Optics. Angewandte Chemie International Edition in English 31(8) (1992): 1075-1077.
- [93] Arduini, A., Fabbi, M., Mantovani, M., Mirone, L., Pochini, A., Secchi, A. and Ungaro, R. Calix[4]arenes Blocked in a Rigid Cone Conformation by Selective Functionalization at the Lower Rim. The Journal of Organic Chemistry 60(5) (1995): 1454-1457.

- [94] Klenke, B. and Friedrichsen, W. A Convenient Access to Iodinated Calix[4]arenes 1. Journal of the Chemical Society, Perkin Transactions 1 (20) (1998): 3377-3380.
- [95] Kadokawa, J.-i., Tanaka, Y., Yamashita, Y. and Yamamoto, K. Synthesis of Poly(spiropyran)s by Polycondensation and their Photoisomerization Behaviors. European Polymer Journal 48(3) (2012): 549-559.
- [96] Brouwer Albert, M. Standards for Photoluminescence Quantum Yield Measurements in Solution (IUPAC Technical Report). in Pure and Applied Chemistry. 2011. 2213.
- [97] Benesi, H.A. and Hildebrand, J.H. A Spectrophotometric Investigation of the Interaction of Iodine with Aromatic Hydrocarbons. Journal of the American Chemical Society 71(8) (1949): 2703-2707.
- [98] Varghese, R., George, S.J. and Ajayaghosh, A. Anion Induced Modulation of Self-Assembly and Optical Properties in Urea End-Capped Oligo(p-phenylenevinylene)s. Chemical Communications (5) (2005): 593-595.
- [99] Sun, X., Wang, Y.-W. and Peng, Y. A Selective and Ratiometric Bifunctional Fluorescent Probe for Al³⁺ Ion and Proton. Organic Letters 14(13) (2012): 3420-3423.

APPENDIX A

May24-2011-dh003
I-KL-25
chula_proton

6.62
6.60
6.58
6.56

4.47
4.43

3.86
3.83

3.16
3.13

1.95
1.93
1.91
1.90

1.01
0.99

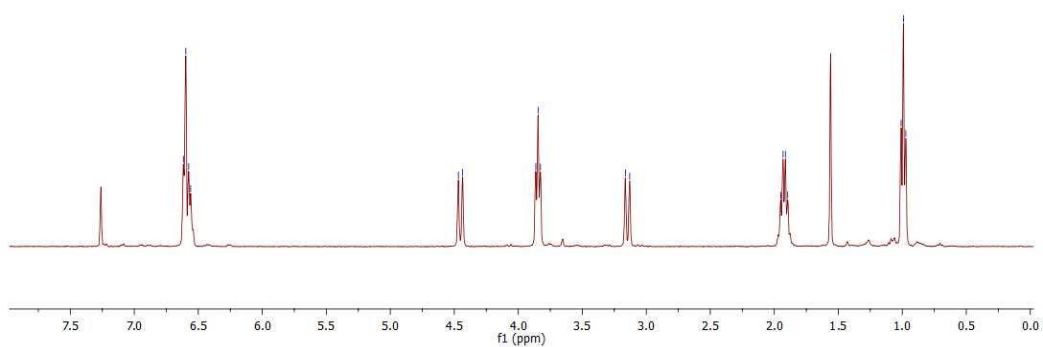
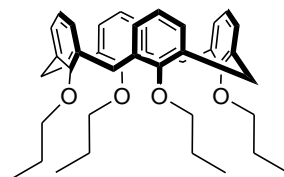


Figure A.1 ^1H NMR of 1 in CDCl_3

Jun03-2011-dh004
I-KL-31
chula_proton

6.99

4.30
4.27

3.82
3.80
3.78

3.07
3.03

1.89
1.87
1.85
1.84

0.97
0.96
0.94

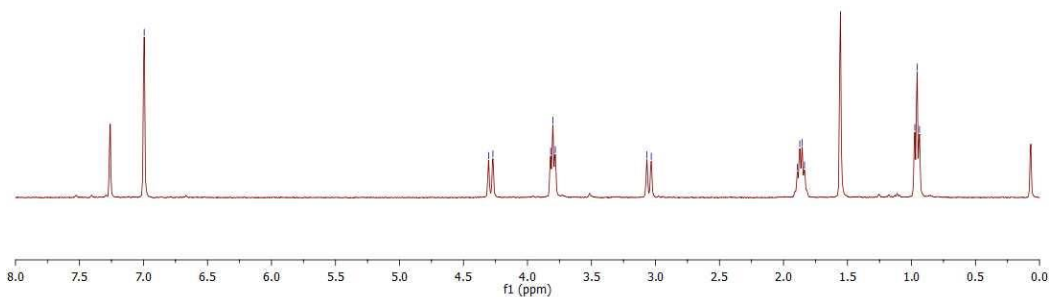
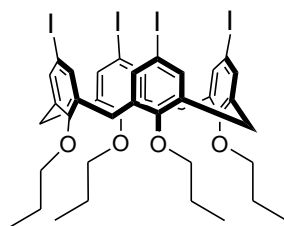


Figure A.2 ^1H NMR of 2 in CDCl_3

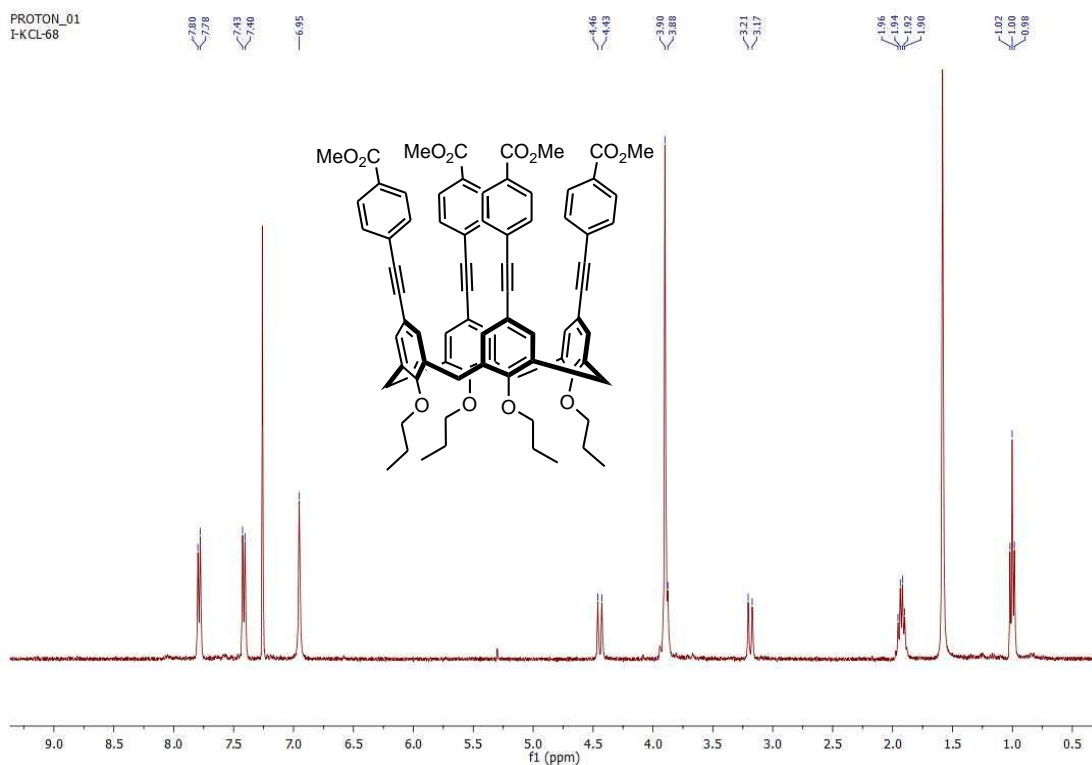


Figure A.3 ¹H NMR of **3a** in CDCl₃

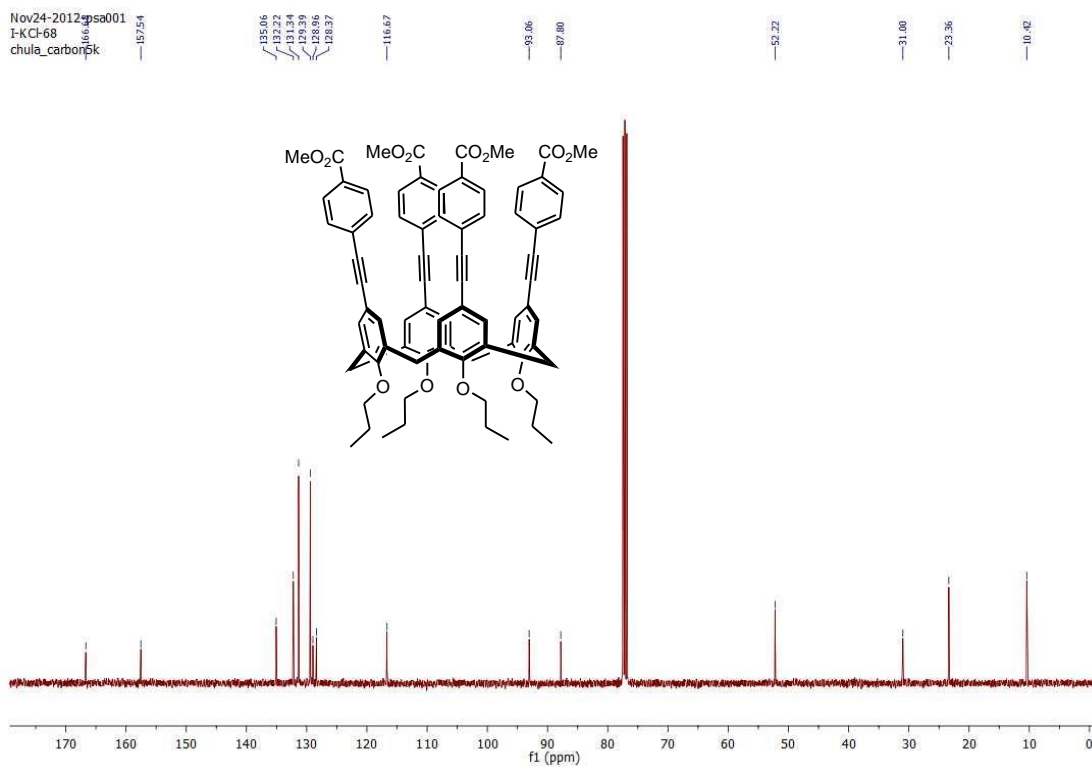
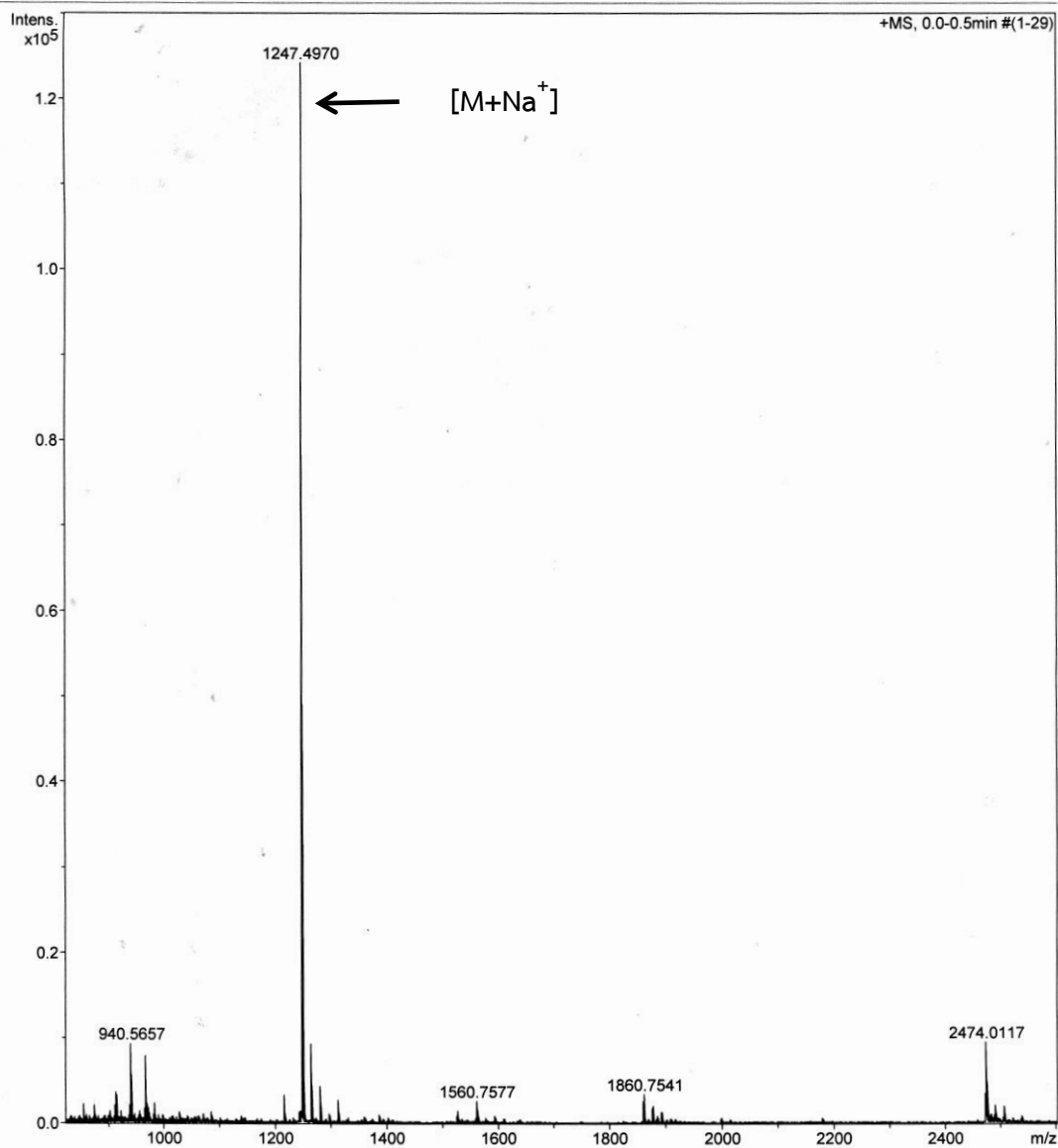


Figure A.4 ¹³C NMR of **3a** in CDCl₃

Generic Display Report

Analysis Info		Acquisition Date	1/4/2013 8:45:41 AM
Analysis Name	D:\Data\Data Service\Year 2013\Small molecule\01042013\I-KCL-68_pos.d	Operator	BDAL@DE
Method	tune_wide.m	Instrument	micrOTOF-Q II
Sample Name	I-KCL-68_pos		
Comment	after tune and cal MS		



Bruker Compass DataAnalysis 4.0

printed: 1/7/2013 3:23:28 PM

Page 1 of 1

Figure A.5 HRMS of 3a.

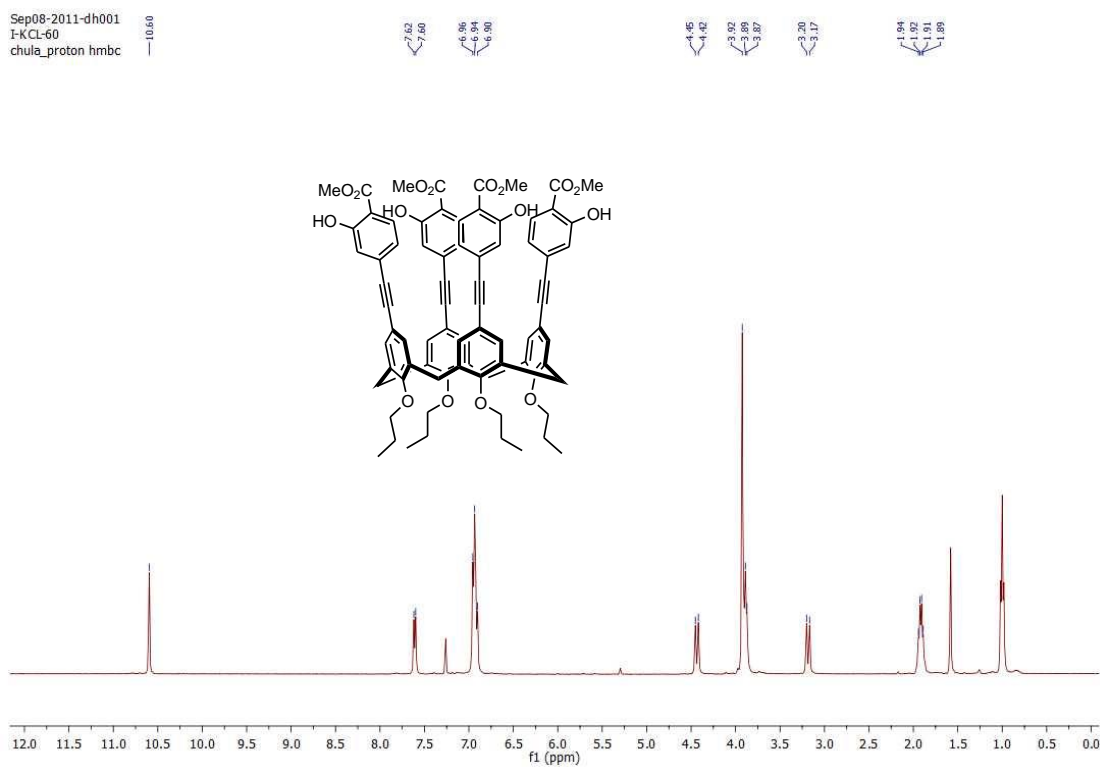


Figure A.6 ^1H NMR of **3b** in CDCl_3

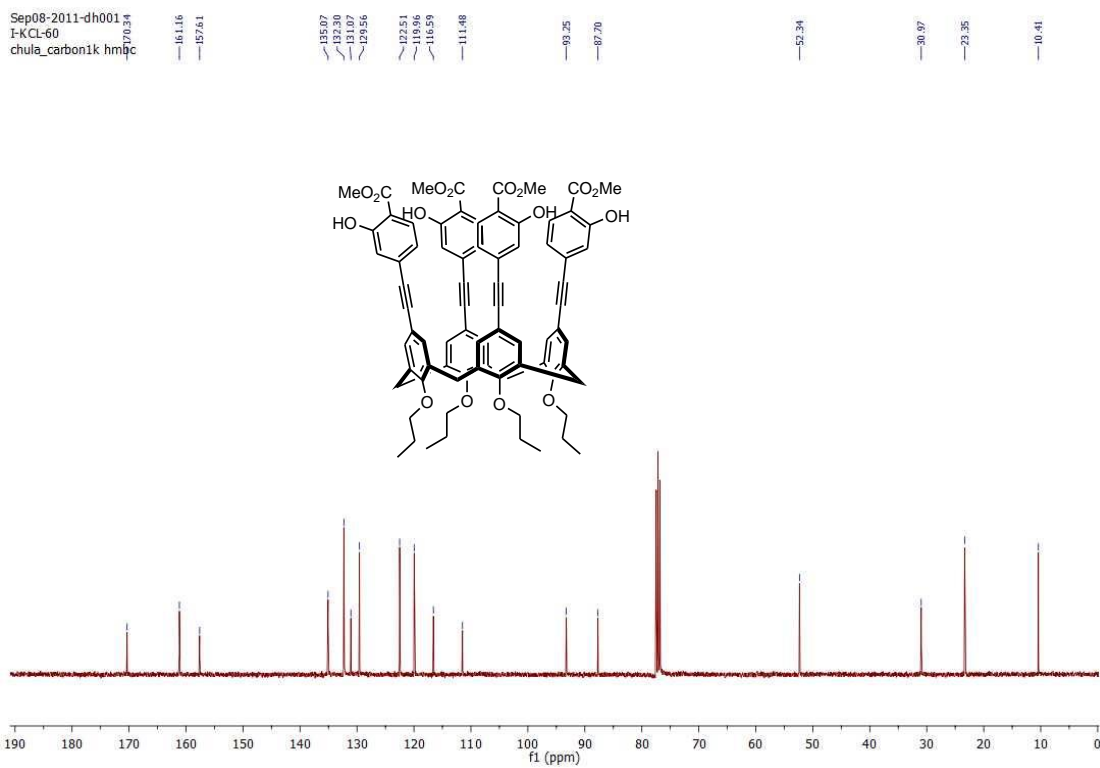


Figure A.7 ^{13}C NMR of **3b** in CDCl_3

Generic Display Report

Analysis Info		Acquisition Date	1/4/2013 8:42:42 AM
Analysis Name	D:\Data\Data Service\Year 2013\Small molecule\01042013\I-KCL-67_pos.d	Operator	BDAL@DE
Method	tune_wide.m	Instrument	micrOTOF-Q II
Sample Name	I-KCL-67_pos		
Comment	after tune and cal MS		

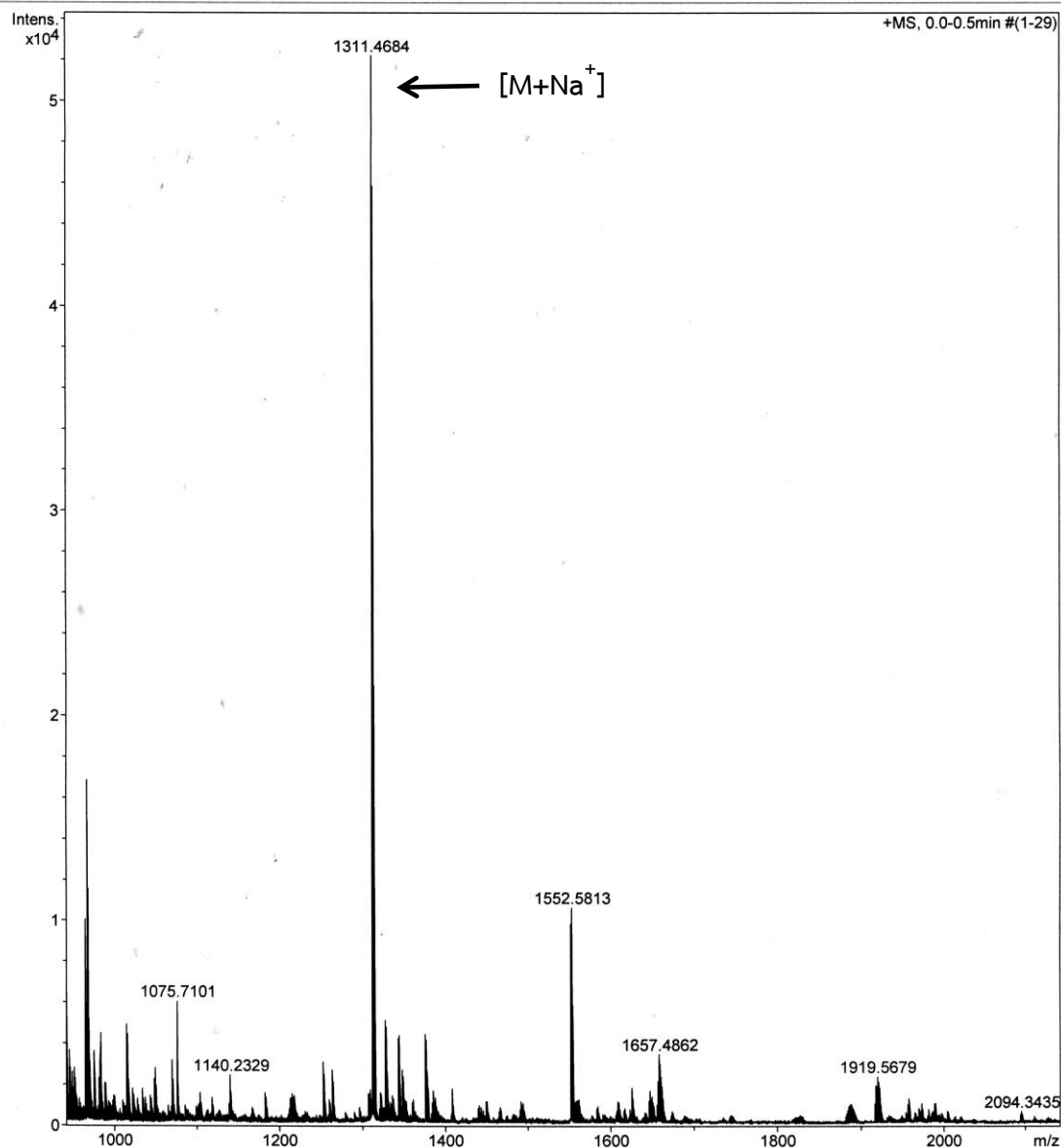
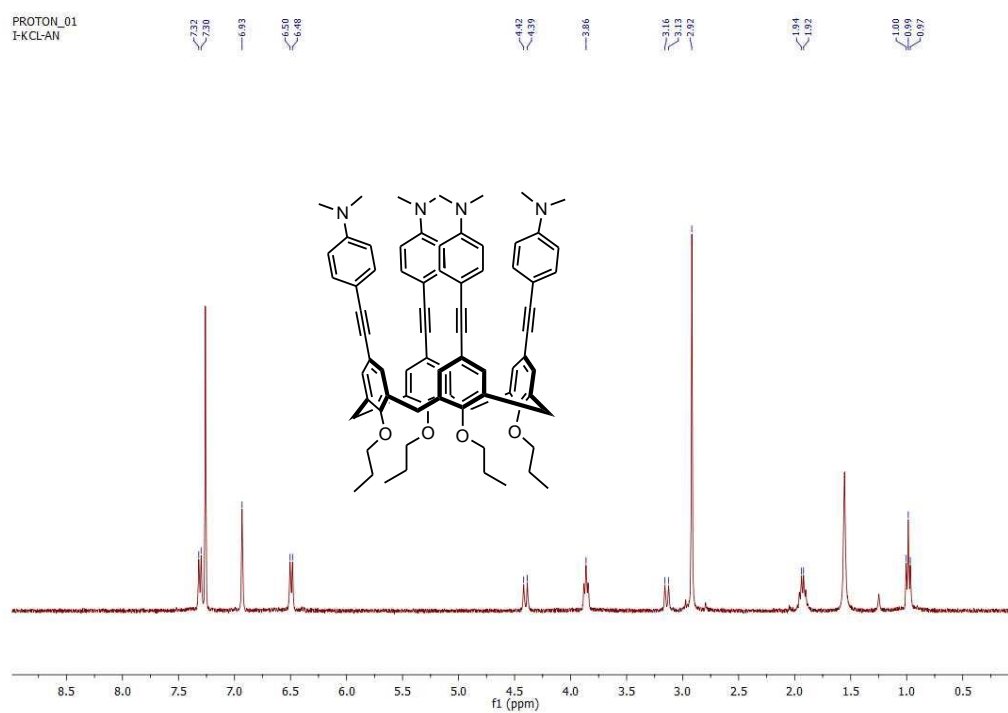
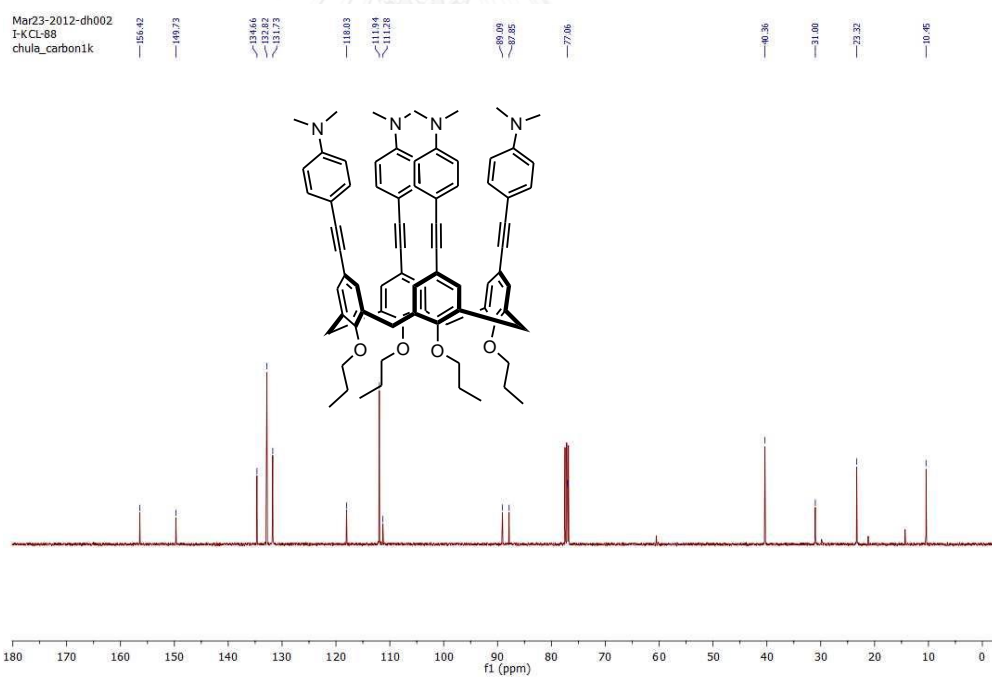


Figure A.8 HRMS of 3b.

Figure A.9 ^1H NMR of ANC in CDCl_3 Figure A.10 ^{13}C NMR of ANC in CDCl_3

Generic Display Report

Analysis Info		Acquisition Date	11/26/2012 10:55:26 AM
Analysis Name	D:\Data\Data Service\Year 2012\Small molecule\11262012\I-KCL-88 pos.d	Operator	BDAL@DE
Method	tune_wide.m	Instrument	micrOTOF-Q II
Sample Name	I-KCL-88 pos		
Comment			

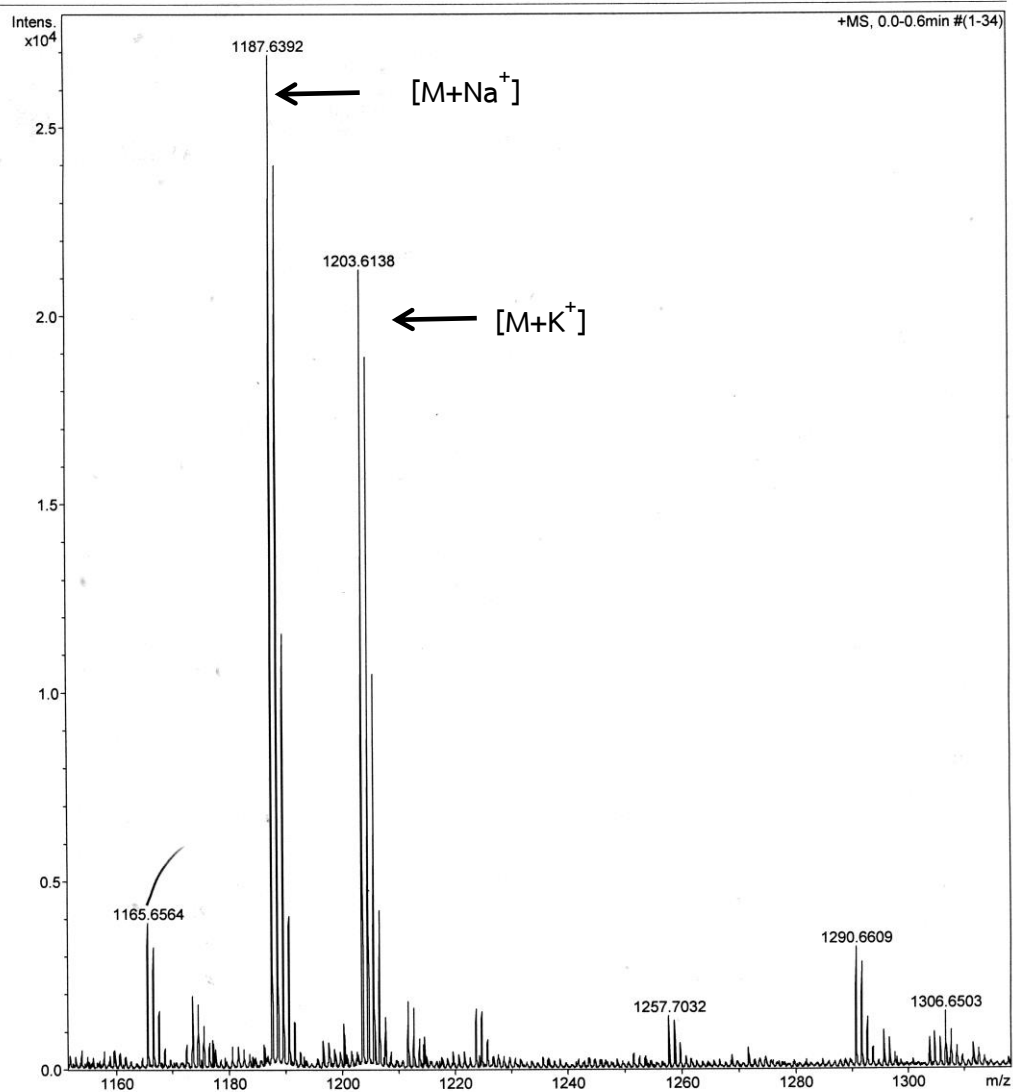


Figure A.11 HRMS of ANC.

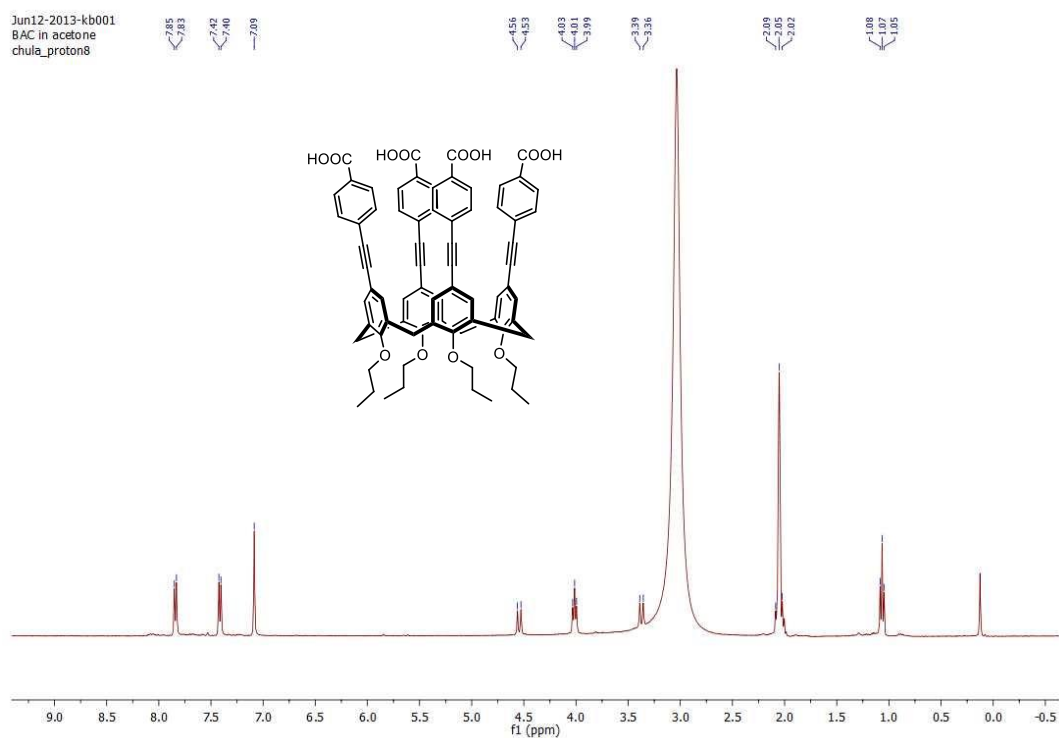


Figure A.12 ^1H NMR of BAC in Acetone- d_6

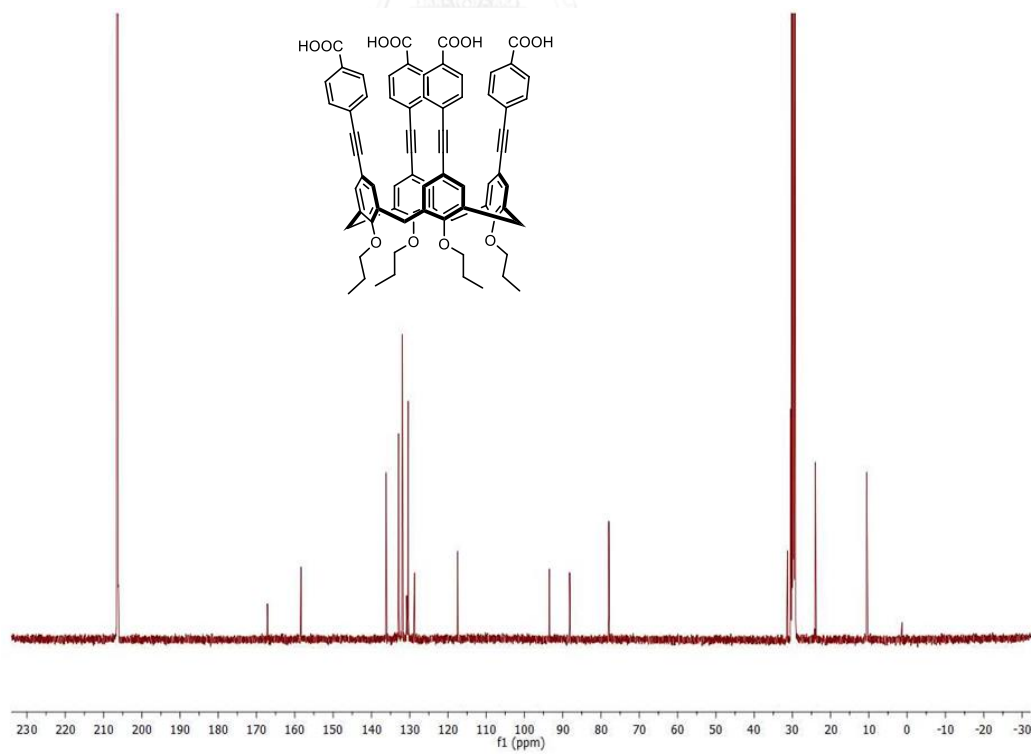


Figure A.13 ^{13}C NMR of BAC in Acetone- d_6

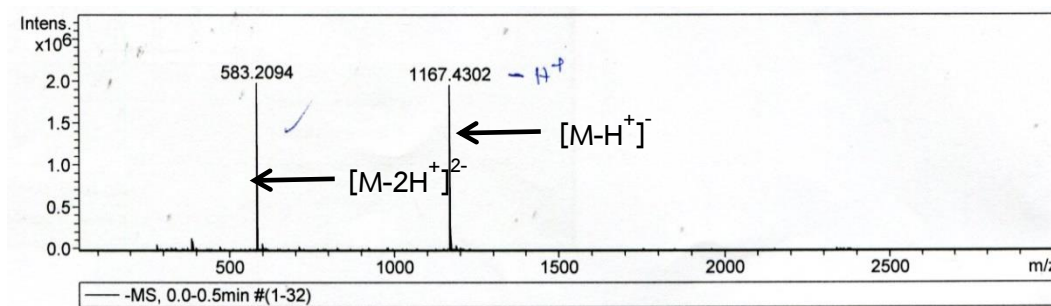
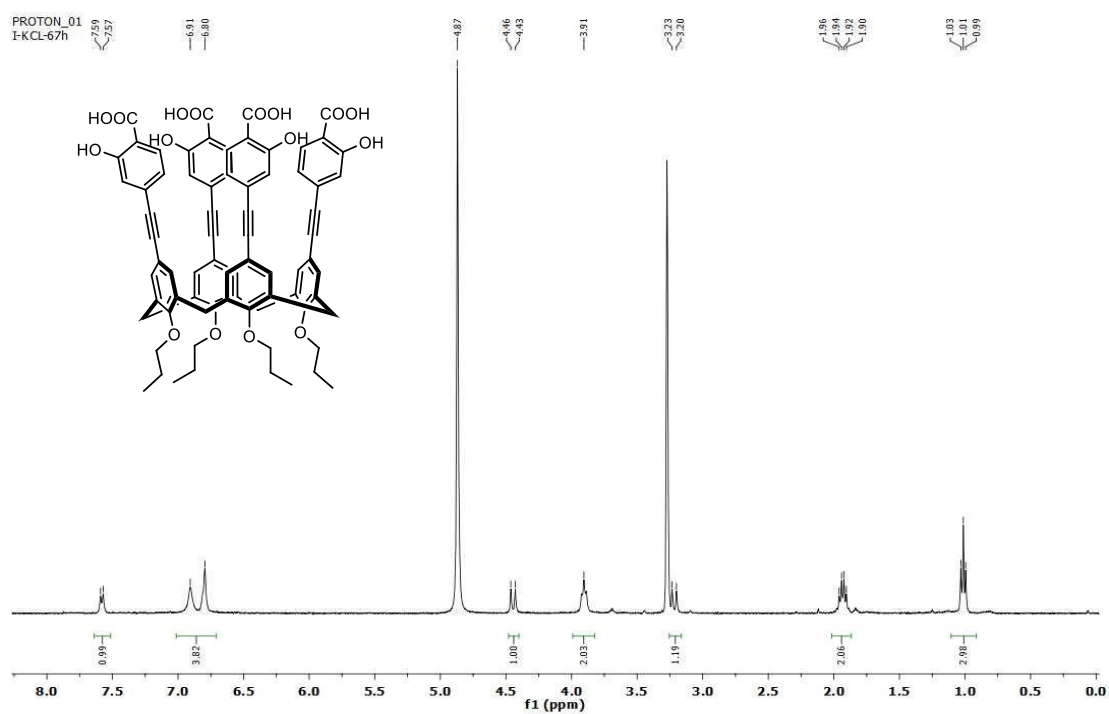


Figure A.14 HRMS of BAC.

Figure A.15 1H NMR of SAC in $MeOH-d_4$

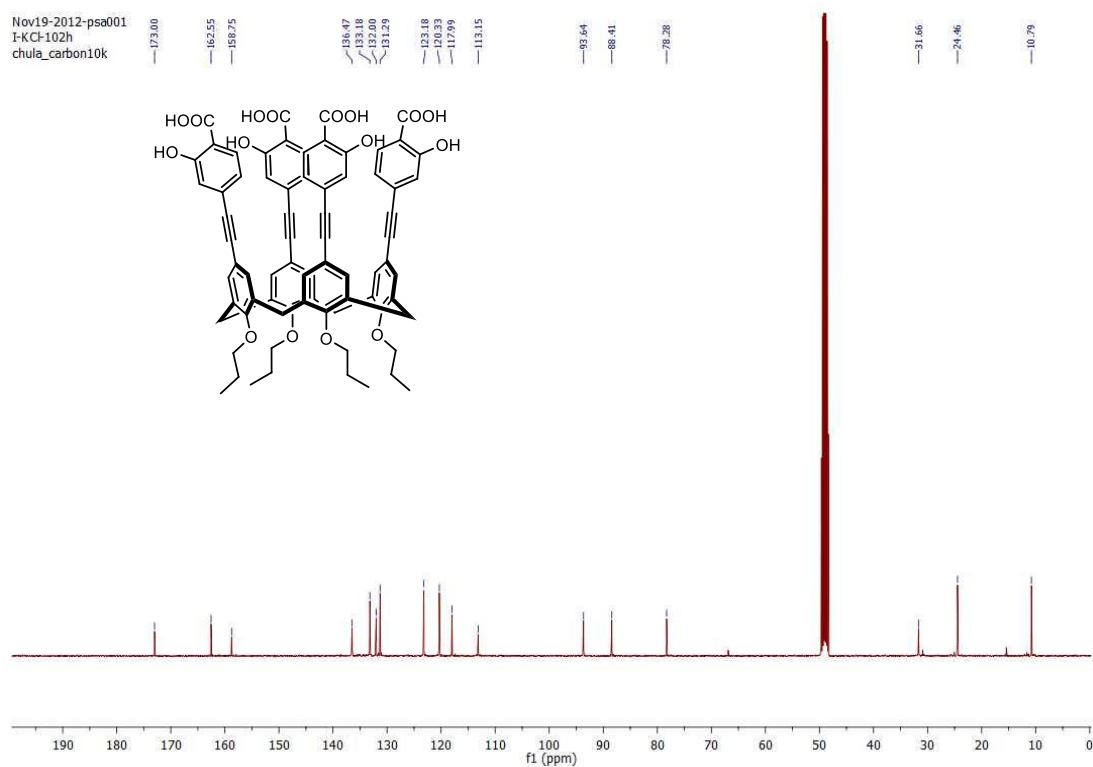


Figure A.16 ^{13}C NMR of SAC in Metanol- d_4

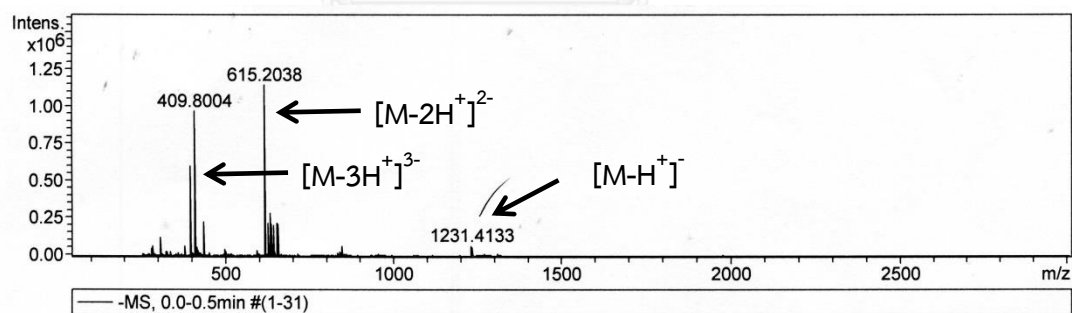


Figure A.17 HRMS of SAC.

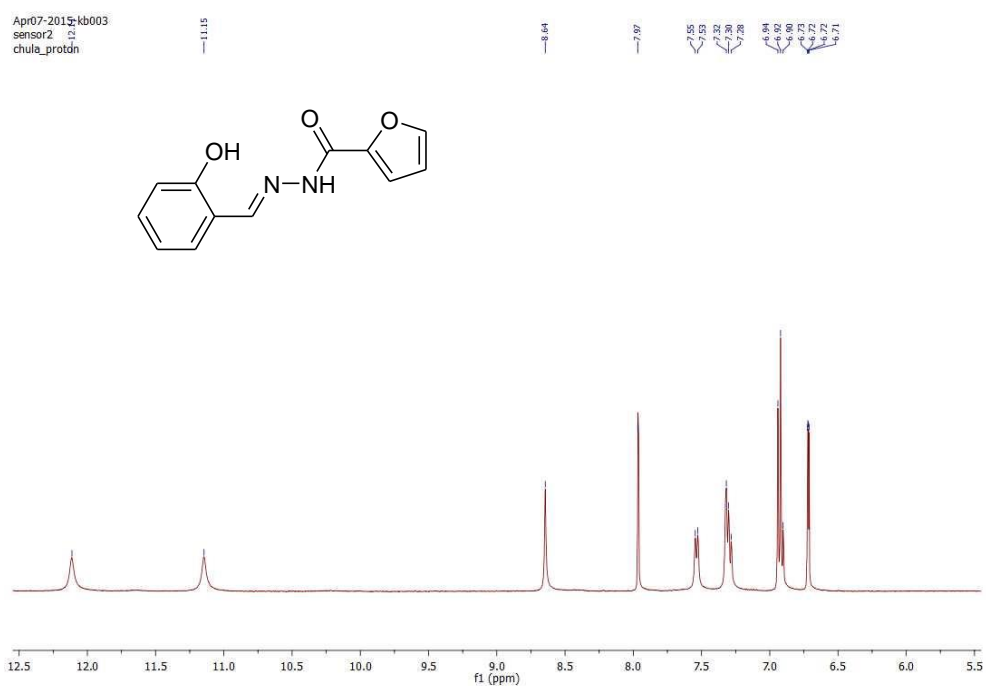


Figure A.18 ^1H NMR of F2 in DMSO-d_6

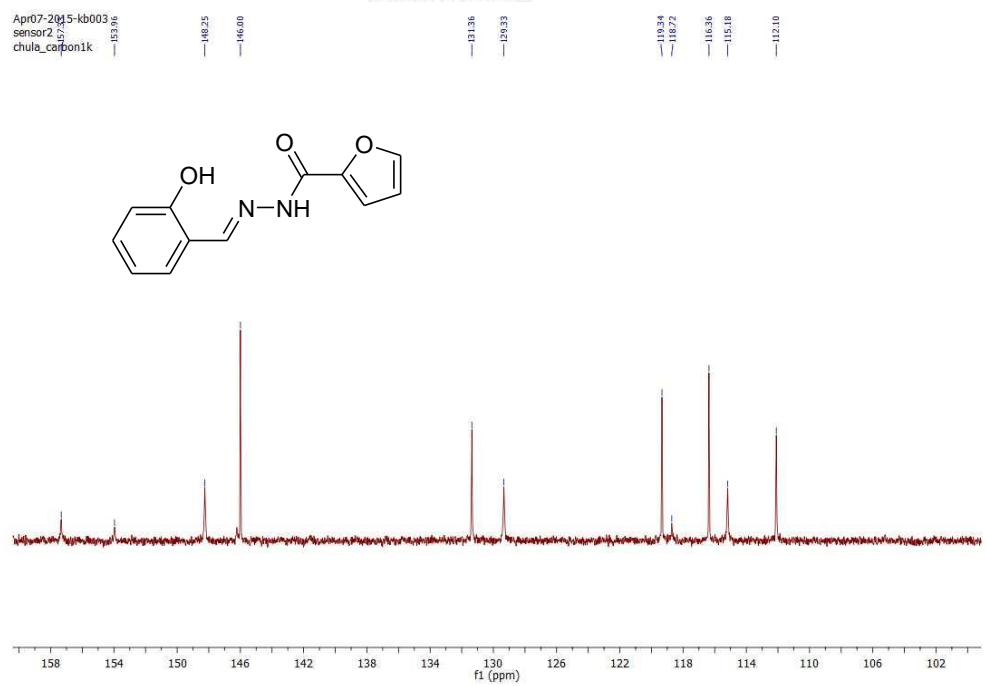


Figure A.19 ^{13}C NMR of F2 in DMSO-d_6

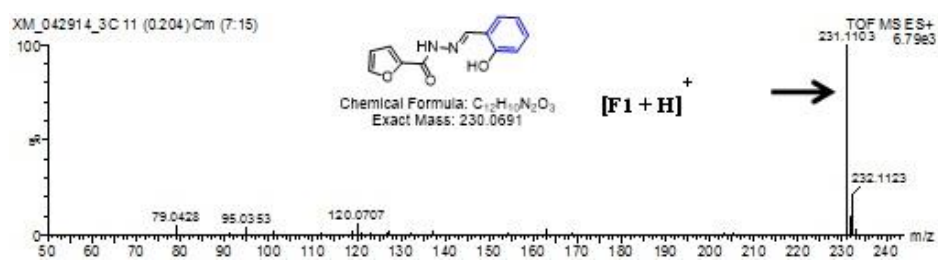
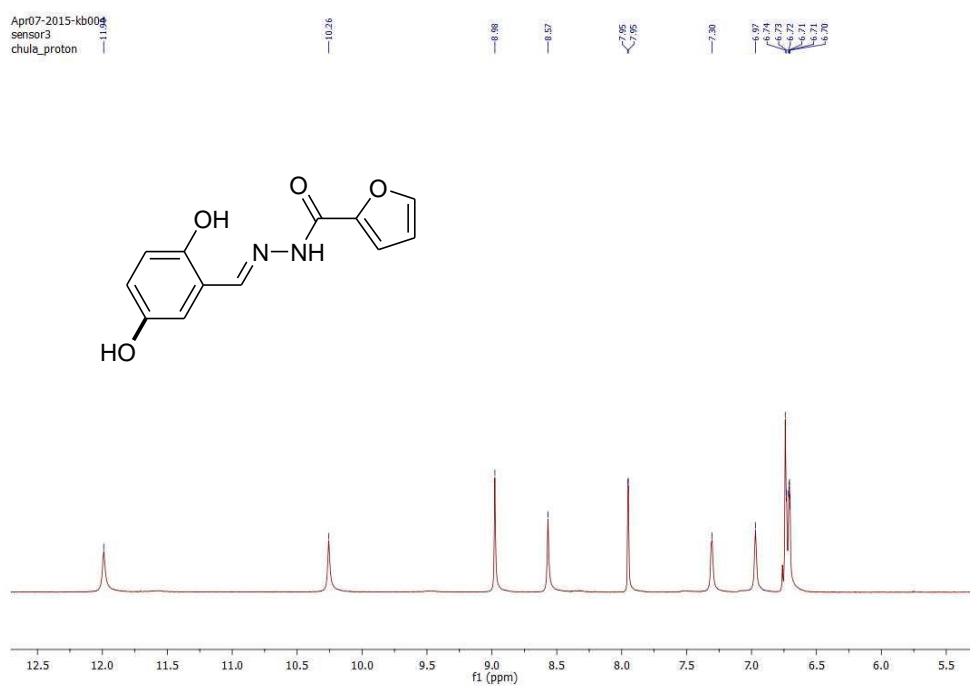


Figure A.20 HRMS of F1.

Figure A.21 1H NMR of F3 in $DMSO-d_6$

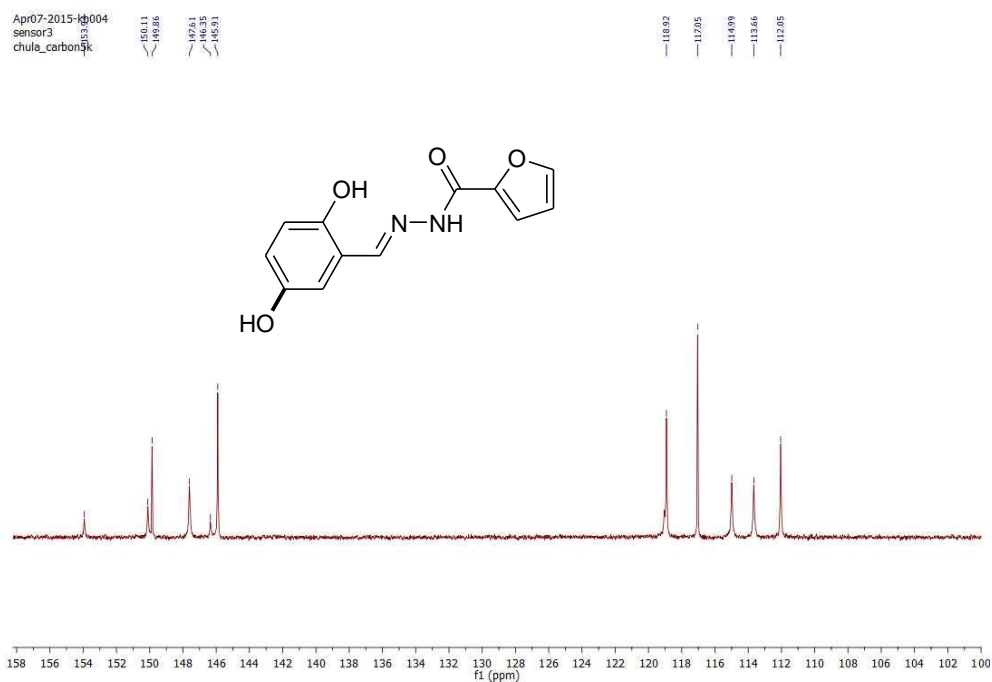


Figure A.22 ^{13}C NMR of F3 in DMSO-d_6

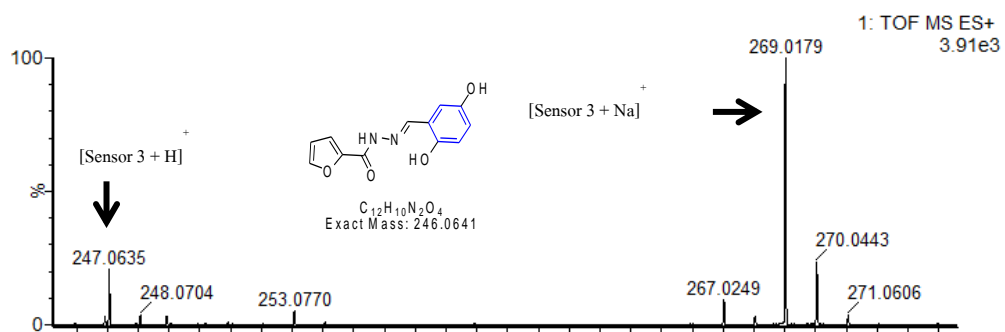


Figure A.23 HRMS of F3.

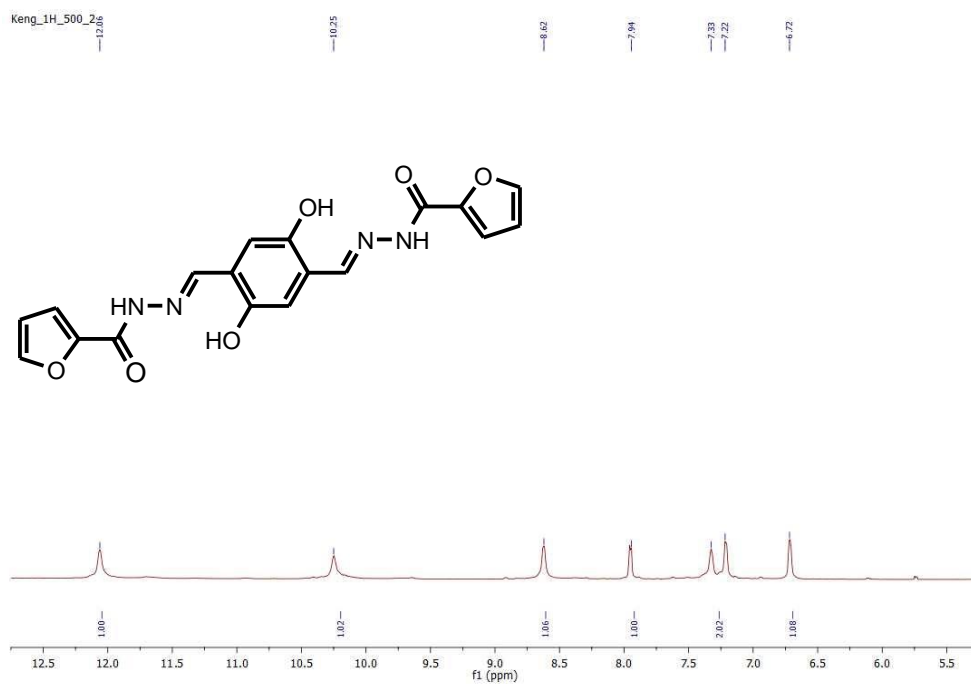


Figure A.24 ^1H NMR of F4 in DMSO-d_6

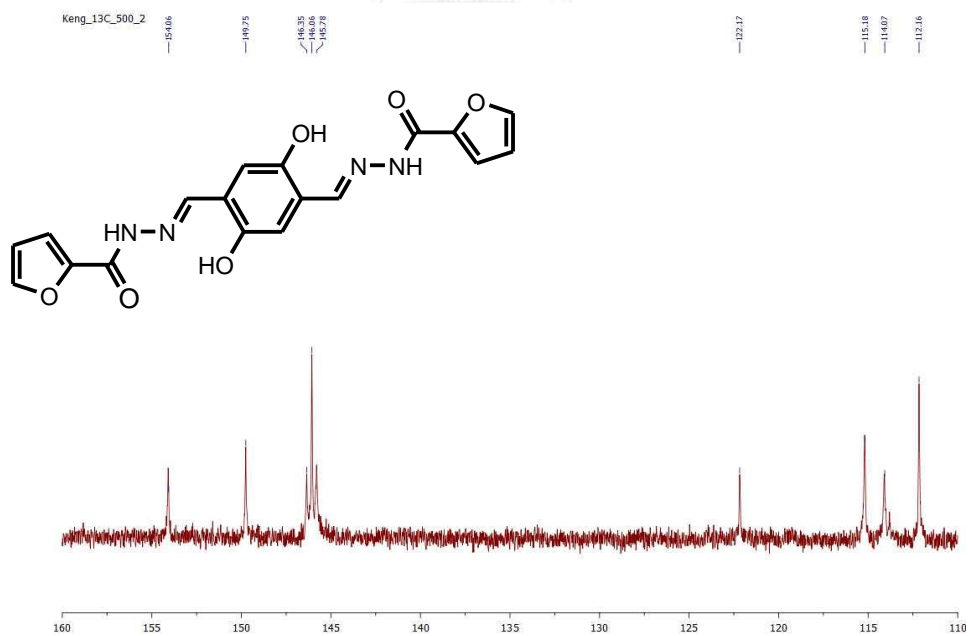


Figure A.25 ^{13}C NMR of F4 in DMSO-d_6

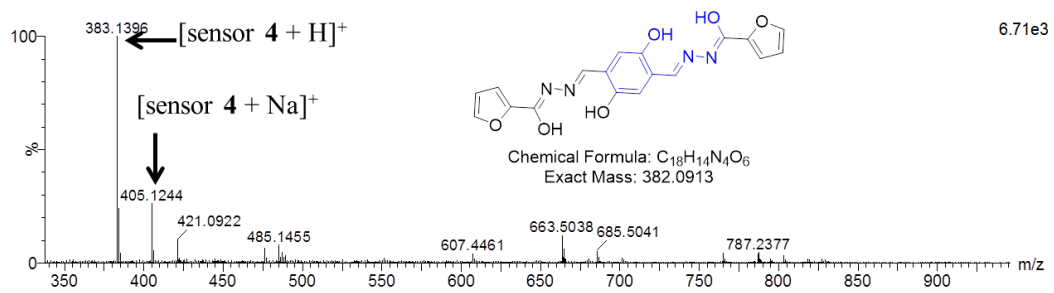


Figure A.26 HRMS of F4.



APPENDIX B

PUBLICATIONS

1. **Boonkitpatarakul, K.**, Yodta, Y., Niamnont, N., and Sukwattanasinitt, M. Fluorescent phenylethynylene calix[4]arenes for sensing TNT in aqueous media and vapor phase. *RSC Advances* 5(42) (2015): 33306-33311.
2. **Boonkitpatarakul, K.**, Wang, J., Niamnont, N., Liu, B., McDonald, L., Pang, Y., Sukwattanasinitt, M. Novel turn-on fluorescent sensors with mega stoke shifts for dual detection of Al^{3+} and Zn^{2+} . *ACS Sens* (2015): DOI: 10.1021/acssensors.5b00136.
3. Pinrat, O., **Boonkitpatarakul, K.**, Paisuwan, W., Sukwattanasinitt, M., and Ajavakom, A. Glucopyranosyl-1,4-dihydropyridine as a new fluorescent chemosensor for selective detection of 2,4,6-trinitrophenol. *Analyst* 140(6) (2015):1886-1893.

VITA

Miss Kanokthorn Boonkitpatarakul was born on October 18th, 1982 in Bangkok, Thailand. She received a Bachelor's Degree of Science, majoring in Chemistry from Faculty of Science, Kasetsart University in 2003. In 2006, she further received a Master Degree in Department of Organic Chemistry Faculty of Science, Mahidol University. Since 2010, she has been a graduate student in Petrochemistry and become a member of Organic Synthesis Research Unit under supervision of Assoc. Prof. Dr. Mongkol Sukwattanasinitt. She graduated with a Ph. D. Degree in Petrochemistry in academic year 2015. During the course of study, she received the scholarship from the Thailand Research Fund through the Royal Golden Jubilee Ph. D. Program (Grant No. PHD/0234/2552).

Her present address is 882/45 Senanikom 1, Phaholyothin road, Senanikom, Jatujak, Bangkok, Thailand 10900.

